

APPLICATIONS OF THE THERMOGRAVIMETRIC ANALYSIS IN THE STUDY OF FOSSIL FUELS

He Huang, Keyu Wang, Shaojie Wang, M. T. Klein and W.H. Calkins*
Dept of Chemical Engineering, University of Delaware, Newark, DE 19716

Key words: thermogravimetric analysis, fossil fuels, characterization

INTRODUCTION

Applications of thermal analysis in fossil fuel research date back as far as the techniques themselves. Thermogravimetry (TG) had been used by Somiya and Hirano in 1930 to determine the volatile yield of many coals (1). Advances in design of thermogravimetric analyzers (TGA) now allow experiments to be carried out simply and fast in high accuracy under various conditions from vacuum to high pressure (2-4). A TG method has been devised for the proximate analysis of coal with the results of the same precision and accuracy as BS and ASTM methods (5).

Thermogravimetric (TG) techniques have been used in our laboratory to characterize fossil fuel samples (6) and to study coal liquefaction kinetics, mechanisms, and processes (7-10). TGA has been providing sensitive, rapid, and reproducible measurements for those purposes. The various weight loss processes determined during the TG analysis reflect the physical and chemical structural changes during the conversion. Thermogravimetric analysis has other desirable features as well. First, only very small samples, usually about 30 mg, are required for each TG scan. Second, by suitable adjustments in the work-up procedures and the TG operating parameters, thermogravimetric analysis reveals important information concerning the reaction pathways. Besides, custom-built thermogravimetric techniques provide very flexible means and unique features for fossil fuel research (11-13).

Development and applications of the TG techniques in our laboratory are reported in this paper. These include 1). characterization of coal structure; 2). determining the liquefaction conversion and measuring the rate of the retrograde reactions occurring during coal liquefaction; 3). evaluating the thermal and catalyzed hydroprocessing of the coal-derived resids; and 4). determining the boiling range of liquid fuels. Various effects including the TG operating variables, such as heating rate, purge gas type (e.g. H_2 or N_2), gas flow rate, and modification of the TG sample pan as well as a method for the development of a custom built thermogravimetric system are also discussed in this paper.

EXPERIMENTAL

Apparatus. The Thermogravimetric Analyses (TGA) were performed with a Model 51 TGA (TA Instruments, New Castle, Delaware).

Procedures. An approximately 30-60 mg sample (e.g. coal, coal liquefaction residue, coal liquid, coal-derived resid, etc.) was loaded in a quartz pan and mounted in the instrument. Selected TG scans were processed using an 11-point smoothing filter of the Linear Regression & Error Analysis procedure (14). The program of manipulation of the TG operating variables was determined by the objectives of the particular experiment.

Materials Studied. Eight coals of rank from lignite to l.v. bituminous were obtained from the Argonne Premium Coal Sample bank. Analytical values of these coals are given in the User's Handbook (15). Two 850°F distillation residue oils (resids), one derived from Wyodak subbituminous coal and another from Pittsburgh bituminous coal, were obtained from the Wilsonville Pilot Plant Runs 259 and 260, and prepared and composited by CONSOL Research. At room temperature, these two resids are solid and only partially soluble in tetralin.

RESULTS AND DISCUSSION

Coal Structure and Composition. A representative TG scan on the Illinois #6 coal is shown in Figure 1. In brief, two stages, i.e., 1) the heating rate at 10 °C/min to 950°C in nitrogen and hold for 7 min; and 2) the oxidation at 950°C, provided measures of Volatile Matter (VM), Fixed Carbon (FC), and Ash. Ash content measured by TGA is in close agreement with that determined by ASTM D3174. When a coal sample is brought to 110 °C in nitrogen and hold for 10 min, the weight loss is a measure of the moisture content (16).

The differential of the weight loss (DTG) curve highlights the various TG processes more clearly. The DTG curve for Illinois #6 shows a pattern which is more complex than many of the other Argonne coals. This becomes even more distinct and complex if the heating rate is slowed down to about 1 °C/min (6).

Thermogravimetric analyses were also run in a hydrogen atmosphere. This provided additional information regarding the structure of coal. (For safety reasons, hydrogen MUST be thoroughly displaced by nitrogen before air or oxygen is introduced.) DTG curves of the eight Argonne Premium Coals in nitrogen and in hydrogen show similar patterns. However,

the Volatile Matter yields at heating rates from 10 °C/min to 200 °C/min are consistently higher, and therefore the Fixed Carbon yields are lower, in hydrogen than in nitrogen. More importantly, the heating rate has a strong effect on the yields of Volatile Matter in either hydrogen or nitrogen. In hydrogen, the Volatile Matter yields decrease somewhat as the heating rate increases. This may be because the pyrolysis time is shorter at higher heating rate, providing less time for reaction with the molecular hydrogen to form more volatile products. However, in nitrogen, the Volatile Matter yields increase with increasing heating rate. This phenomenon may be because, at the low heating rates, the unquenched free radicals react to form more retrograde products (fixed carbon). This is consistent with the flash pyrolysis process, where the oil and gas product yields increase with increasing heating rate.

TGA provides an objective measure of coal rank. DTG curves scanned in 100 cm³(STP)/min nitrogen at 10 °C/min for the eight Argonne Premium Coals (which were dried in a vacuum oven with a nitrogen purge at 105 °C for 48 hours before use) are shown in Figure 2. These coals range ranking from lignite to l.v. bituminous. This plot clearly shows the gradual shift of peak temperature as the coal rank increases from Lignite to low volatile bituminous coal. However, the peak height increases to a maximum at about 81 wt% (daf) Carbon and then decreases as the rank increases.

Coal Liquefaction Studies. A Short-Contact-Time Batch Reactor (SCTBR) was used to run coal liquefaction. This reactor apparatus allows the heat up and quenching of the process stream to and from reaction temperature in about 0.3 seconds, respectively. The design and operation of such a SCTBR reactor system have been described in detail elsewhere (17,18). After a liquefaction run, the product mixture was filtered and the solid residue washed with fresh tetralin thoroughly, then rinsed with methylene chloride to remove residual tetralin, and dried in a vacuum oven with a nitrogen purge at about 105 °C for 48 hours. This resulted in the production of a liquid filtrate, which consisted mainly of tetralin and dissolved coal liquids, and a solid filter cake, of unconverted and/or partially converted solid coal residue.

During coal liquefaction, the coal liquids are extracted into the tetralin solvent. However, the mineral matter of the coal remains with the solid coal residue and is insoluble in tetralin, as proven by the TG scan on the liquid filtrate (8,19). Since the ash is not consumed during the liquefaction and remains in the solid, conversion to the tetralin-soluble oils can be derived based on an ash-balance (8,17):

$$\text{Conversion} = \left(1 - \frac{A_o}{A_s}\right) \times 100\% \quad (1)$$

where A_o and A_s are the weight fractions of ash in the control sample and in the liquefaction residue, respectively. The control sample is the original coal which is processed exactly as a liquefaction residue except at ambient temperature. When the liquefaction is carried out in the presence of an inorganic catalyst, the conversion calculation must include an ash value corrected for the ash derived from the catalyst.

The thermal and catalyzed liquefaction conversions of Illinois #6 coal in tetralin at 390 °C are shown in Figure 3. In the thermal liquefaction, three distinct phases in the process were observed, i.e., a very rapid conversion followed by an induction period and then a slower liquefaction of the coal structure. The initial rapid conversion in the first minute is due to the physical extraction of a soluble fraction of the coal into the hot tetralin. This is followed by an induction period and then the slow conversion of the coal structure to liquid products. The induction period observed is actually a pseudo induction period. This induction period is a transition interval which is due to the simultaneous occurrence of two processes, a very rapid extraction and a relatively slower liquefaction of the coal structure. In fact, as the temperature increases, the induction period steadily becomes less pronounced as the rate of break down of the coal structure increases and becomes closer in reaction rate to the extraction step itself (10). That the induction period is not due to the build up of free radicals is also proven by ESR data (20,21). In the catalyzed liquefaction, the pseudo induction period is, as expected, diminished and the subsequent conversion is much faster for the catalyzed than the thermal liquefaction. More importantly, the retrograde process, leading to form tar, coke and char, is very significantly reduced in the presence of catalyst and hydrogen as is shown by the Fixed Carbon content in the residue as a function of liquefaction time (Figure 4). When the catalyzed liquefaction was run at higher temperature, the Fixed Carbon of the residue was even further reduced (Figure 5), suggesting that the precursors of the retrograde processes are being hydrogenated and stabilized during the catalyzed liquefaction. Liquid yields were thereby significantly improved (Figure 6).

DTG curves for partially converted coal liquefaction residues of Illinois #6 coal after liquefaction in tetralin at 390°C under 1000 psig nitrogen at selected contact times are

shown in Figure 7. The gradual disappearance of the two smaller peaks (one of them identified as FeS₂ conversion to FeS and S) clearly indicates that some chemical changes in the solid coal are taking place before the coal actually becomes liquid. In addition, the sensitivities of the production of VM in the residues to heating rate and to atmospheres of nitrogen and hydrogen are significantly changed as shown in Figures 8a and 8b for the unreacted original Illinois #6 coal and a liquefaction sample of Illinois #6 taken after 30 seconds at 390 °C, respectively. The profound changes shown in that short time suggests that even short exposure to donor solvent can significantly change the character of the coal before much actual liquefaction has taken place. This change may merely be the removal of a very unstable volatile fraction or actual stabilization by hydrogen transfer from the donor solvent.

Evaluating the thermal and catalyzed hydroprocessing of the coal-derived resids. The Short-Contact-Time Batch Reactor (SCTBR) was again used for the thermal and catalyzed hydroprocessing of the coal-derived resids. The resid reaction product workup procedure and determination of the thermal and catalyzed resid conversion have been described in detail elsewhere (8). The conversion of resid to tetralin soluble material was determined by relating the inorganic matter (ash) in the reacted resid with that of the unreacted resid. Un-catalyzed conversion of tetralin-insoluble resids to tetralin soluble products in this study was very low (< 10 wt%) under coal liquefaction conditions (410 - 440 C, 1500 psig H₂, 2 - 5 of tetralin to resid ratio). But, up to 80 wt% (ash-free basis) was solubilized in tetralin using sulfided Ni/Mo on alumina catalyst at 434°C for 10 min. Hydroprocessing at liquefaction conditions (see above), and particularly in the presence of Ni/Mo on alumina catalyst, was effective for converting tetralin-insoluble to tetralin-soluble material, and for reducing the average molecular weight (8). Up to 50 wt% of the resid was already tetralin soluble even at room temperature. Therefore, the tetralin solubility cannot be used as a measure of the resid converted to low boiling fuels. The actual conversion of resid represents the portion of the resid which is broken down in the hydroprocessing to low molecular weight material boiling below 850 °F. For that reason, additional technique(s) is required for measuring the degree to which the resids is converted to lower boiling products (i.e. below 850 °F).

An analytical TGA method for boiling range measurement, SimDis TGA, has been developed for that purpose. This SimDis TGA technique requires a change in the conventional TGA sample pan. It was devised with a small aperture at the top of the pan. The fundamentals, methodology, and experimental details of the SimDis TGA technique have been reported in the Symposium on New Analytical Methods for Characterizing Fossil Fuels and Derived Products in Chicago in 1995 (22). The boiling point distribution of Wilsonville # 258 resid liquid sample, which was determined by the SimDis TGA technique, is shown in Figure 9. This resid sample was hydroprocessed in tetralin using sulfided molybdenum naphthenate catalyst at 403°C for 60 minutes. The fraction of the resid liquid boiled below 850 °F (i.e. 850 °F) was 93.8 wt%, in which tetralin fraction was included. The following equation:

$$\text{Conversion (850 }^\circ\text{F)} = \text{TSF} \times \left(1 - \frac{\text{850 }^\circ\text{F}^+ \text{ in tetralin}}{\text{RSF in tetralin}}\right) \times 100\% \quad (2)$$

was used to evaluate the resid conversion to 850 °F during the thermal and catalyzed hydroprocessing. In Equation 2, TSF (Tetralin Soluble Fraction) was determined by ash content in the solid residue (8); RSF (Resid Soluble Fraction) and 850 °F⁺ fractions in tetralin were determined by running the ramp and SimDis TGA methods (8,22) on the resid liquid products, respectively. Preliminary studies show that, for the illustrative sample in Figure 9, TSF (Tetralin Soluble Fraction) determined by ash content of the solid residue was 67.8 wt%; 850 °F⁺ fractions in tetralin determined by the ramp method was 8.62 wt%. Conversion of the Wilsonville #258 resid hydroprocessed under those conditions to 850 F⁺ was 19.0 wt%.

Determining boiling point distribution of liquid fuels. In addition to the SimDis TGA method, which is capable of measuring the boiling point up to 1000 °C and briefly described in previous section, a custom-built thermogravimetric apparatus for distillation of liquid fuels was also developed in our laboratory (23). As an example, boiling point distribution of a crude oil analyzed using the custom-built thermogravimetric apparatus is illustrated in Figure 10.

CONCLUSION

Thermogravimetric analysis (TGA) of coal and resid liquids and coal and resid solid residues, which were produced in coal liquefaction and coal-derived resid hydroprocessing in the SCTBR (Short-Contact-Time Batch Reactor) apparatus, provides a sensitive, rapid, and reproducible means of studying the kinetics and mechanisms of fossil fuel conversion

processes. SimDis TGA and the custom built thermogravimetric system for distillation provide unique means to characterize liquid fuels for the boiling point distribution.

Thermogravimetric Analysis (TGA) provides information concerning the various weight loss processes that can be a reflection of the physical and chemical structure of fossil fuel samples. More importantly, this technique is also capable of yielding TG scanning parameters, such as Volatile Matter, Fixed Carbon, Ash, etc. to be used to monitor the fossil fuel conversion processes. A significant example is to determine the onset and rate of the retrograde reactions during the coal liquefaction process.

ACKNOWLEDGMENTS

The support of these studies by the Department of Energy under DE22-93PC93205 and by subcontracts from CONSOL Inc. under U. S. DOE Contract No. DE-AC22-89PC89883 and DOE Contract No. DE-AC22-94PC93054 is gratefully acknowledged.

The assistance and advice of F.P. Burke, R.A. Winschel and S.D. Brandes of CONSOL Inc in preparation and analysis of the resid and catalyst samples used in resid hydroprocessing are gratefully acknowledged. The use of Argonne Premium Coal Samples provided by Dr. Karl Vorres is also acknowledged.

Additional funds for purchase of thermal analysis equipment was provided by the University of Delaware.

REFERENCES

1. Somiya, T.; Hirano, S. *J. Chem. Soc. Ind. (Japan)* 1930, **33**, 737.
2. Schwartz, H.E.; Brownlee, R.G.; Boduszynski, M.; Su, F. *Anal. Chem.* **1987**, **59**, 1393.
3. Nie, X.; McClennen, W.H.; Liu, K.; and Meuzelaar, H.L.C. *ACS Fuel Chem Div Preprints* **38** (4), 1147 (1993).
4. Liu, K.; Jakab, E.; McClennen, W.H.; Meuzelaar, H.L.C. *ACS Fuel Chem Div Preprints* **38** (3), 823 (1993).
5. Ottaway, M. *Fuel* **1982**, **61**, 713.
6. Huang, He; Wang, Keyu; Klein, M.T.; W.H. Calkins *ACS Fuel Chem Div Preprints* **40** (3), 465 (1995).
7. Huang, He; Wang, Keyu; Calkins, W.H.; Klein, M.T. *ACS Fuel Chem Div Preprints* **39** (3), 741 - 746 (1994).
8. Huang, He; Calkins, W.H.; Klein, M.T. *I&EC Research* **33**, 2272-2279 (1994).
9. Huang, He; Wang, Keyu; Klein, M.T.; W.H. Calkins *Coal Science and Technology 24: Coal Science*, Eds J.A. Pajares and J.M.D. Tascon, Vol. II, p. 1207 (1995).
10. Huang, He; Wang, Keyu; Wang, Shaojie; Klein, M.T.; W.H. Calkins *ACS Fuel Chem Div Preprints* **40** (3), 550 (1995).
11. Massoth, F.E. *Chem. Tech.* 1972, May, 285.
12. Sears, J.T.; Maxfield, E.A.; Tamhankar, S.S. *Ind. Eng. Chem. Fundam.* 1982, **21**, 474.
13. Dean, J.W.; Dadyburjor, D.B. *Ind. Eng. Chem. Res.* 1988, **27**, 1754.
14. Wang, Keyu; Wang, Shaojie; Huang, He; Klein, M.T.; Calkins, W.H.; paper to be presented in the *Symp. on the Thermal Analytical Techniques*, March 24-29, 1996, in New Orleans.
15. Vorres, K.S. 'User's Handbook for the Argonne Premium Coal Sample Program' *ANL/PCSP-93/1*.
16. He Huang, D.M. Bodily, and V.J. Hucka *Proceedings 1993 International Conference on Coal Science*, 411-414.
17. Huang, He; Calkins, W.H.; Klein, M.T. *Energy and Fuels* **8**, 1304-1309 (1994).
18. Huang, He; Fake, D.; Calkins, W.H.; Klein, M.T. *Energy and Fuels* **8**, 1310-1315 (1994).
19. Calkins, W.H.; Huang, He; Klein, M.T. *Proceedings 1994 Pittsburgh Coal Conference* pps. 475-480.
20. Huang, He; Provine, W.D.; Jung, B.; Jacintha, M.A.; Rethwisch, D.G.; Calkins, W.H.; Klein, M.T.; Dybowski, C.R.; Scouten, C.G. *Proceedings of the International Conference on Coal Science, 1993*, Ed. K.H. Michaelian, Vol. I, 266.
21. Provine, W.D.; Jung, B.; Jacintha, M.A.; Rethwisch, D.G.; Huang, He; Calkins, W.H.; Klein, M.T.; Scouten, C.G.; Dybowski, C.R. *Catalysis Today*, **1994**, Ed. D.B. Dadyburjor and J.W. Zondlo, Vol. **19**, No. 3, 409.
22. Huang, He; Wang, Keyu; Wang, Shaojie; Klein, M.T.; W.H. Calkins *ACS Fuel Chem Div Preprints* **40** (3), 485 (1995).
23. Huang, He; Wang, Keyu; Wang, Shaojie; Klein, M.T.; W.H. Calkins paper to be presented in the *Symp. on the Thermal Analytical Techniques*, March 24-29, 1996, in New Orleans.

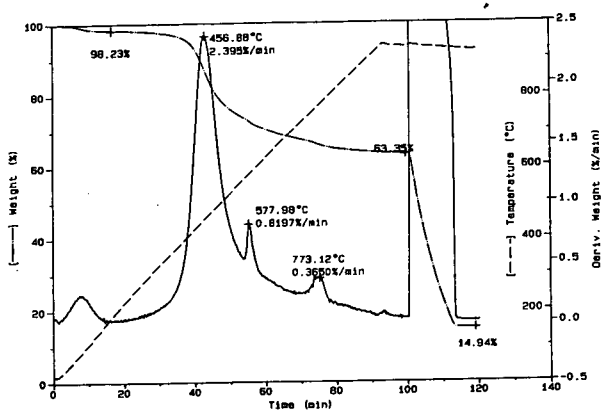


Figure 1 A TG scan of Illinois #6 coal at 10 C/min

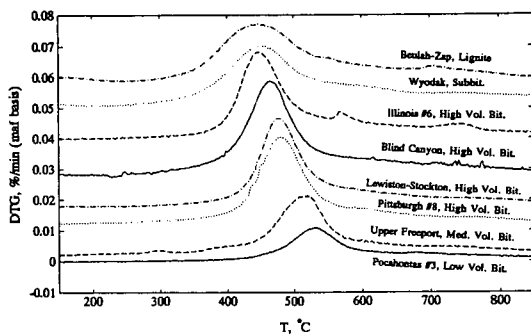


Figure 2 DTG profiles of the eight Argonne coals

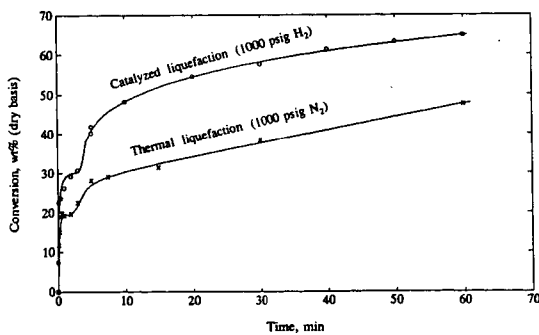


Figure 3 Conversion vs time of the thermal and catalyzed (about 0.9 wt% Mo of sulfided molybdenum naphthenate) liquefaction of Illinois #6

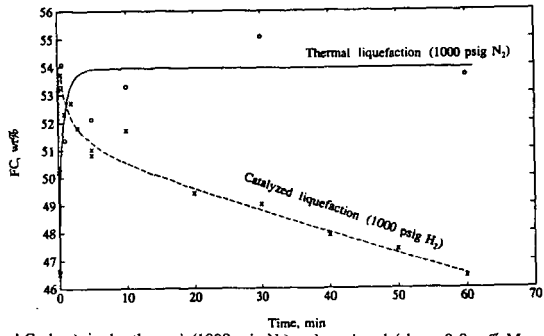


Figure 4 FC (Fixed Carbon) in the thermal (1000 psig N₂) and catalyzed (about 0.9 wt% Mo and 1000 psig H₂) liquefaction residues determined by TGA

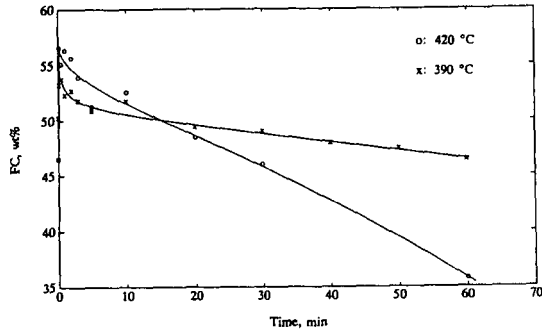


Figure 5 FC (Fixed Carbon) in the catalyzed (about 0.9 wt% Mo) liquefaction residues determined by TGA

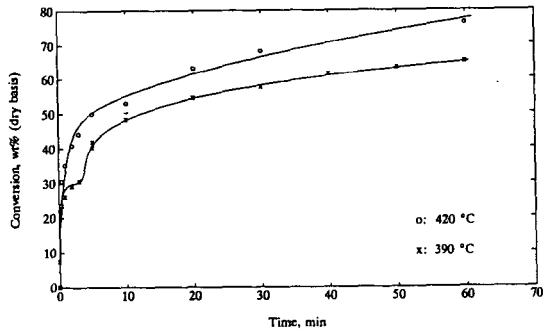


Figure 6 Conversion of the Illinois #6 bituminous in catalyzed (about 0.9 wt% Mo) coal liquefaction under 1000 psig H₂

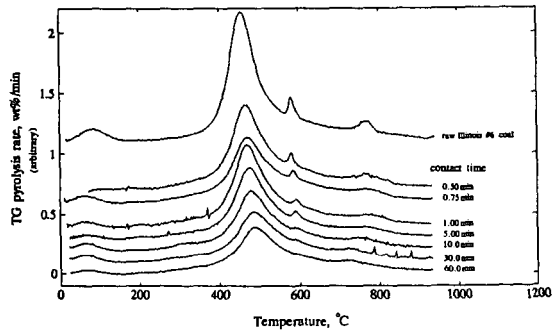


Figure 7 DTG profiles for the liquefaction residues of the Illinois #6 bituminous at the selected contact times

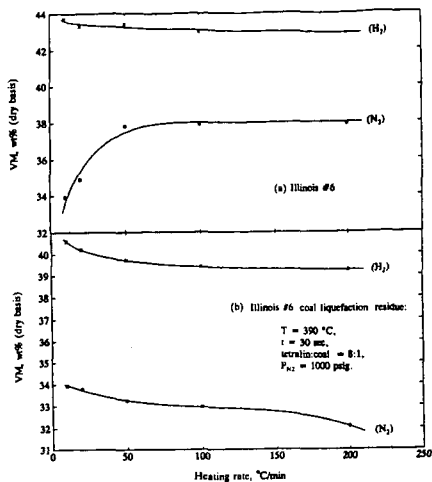


Figure 8 Effect of heating rate and type of purge gas on the VM yields of a). raw Illinois #6 coal and b). its liquefaction residue

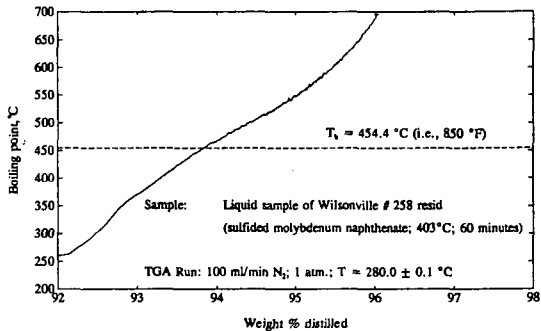


Figure 9 Boiling point distribution of the hydroprocessed reisd liquid determined by SimDis TGA

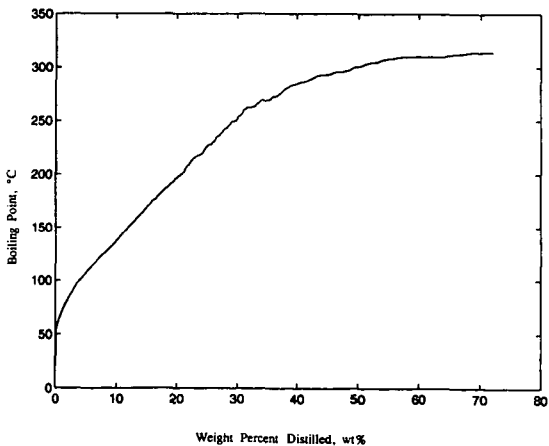


Figure 10 Weight percent distilled vs boiling point of a filtered crude oil determined by a custom built TG for distillation

APPLICATION OF THERMAL ANALYSIS TECHNIQUES IN ACTIVATED CARBON PRODUCTION

Gwen L. Donnals, Joseph A. DeBarr, Massoud Rostam-Abadi, Anthony A. Lizzio,
Todd A. Brady, Illinois State Geological Survey, Champaign, Illinois 61820

Keywords: thermal analysis, activated carbons

INTRODUCTION

Several current research programs at the Illinois State Geological Survey (ISGS) relate to the development of activated carbons from Illinois coal, fly ash, and scrap tires [1-5]. Preparation of activated carbons involves thermal processing steps that include preoxidation, pyrolysis and activation. Reaction time, temperature and gas composition during these processing steps ultimately determine the nature of the activated carbon produced. Thermal analysis plays a significant role in developing carbons by providing fundamental and engineering data that are useful in carbon production and characterization for process development.

EXPERIMENTAL

Thermal analysis instruments and their applications are useful for characterizing activated carbon precursors and intermediate and final products. Instruments available in the Thermal Analysis Laboratory at the ISGS include both atmospheric (Cahn TG-131) and high pressure (SRE Model TL-TGA 1900/600) thermogravimetric analyzers (TGA and PTGA). Evolved gases from a controlled fixed-bed thermal reactor are monitored by non-dispersive infrared CO and CO₂ analyzers (Rosemount model 880) and a quadrupole mass spectrometer (Fisons model MMP300-D). All instruments are computer interfaced to allow data collection and rapid data reduction and analysis.

Proximate analysis is performed in the TGA to determine the amounts of moisture, volatile matter, fixed carbon and ash content in activated carbons. In a typical analysis, 50 mg of sample is heated in a platinum pan at 50°C/min to 950°C in N₂ flowing at 75 cc/min (STP). The temperature is held constant at 950°C for 10 minutes, then reduced to 750°C. Air is introduced at 750°C until the oxidation reaction is complete and no further weight loss is observed.

Activation studies are done in the TGA to determine appropriate conditions for activation of carbon samples in larger scale test facilities [6]. Reactivity is determined in the TGA using air at 380-500°C, CO₂ at 920-1000°C, or steam at 860-960°C. Typically, 2-10 mg of sample is heated in N₂ to a predetermined reaction temperature. Once the temperature and weight stabilize, appropriate reaction gas is substituted for the N₂ and weight loss is monitored as a function of time.

SO₂ removal efficiencies from simulated combustion flue gas by activated carbons is determined in the TGA [7]. In a typical run, 30-50 mg of sample is heated at 20°C/min in flowing N₂ to 360°C to remove surface impurities. The sample is then cooled to 120°C in N₂ and the gas stream is switched to a mixture of 5% O₂, 7% H₂O, balance N₂. Because at this temperature O₂ and H₂O are adsorbed onto the carbon, the sample weight is allowed to stabilize before SO₂ (2500 ppmv) is introduced into the TGA. Uptake of SO₂ is monitored for up to 60 h.

Methane adsorption capacities of activated carbons are determined using the PTGA [2]. The samples are degassed at 150°C for 3 h in N₂ prior to adsorption of methane. Adsorption of methane is done at 25°C at pressures of 0, 100, 200, 300, 400 and 500 psig. The rate of methane uptake and the adsorption capacity (g methane/g char) are recorded by a computerized data acquisition system.

The nature and extent of oxygen functional groups on the carbon surface are determined by temperature programmed desorption (TPD) [8]. TPD experiments are performed in a 2.5 cm ID stainless steel fixed-bed reactor system. In a typical run, 0.5 g of sample is heated at 5°C/min to 1000°C in N₂ flowing at 0.5 L/min. Temperature is held at 1000°C until evolved CO and CO₂ return to baseline concentrations, indicating complete desorption. Concentrations (ppm) of CO and CO₂, time and temperature are recorded by a computerized data acquisition system. The areas under the CO and CO₂ curves are converted to the amount of oxygen present on the carbon surface.

RESULTS AND DISCUSSION

Carbon production

Partial gasification during activation serves to develop surface area and porosity in char. The overall surface area and type of pore structure of the activated carbon may be controlled by the rate and

extent of gasification during activation. Chars may be activated with oxygen, steam, CO₂, or a mixture of these gases. At a given temperature, the relative rates of reaction for these gases range over several orders of magnitude, with O₂ > steam > CO₂. Thermogravimetry (TG) provides a method for directly monitoring both the rate and extent of activation as the reaction proceeds. This allows for good control of process conditions when preparing an activated carbon with characteristics needed for a particular application. Figure 1 shows the activation profile of a carbon prepared from a utility fly ash. Initial activation was done at 950°C in CO₂ for 1 hour, with a weight loss of only 5%. Surface areas of activated carbons, not corrected for ash content, generally increase monotonically during activation up to about 80% weight loss (conversion) [9]. After 1 h, the gas composition was changed to 50% steam/50% CO₂, which resulted in a total weight loss of 30% in 2 h. Using the data from Figure 1, a larger sample was prepared in a horizontal tube furnace that had surface area and adsorption properties similar to the sample prepared in the TGA.

Carbon Characterization

Carbons with a variety of surface areas and pore size distributions have been developed at the ISGS for various applications. One such application is the removal of contaminants from flue gas streams of waste incinerators [10]. STEAG, of Essen, Germany, has developed a process in which a bed of low surface area, low cost carbon is used to remove contaminants such as particulate matter, dioxins, furans, mercury, SO₂, other acid gases and heavy metals from flue gas. The ISGS was asked to prepare a low surface area, low cost activated carbon from Illinois coal for testing in the STEAG a/cTM process. Process variables, developed to prepare gram quantities of carbons in the laboratory, were used ultimately to prepare 500 pounds of activated carbon for tests in STEAG's pilot plant [11]. STEAG believes that the SO₂ adsorption behavior of a carbon is indicative of its ability to remove other contaminants from flue gas streams using their process [12]. Surface area and SO₂ adsorption behavior of the activated carbons prepared in each stage of scale up were used as guides to ensure that a carbon was produced with desired properties for the STEAG process. TG provided a rapid method for determining the relative rates of SO₂ adsorption and equilibrium SO₂ adsorption capacity of a carbon using only milligram quantities of sample. Figure 2 shows the kinetics of SO₂ adsorption in a simulated flue gas for the ISGS carbon and the carbon STEAG currently uses in their process (Herdofenkoks). Although the surface area of the Herdofenkoks was nearly three times that of the ISGS carbon, the initial rate of SO₂ adsorption was much greater for the ISGS carbon. This carbon has proven effective in STEAG's process during pilot plant tests.

TG has been used to study the effect of adsorption temperatures, gas compositions and carbon characteristics on SO₂ adsorption by carbons [13]. Figure 3 shows SO₂ adsorption by an air activated carbon heated to different temperatures in inert gas after activation. These carbons all had surface areas of about 300 m²/g, suggesting that surface area is not a good indicator of SO₂ adsorption [13]. Corresponding TPD profiles for the air activated carbons show that as the parent carbon was heated to higher temperatures, less oxygen was present on the surface of the carbon (Figure 4). These results suggest that SO₂ capacity is inversely related to the amount of oxygen on the surface of the carbon. Similar data have been found for other carbons. These results were used to propose a new mechanism for SO₂ adsorption on activated carbons [14].

TG also permits rapid evaluation of the thermal regeneration of carbons, and may be used to predict the life cycle of adsorbents in different applications. Adsorption/desorption cycles were performed in the TGA to determine regenerative properties of an activated carbon prepared from Illinois coal by steam activation, followed by HNO₃-treatment and thermal desorption at 925°C [4]. After initial SO₂ adsorption, the carbon was regenerated in the TGA by heating to 360°C. Regeneration of the carbon in this manner resulted in a significant decrease in the SO₂ adsorbed in subsequent adsorption/desorption cycles (Figure 5). These results have been explained by the formation of stable oxygen complexes on the surface of the carbon that inhibit adsorption of SO₂ [4]. It is thought that regeneration of this carbon at higher temperatures would restore its original SO₂ capacity, but this remains to be determined.

Carbons prepared from different precursors such as coal, fly ash and tires may have different adsorption properties not only because of their structure, but also due to different composition. A significant portion of the carbonaceous material is lost during pyrolysis and activation, and non-volatile mineral matter present in the precursor is concentrated in the remaining carbon product. Proximate analysis of activated carbons can be done rapidly with TG to provide information on the moisture, volatile matter, fixed carbon, and mineral matter present in the carbon. Figure 6 shows proximate analyses for a fly ash carbon and three steam activated chars made from Illinois coal.

Activated carbon may be used for onboard methane storage in natural gas vehicles. This storage technology is less expensive, occupies less space and costs less to refuel than compressed natural gas storage, and may result in vehicles that are lighter and have much greater storage density at low

pressure (< 35 atm). Activated carbons that might be suitable for this application have been prepared at the ISGS from both Illinois coal and scrap tires [2]. Pressurized TGA allows methane adsorption isotherms to be measured for small quantities of sample as shown in Figure 7. Shown for comparison is the isotherm for a commercial activated carbon Calgon BPL. Activated carbons prepared from scrap tires exhibit a wide range of adsorption capacities. Methane adsorption capacities (g methane/g char) of some tire-derived carbons were within 10% of the BPL carbon.

SUMMARY

Thermal analysis techniques have been used at the ISGS as an aid in the development and characterization of carbon adsorbents. Promising adsorbents from fly ash, tires, and Illinois coals have been produced for various applications. Process conditions determined in the preparation of gram quantities of carbons were used as guides in the preparation of larger samples. TG techniques developed to characterize the carbon adsorbents included the measurement of the kinetics of SO₂ adsorption, the performance of rapid proximate analyses, and the determination of equilibrium methane adsorption capacities. Thermal regeneration of carbons was assessed by TG to predict the life cycle of carbon adsorbents in different applications. TPD was used to determine the nature of surface functional groups and their effect on a carbon's adsorption properties.

REFERENCES

1. Lizzio, A.A. and Rostam-Abadi, M., "Production of Carbon Molecular Sieves from Illinois Coal," *Fuel Processing Technology*, 34, pp 97-122, 1993.
2. Brady, T.A., "Adsorbent Carbons from Waste Tires for Natural Gas Storage," M.S. Thesis in Environmental Engineering in Civil Engineering, University of Illinois at Urbana-Champaign, 1996.
3. Sun, J., Rood, M.J., Rostam-Abadi, M., Lizzio, A.A., "Natural Gas Storage with Activated Carbon from a Bituminous Coal," special issue of *Gas Separation and Purification*, in press.
4. Lizzio, A.A., DeBarr, J.A., Donnals, G.L., Kruse, C.W., Rood, M.J., Gangwal, S.K., "Production and Use of Activated Char for Combined SO₂/NO_x Removal," Final Technical Report, Illinois Clean Coal Institute, Carterville, Illinois, 1995.
5. DeBarr, J.A., Rapp, D.M., Rostam-Abadi, M., Lytle, J.M., Rood, M.J., "Valuable Products from Utility Fly Ash," First Quarterly Technical Report, Illinois Clean Coal Institute, Carterville, Illinois, 1995.
6. Lizzio, A.A., DeBarr, J.A., Donnals, G.L., Kruse, C.W., Rood, M.J., Gangwal, S.K., "Production and Use of Activated Char for Combined SO₂/NO_x Removal," Third Quarterly Technical Report, Illinois Clean Coal Institute, Carterville, Illinois, 1994.
7. DeBarr, J.A., Lizzio, A.A., Daley, M.A., "Adsorption of SO₂ on Bituminous Coal Char and Activated Carbon Fibers from Phenol Formaldehyde," ACS preprints, Fuel Chemistry Division, 1996.
8. DeBarr, J.A., Lizzio, A.A., "New Insights on the Mechanism of SO₂ Removal by Carbon," Proceedings of the 22nd Biennial Conference on Carbon, San Diego, CA, July 1995.
9. Lizzio, A.A. and Radovic, L.R., "On the Usefulness of Total Surface Area for Predicting Carbon Gasification Reactivity Profiles", 19th Biennial Conference on Carbon, University Park, PA, 1989.
10. Brueggendick, H. And Pohl, F.G., "Operating Experience with STEAG's Activated Carbon Process-a/c/tTM in European Waste Incineration Plants," Proceedings of Tenth Annual International Pittsburgh Coal Conference, Pittsburgh, PA, 1993.
11. Lizzio, A.A., DeBarr, J.A., Kruse, C.W., "Development of Low Surface Area Char for Cleanup of Incinerator Flue Gas," Proceedings of the 22nd Biennial Conference on Carbon, San Diego, CA, July 1995.
12. Rummenhol, V., Presentation to Illinois Coal Development Board, Illinois Clean Coal Institute and Illinois State Geological Survey, Champaign, IL, March 2, 1994.
13. DeBarr, J.A., "The Role of Free Sites in the Removal of SO₂ from Simulated Flue Gases by Activated Char," M.S. Thesis in Environmental Science, University of Illinois at Urbana-Champaign, 1995.
14. Lizzio, A.A., DeBarr, J.A., "The Mechanism of SO₂ Removal by Carbon," ACS preprints, Fuel Chemistry Division, 1996.

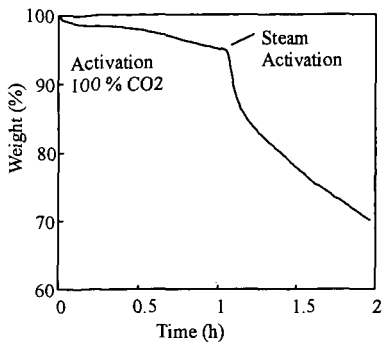


Figure 1. Activation profile of carbon prepared from a utility flyash.

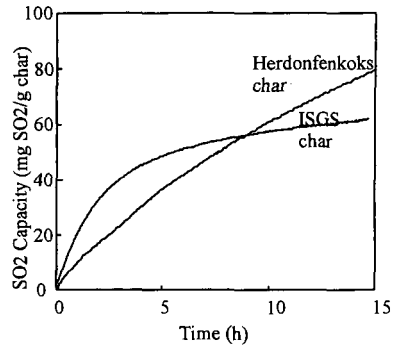


Figure 2. SO₂ adsorption of IGS and Herdonfenkoks chars.

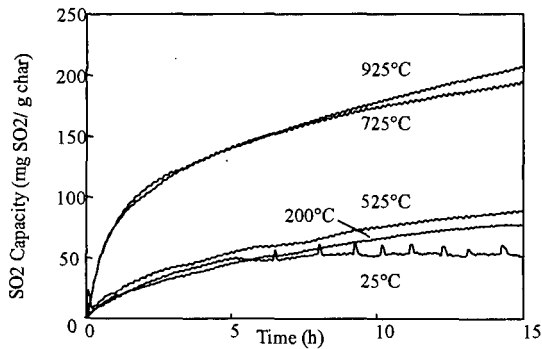


Figure 3. SO₂ adsorption profiles of air activated carbons heated to different temperatures.

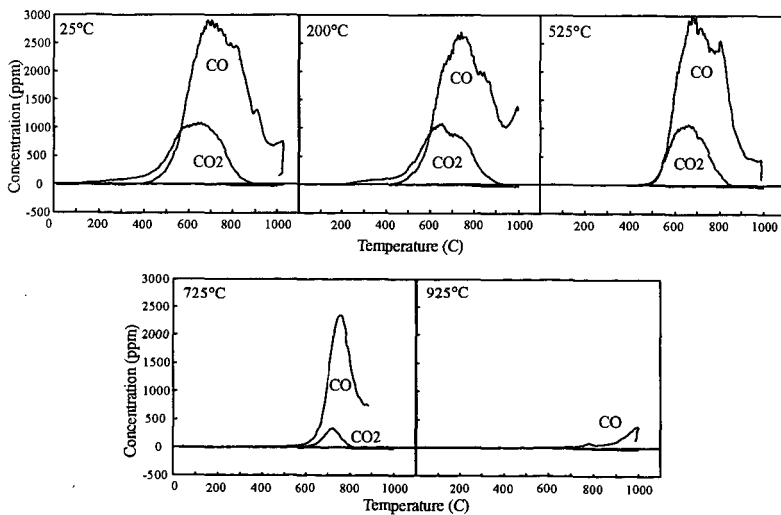


Figure 4. TPD profiles of air activated carbons heated to different temperatures.

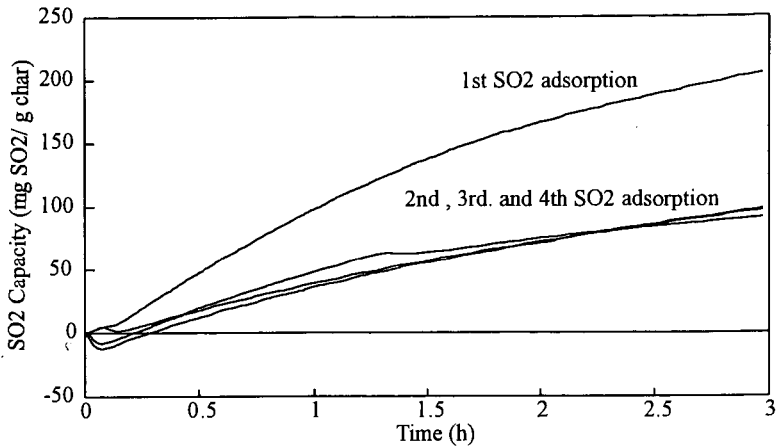


Figure 5. Thermal regeneration of nitric acid treated IBC-102 char.

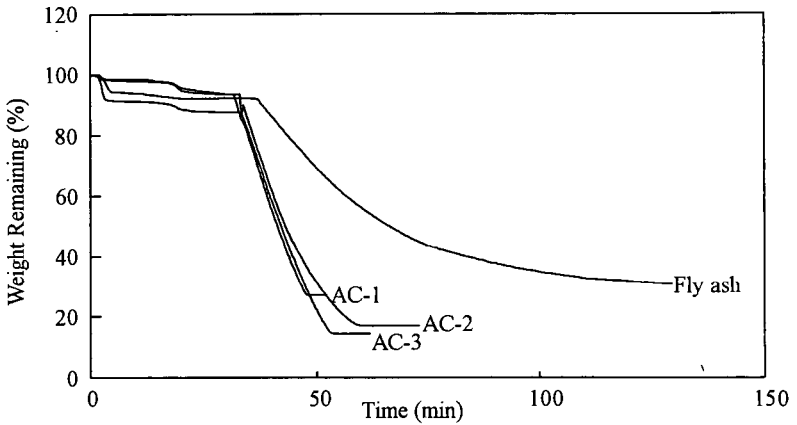


Figure 6. Proximate analysis of activated carbons.

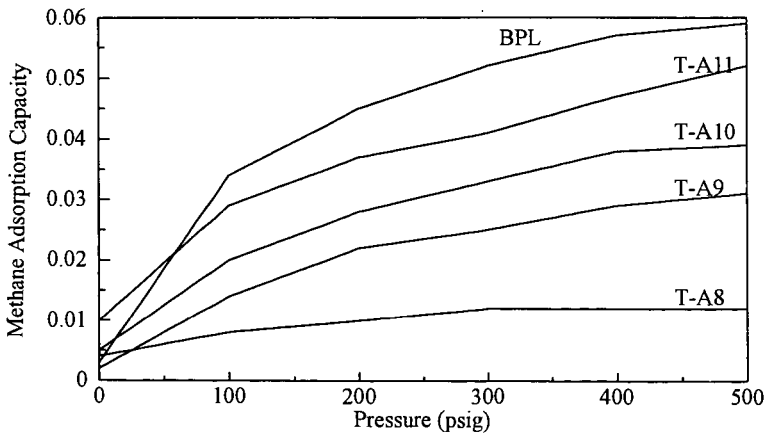


Figure 7. Methane adsorption capacity for carbons (g methane/g char at 298K).

AN EXAMINATION OF BURNING PROFILES AS A TOOL TO PREDICT THE COMBUSTION BEHAVIOR OF COALS

Sarma V. Pisupati

*Energy and Fuels Research Center
The Pennsylvania State University
C211 Coal Utilization Laboratory
University Park PA 16802*

Keywords: Burning profiles, Combustion behavior, DTGA

Introduction

Thermal analytical techniques such as thermogravimetric analyzer (TGA) have been used extensively in characterizing the thermal behavior of coals. Intrinsic reactivity (expressed as instantaneous, average and time required for 50% burnoff (τ_{50})), volatiles release profiles and burning profiles are common parameters used to predict combustion behavior in a large combustion system. The burning profile provides information on the combustion rate including intensity of reaction, heat release rate and residence time requirements for a fuel compared to those of a fuel with known combustion characteristics. The technique for determining the burning profile was developed by Babcock and Wilcox as a method for evaluating fuels to select the optimum boiler design (Wagoner and Duzy, 1967). The technique has been modified by others (Cumming, 1984; Cumming and McLaughlin, 1982; Morgan et al., 1986, 1987; Smith et al., 1981) to characterize the combustion behavior of coals in a laboratory. However, information on the validity of these profiles to industrial scale and utility boilers is scarce.

Penn State Energy and Fuels Research center evaluated combustion behavior of coals in various devices ranging from drop tube reactor to an industrial scale boiler. This paper summarizes the observations, and discusses the applicability of the data from the profiles to predict the combustion behavior.

What is a Burning Profile ?

A burning profile is a plot of the rate at which a solid fuel sample changes weight as a function of temperature, when heated at a constant rate. Cumming and McLaughlin (1982) used four characteristic temperatures to interpret a burning profile; 1) the first initiation temperature where the weight first begins to fall (T_{VM}); 2) the second initiation temperature where the rate of weight loss accelerates due to the onset of combustion of char (T_{FC}); 3) the peak temperature (PT) where the rate of weight loss is a maximum; and 4) the burnout temperature, where the weight becomes constant at the completion of burning (BT). Cumming (1984) later proposed in lieu of the above four characteristic temperatures, a weighted mean apparent activation energy value which correlated well with the PT. These characteristic temperatures as proposed by Cumming and McLaughlin (1982) have been used with minor modifications by Morgan et. al. (1986, 1987) to interpret burning profiles.

Literature Review

Wagoner and Winegartner (1973) reported a successful combustion evaluation of fluid coke from a California crude and a delayed coke derived from a Louisiana crude oil with respect to a reference combustion profile of Pocahontas coal. These profiles were reported to predict the performance of these fuels in an industrial boiler. Smith et al. (1981) later evaluated the relative ease of combustion of sixty-six coals ranging in rank from lignite to low-volatile bituminous and with low mineral matter contents. The activation energies obtained varied from 4 KJ mol⁻¹ in the high temperature, diffusion controlled zone to 290 KJ mol⁻¹ in the chemical reaction controlled, low-temperature zone.

Morgan et al. (1986) correlated the BTs from the burning profiles to predict burnout values based on a model that uses data on oxidation rates of chars prepared in an entrained flow reactor and coal properties. Nine coals were ranked based on their performance in a pilot scale pulverized coal combustor and the ranking correlated well with the characteristic temperatures from the burning profiles of the coals. Superior burnout has been reported with coals having low burnout temperatures.

Wagoner and Winegartner (1973) reported that the Pocahontas coal with a volatile matter content of 14-16.5% and a Bureau of Mines char with a 5% volatile matter should have identical combustion characteristics based on their burning profiles. But, Demeter et al. (1973) found that in a 500 lb/hr experimental coal combustor the Pocahontas coal burnt with out any auxiliary fuel or

preheat of the primary air whereas the Bureau of Mines char needed preheat or auxiliary fuel to burn successfully.

Experimental

In this study combustion behavior of coals as evaluated in a drop tube reactor, a research boiler generating 1,000 lb/h steam and a 15,000 lb/h (steam) industrial scale demonstration boiler is reported. For coals tested in these devices, burning profiles were obtained in a Perkin Elmer TGA.

The experimental variables in the TGA which were found to affect the rate of burning and hence the burning profile included heating rate, sample weight, shape and material of construction of the sample pan and the heat capacity of the pan. Although the experimental conditions originally employed by Wagoner and Duzy (1967) allow the combustion rate to be limited by the diffusion rate of oxygen, as shown by Smith et al. (1981), and the temperature of the sample may not have been representative of the temperature of the burning fuel, the burning profile data obtained in the TGA seemed to produce consistent results in the evaluation of the relative combustion performance of unknown fuels with different equipment in different laboratories.

The results during optimization of test conditions indicated a good reproducibility of characteristic temperatures ($\pm 1.8^\circ\text{C}$). The effect of heating was determined using an Upper Freeport seam coal for heating rates of 5, 10, 15, and $20^\circ\text{C min}^{-1}$ and a sample weight of 5 mg. The results are shown in Table 1. It is seen from the results that as the heating rate was increased the characteristic temperatures proportionately increased which did not change the relative ranking of a coal. At higher heating rates some low rank coals ignited and therefore, led to uncontrolled temperature of the sample. Hence, a heating rate of $10^\circ\text{C min}^{-1}$ was used in this study. The effect of sample amount was not as significant as that of heating rate and a sample size of 5 mg was used.

Table 1. Effect of Heating Rate on Characteristic Temperatures

Heating Rate	5°C/min	10°C/min	15°C/min	20°C/min
Initial Temperature (IT)	325.6	337.5	350.0	347.0
Peak Temperature (PT)	494.1	505.1	522.6	618.3
Burnout Temperature (BT)	542.0	616.0	618.3	630.0

The following characteristic temperatures as defined in earlier work (Pisupati et al., 1991 and Pisupati and Scaroni, 1993) were obtained for each sample. The Initial Temperature (IT), is defined as the temperature at which the rate of weight loss exceeded $0.1\% \text{ min}^{-1}$ after the initial moisture loss peak. The Peak Temperature (PT) is defined as the temperature at which the rate of weight loss was maximum and the Burnout Temperature (BT) is the temperature at which the rate of weight loss decreased to $1.0\% \text{ min}^{-1}$.

Results and Discussion

In an earlier study conducted in the laboratory, a set of five fresh and companion crop coals was used to investigate the influence of natural weathering (in-situ) and low-temperature oxidation on the combustion behavior of the coals. In the study a fresh coal sample was oxidized in the laboratory for 2 hours, and for 72 hours in stagnant air to oxidize the coal to a similar level to that of the naturally weathered crop coal. Combustion behavior of the suite of coals was determined in the laboratory by obtaining burning profiles and the combustion efficiency in a drop tube reactor. The characteristic temperatures were derived from the burning profiles. Figure 1 shows the profiles for the Fort Palmer fresh and crop coals. Analogous profiles were obtained for other samples. The initial negative weight change in the burning profiles is due to the loss of moisture. The second positive peak at around 300°C for the fresh coal samples is attributed to the adsorption of oxygen, and represents a weight gain of about 3%. Adsorption of oxygen by the significantly oxidized crop coals was not apparent and these coals had lower initial temperatures (approximately $20\text{--}115^\circ\text{C}$ less) than the corresponding fresh coals. This can be explained as follows. Desorption of the preoxidized oxygen in the crop coals creates unoccupied sites for further oxygen adsorption and subsequent desorption, thereby initiating significant weight loss at much lower temperatures.

For these oxidized coals, it was observed that there were two distinct peaks. The lower peak is attributed to the decomposition of the carbon-oxygen complex and to the devolatilization of the coal. The height of this peak for the crop coals was proportional to the degree of oxidation. These profiles indicated that combustion is expected to be complete for the crop coals at lower temperatures than for their companions for otherwise the same operating conditions.

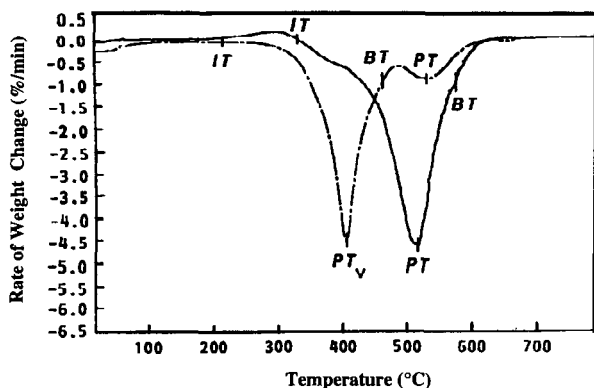


Figure 1. Burning Profiles for the Fort Palmer Fresh (—) and Crop (- -) Coals

The combustion efficiencies were conducted in a vertical, electrically heated drop tube reactor (DTR). Details of the reactor can be seen elsewhere (Pisupati and Scaroni, 1993). A relatively low combustion temperature of 1,300°C was used to accentuate the differences in combustion efficiencies. A coal feed rate of 0.33 g min⁻¹ and a total combustion air of 4 l min⁻¹, which corresponds to an excess air of 25%, was used. The results from the combustion studies in the drop tube reactor were consistent with observations from the burning profiles. Figure 2 shows a correlation between the burning profile data and the combustion efficiency determined in the DTR. The figure indicates that the lower the initial temperature, the higher the combustion efficiency.

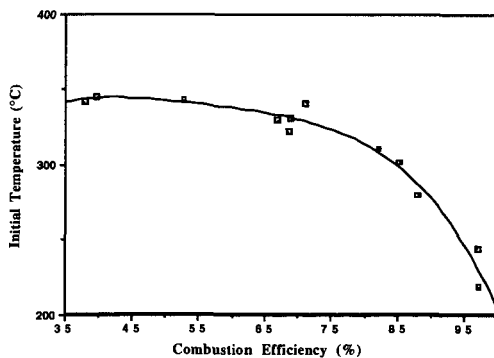


Figure 2. Initial temperatures (IT_{bp}) Obtained from Burning Profiles as a Function of Combustion Efficiency Determined in the DTR.

In another study, combustion behavior of two Pennsylvania bituminous coals, an Indonesian subbituminous coal, and blends of PA and Indonesian coals was determined in a research boiler. Burning profiles were obtained for these coals and blends in the TGA prior to the combustion tests in the boiler. The compositional analysis of the coals is provided in Table 2.

The combustion tests were conducted in a 1,000 lb steam/h water tube research boiler with a maximum thermal input of 2 million Btu/h. The boiler is a standard Cleaver Brooks "A-frame" water tube boiler. The combustion chamber is 3 ft wide, 3 ft high and 7 ft long. To promote evaporation and ignition of difficult-to-burn fuels, a ceramic quarl extends the length of the combustion chamber by two feet. The quarl and the boiler are preheated by burning natural gas prior to introducing of the test fuel until the surface temperature was approximately 900°F. The

Table 2. Proximate Analysis (wt.%, d.b.)

	100% PA	80% PA - 20% Indonesian	50%PA - 50% Indonesian	100% Indonesian	100% Upper Freeport (PA)
Volatile Matter	20.47	25.17	32.74	46.20	31.89
Fixed Carbon	67.19	64.70	60.13	52.14	61.61
Ash	12.34	10.13	7.13	1.66	6.50
Moisture (as-fired)	1.69	7.46	12.73	21.44	7.14
H.H.V.(Btu/lb as fired)	13,680	12,679	11,617	10,098	13,680

preheated quartz acts as a source of radiant heat to help support the flame. Pulverized coal was fed from a two foot diameter hopper to an eductor via a 1.5-inch diameter screw feeder. The pulverized coal was entrained by dense phase transport (≈ 1 lb of air/lb of coal) into an annular section and then through a swirler. The feed rate of pulverized coal was monitored by load cells. Slowly, the coal firing rate was increased while reducing simultaneously the natural gas rate until the desired load was obtained on coal. A thermal input of approximately 1.6 MBTU/h was held constant throughout the testing. The combustion gases, at the end of the radiant section, are split into two convective passes, one on each side of the radiant combustion chamber. The gases exiting the convective section are cooled to below 500°F in an economizer located on top of the combustion chamber and then pass into a baghouse. The products of combustion (O_2 , CO_2 , CO , NO_x and SO_2) are monitored at the economizer outlet with a series of on-line gas analyzers. The ash samples were collected and analyzed for moisture and unburnt carbon to calculate the carbon burnout using the ash tracer technique as follows:

$$\text{Combustion Efficiency (\%)} = \left[1 - \frac{A_c(100 - A_r)}{A_r(100 - A_c)} \right] \times 100$$

where, A_c = wt. percent ash in the coal, and A_r = wt. percent ash in the residue

Figure 3 shows a correlation between the Initial temperatures (from the burning profiles in a TGA) and the combustion efficiencies determined in the boiler. The plot shows a good correlation between the burning profile data and the combustion efficiencies as determined in the boiler. However, the flue gas oxygen levels were 5.5 and 5.9% for the Indonesian and PA coals, whereas for the Upper Freeport coal the boiler oxygen level was 6.5% and therefore, the combustion efficiency was slightly higher than expected from the interpolation. This underscores the importance of the operating conditions and sample characteristics.

Two bituminous coals were fired in a 15,000 lb/h industrial scale, demonstration boiler as micronized coals (80% passing through US standard 325 mesh instead of 80% passing 200 mesh). The boiler is a D-type package boiler designed for fuel oil. The boiler and auxiliaries are adapted with minor modifications to burn coal and coal-water slurry fuels. Details of the boiler can be found elsewhere (Pisupati et al., 1993). The combustion efficiency data obtained in the demonstration boiler is shown on Figure 3 as open diamonds. The combustion efficiency obtained for both coals was varying from 90 to 95% depending on the operating conditions such as excess air and fuel firing rate etc. The data plotted were for the conditions when the boiler oxygen was 3.2% and the firing rate was 14.8 MMBtu/h for both coals. The initial, peak, and the burnout temperatures for the Brookville bituminous coal were 310.8, 492.4 and 555°C, respectively. The initial, peak, and the burnout temperatures for the Kentucky bituminous coal were 313.8, 508.8 and 577.5°C, respectively. Very close initial temperatures reflected in close combustion efficiencies in the boiler under identical conditions. This also shows that the initial temperatures correlate well with the combustion efficiency. This probably is due to the earlier decomposition and thereby causing physical and chemical structural changes of the residual char earlier and hence a change in the reactivity.

Combustion Studies of blends of coals

One of the puzzling questions has been whether the characteristic temperatures obtained from burning profile hold good for blends of coals. Cumming (1989) has reported that the burning profile of a blend of coals of different rank (bituminous and anthracite) indicates that the fuels burn without interaction. Similar observations were made at this laboratory with bituminous and anthracite blends. However, blends of bituminous and lower rank coals indicated a linear correlation. Artos and Scaroni (1993) have shown that when a bituminous coal is blended with a subbituminous coal, the initial temperatures (IT) were proportionately lower with increasing

percent of a subbituminous coal. The study also showed a linear increase in the combustion efficiency in the DTR with the addition of the subbituminous coal.

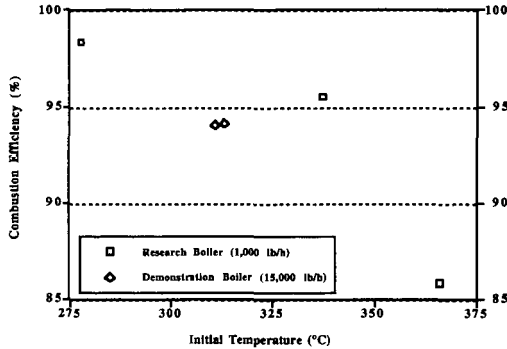


Figure 3. Correlation between the Initial Temperatures and the Combustion Efficiencies obtained in the 1,000 lb/h Research Boiler and in the 15,000 lb/h Demonstration Boiler.

In this study, an Indonesian subbituminous coal was blended with a Pennsylvania bituminous coal and the burning profiles and combustion behavior was determined in the TGA and the Research Boiler, respectively. The burning profiles are shown in Figure 4 for the Indonesian coal and blends with PA coal in various proportions. It can be clearly seen that there is a clear progressive increase in the characteristic temperatures with the increase in the proportion of the PA coal. This study confirms the observations of Artos and Scaroni (1993). The difference between the IT and the BT for the blends is higher indicating the initial decomposition starts at a lower temperature corresponding that of the lower rank coal in the blend and the combustion is not complete until the component with lower reactivity is burned. This suggests that there possibly is no influence of one coal on the other in a TGA. However, since there is a good correlation between the initial temperature and the combustion efficiency it may be concluded that blending coal which decomposes at lower temperature with less reactive coal, the former influences the combustion behavior of the latter in a boiler with self sustaining flame.

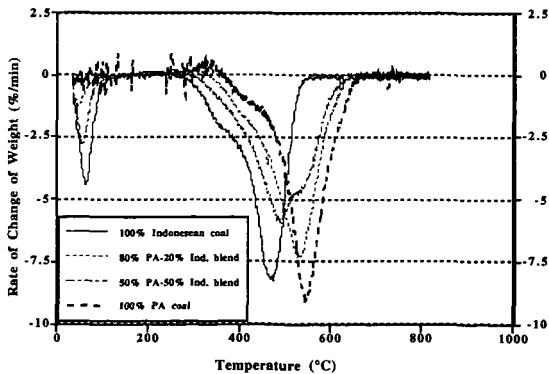


Figure 4. Burning Profiles of Pennsylvania Bituminous Coal Blends

Figure 5 shows a correlation between the initial temperature and the combustion efficiency obtained in the 1,000 lb/h research boiler for the coals and coal blends.

Summary

Burning profiles of a suite of coals ranging from fresh coals to severely weathered coals, and subbituminous coals and bituminous coals were obtained. Combustion efficiencies were also determined in a Drop tube reactor, 1,000 lb/h research boiler, and a 15,000 lb/h industrial scale demonstration boiler. A good correlation was obtained between the initial temperature and the

combustion efficiency obtained under identical conditions was observed. A burning profile appears to be a good tool for evaluation of the relative combustion characteristics of fuels at a laboratory scale, when it is difficult, or there is not enough fuel, to test fire in a large installation.

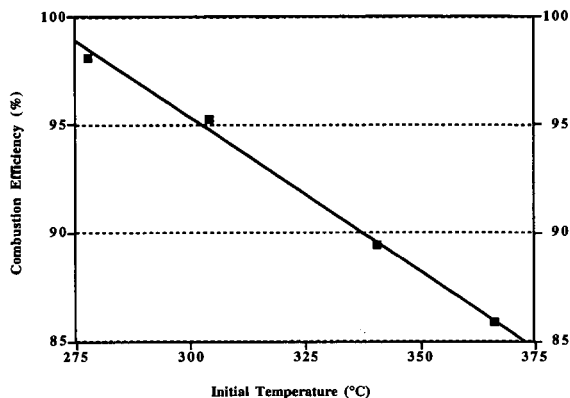


Figure 5. Correlation Between the Initial Temperatures and the Combustion Efficiencies Obtained in the Research Boiler

Because various investigators employed experimental conditions that were different from those originally proposed by Wagoner and Winegartner (1973), yet still obtained reproducible and interpretable results, it can be concluded that any laboratory using the technique of determining burning profiles to characterize the combustion behavior of coals can use their own reference standard conditions as long as all the samples (both the reference and unknown fuel) are tested under those standard conditions to obtain interpretable and meaningful data. However, it is not yet clear whether these profiles could predict the combustion efficiency of coal-water slurry fuels. The data generated under identical conditions may predict the combustion behavior of an unknown fuel under similar conditions. Those conditions may not be the optimum conditions for the fuel.

Acknowledgments

The author thanks the staff of the Energy and Fuels Research Center for generating some of the data used in this paper, and Bruce Miller for sharing some of the Demonstration Boiler data.

References

- Artos, V. and Scaroni, A. W., (1993) *Fuel*, 72, 927.
- Cumming, J. W. and Mc Laughlin, J. (1982) *Thermochemica Acta*, 57, 253.
- Cumming, J. W. (1984) *Fuel*, 63, 1436.
- Cumming, J. W. *Thermochemica Acta*, 1989, 155, 151
- Demeter, J. J., McCann, C. R. and Bienstock, D. (1973) *ASME Paper No 73-WA/Fu2*, presented at the Winter Annual Meeting, ASME, New Orleans, LA.
- Morgan, P. A., Robertson, S. D. and Unsworth, J. F., *Fuel*, 1986, 65, 1546.
- Morgan, P. A., Robertson, S. D. and Unsworth, J. F., *Fuel*, 1987, 66, 210.
- Pisupati, S. V., Scaroni, A. W. and Stoessner, R. (1991) *Fuel Processing Tech.*, 72, 779.
- Pisupati, S. V., Britton, S. A., Miller, B. G. and Scaroni, A. W. (1993) *Proceedings of the 18th International Technical Conference on Coal Utilization and Fuel Systems*, Coal and Slurry Technology Association, April 26-29, Clearwater, Florida, FL, pp. 349 - 360.
- Pisupati, S. V. and Scaroni, A. W., (1993) *Fuel*, 72, 779.
- Smith, S. E., Neavel, R. C., Hippo, E. J. and Miller, R. N. (1981) *Fuel*, 60, 462.
- Wagoner, C.L. and Duzy, A. F., ASME Paper 67-WA/FU-4, Winter Annual Meeting and Energy Systems Exposition, American Society of Mechanical Engineers, Pittsburgh, 1967.
- Wagoner, C. L. and Winegartner, E. C. *Trans ASME Ser. A, J. Eng. Power*, 1973, 95, 119.

EFFECT OF PRESSURE ON PREPARATION OF SO₂ SORBENT FROM LEONARDITE AND ON SO₂ ADSORPTION BY LIMESTONE AND DOLOMITE AS DETERMINED FROM PRESSURE THERMOGRAVIMETRIC ANALYSIS

R.C. Timpe, R.W. Kulas, and B.C. Young
University of North Dakota Energy and Environmental Research Center
15 North 23rd Street
Grand Forks, North Dakota 58203

Keywords: Pressure TGA, SO₂ adsorption, limestone

ABSTRACT

Control of SO₂ with limestone or dolomite is state-of-the-art at the present time, but activated carbon in the form of low-rank coal char also has some promise. A process for production of the sorbent includes selection of temperature regime, pressure, activation gas, residence time, and additive. The effect of pressure on the behavior of sorbent during SO₂ removal from flue gas or during production of sorbent carbon is the parameter least found in the literature. Pressure thermogravimetric analysis (pTGA) provides a simple means of studying this effect.

In this study, a fully calcined and a partially calcined dolomite and limestone were tested for SO₂ sorbent characteristics under pTGA at 840°C at 160 psig. The stones were characterized by capacity and rate of sorption of SO₂.

A leonardite was carbonized at 480°C and activated at 800°C under nitrogen at ambient, 150, 300, and 450 psig. Each char was then exposed to a flowing gas mixture containing argon and SO₂. The char produced at lower pressures adsorbed more SO₂ than those produced at successively higher pressures as determined by TGA and confirmed by American Society for Testing and Materials (ASTM) total sulfur measurements.

INTRODUCTION

Combustion of coal provided approximately 55% of the available electric power in the United States in 1993 with the burning of approximately 814,000 tons (1) of coal. As the demand for electricity increases, the demand for coal will also increase, resulting in accelerated depletion of our coal supplies. At present, the quality of the coal mined to produce this electricity, in terms of pollutants such as sulfur, nitrogen, and heavy metals liberated to the environment, is relatively clean compared to much of the remaining minable coal reserves. Government, utilities, and researchers have been aware of the potential environmental consequences of burning "dirtier" coal for more than three decades and have been attempting to deal with the problem through application of known technology and development of newer, more efficient, less costly methods of emission control. Both precombustion and postcombustion methods have been attempted as means to remove potential pollutants from coal before they enter the environment. Industrially, precombustion cleaning of bituminous coal by physical means, e.g., float-sink, froth floatation, magnetic separation, has met with mild success, while cleaning by chemical means, e.g., molten caustic leaching, has been generally discounted as being too costly. Similarly, physical or chemical cleaning of low-rank coal results in excessive cost for the product.

For lack of economically and technically feasible precombustion cleaning methods, most environmental protection from the emissions from coal combustion is currently done by cleaning stack gas from the utility. Sorbents such as limestone (CaCO₃) and dolomite (CaCO₃-MgCO₃) are commonly used for scrubbing SO₂ from the gas. Well-known processes such as those of Pure Air's Advanced Scrubber, Chiyoda's CT-121 Scrubber, S-H-U wet limestone scrubber, LIFAC sorbent injection system, Bechtel's Confined Zone Dispersion Process, AirPol Gas Suspension Adsorption Process, the Babcock and WILCOX LIMB process, and Consolidation Coal's Coolside Process all make use of limestone in either the raw or calcined form as the sorbent for SO₂ emissions (2). Factors concerning the cleaning efficiency of the stones include partial pressure of SO₂, contact time, degree of calcination, surface area, temperature, and surface incidence of inert material. Each of these factors can be studied using thermal analysis techniques. Pressure thermogravimetric analysis is particularly useful for these studies since it allows the determination of the effect of all of these factors.

Similarly, preparation of sorbents such as activated carbon is affected by each of the properties above.

EXPERIMENTAL

Prior to testing, the dolomite and limestone samples were crushed in a hammer mill and then further reduced in size on a Braun mill. The samples were reconstituted by recombining sieve fractions and mixing thoroughly.

Two tests were performed on each of the two CaCO_3 -based samples using the pressure thermogravimetric analyzer (pTGA). The test methods used to determine SO_2 uptake from a mixed gas stream by each sample were as follows:

The samples were crushed in mortar and pestle to pass 20-mesh screen ($0.84 \text{ mm} = 840 \mu\text{m}$). The samples were classified into four size fractions by sieving. Class sizes were 250–840 μm , 150–250 μm , 75–150 μm and $< 75 \mu\text{m}$. To obtain test results which would represent sorption results characteristic of the bulk material, size fractions were recombined prior to pTGA testing.

Method 1. Approximately 20 mg of crushed reconstituted sample was loaded onto the sample pan of an SRE 1990/600 pTGA. The cover was replaced, and the sample chamber was pressurized to 160 psig with N_2 and the gas flow adjusted to nominally 100 mL/min. Heatup was approximately $100^\circ\text{C}/\text{min}$ to 840°C , and the sample was calcined at that temperature for up to 150 minutes. Nitrogen flow was then replaced by a synthetic sulfated combustion gas mixture containing 13% CO_2 , 3.5% O_2 , and 0.25% SO_2 (balance N_2), and flow was continued for at least 60 minutes. The tests were terminated and the system cooled down under flowing N_2 .

Method 2. Approximately 20 mg of crushed reconstituted sample was loaded onto the sample pan of the SRE 1990/600 pTGA. The cover was replaced, and the sample chamber was pressurized to 160 psig with a gas mixture containing 13% CO_2 and 3.5% O_2 (balance N_2) and the gas flow adjusted to nominally 100 mL/min. Heatup was approximately $100^\circ\text{C}/\text{min}$ to 840°C , and the sample was held at that temperature for up to 90 minutes (for half-calcination). The synthetic sulfated combustion gas mixture containing 13% CO_2 , 3.5% O_2 , and 0.25% SO_2 (balance N_2) was then introduced, and the tests were completed as in Method 1.

The effect of pressure on the sorption capacity of activated char prepared from a North Dakota leonardite was studied. The sample was carbonized at 480°C under N_2 at each of four pressures: 450 psig, 300 psig, 150 psig, and ambient pressure. Each sample was activated under N_2 at 800°C at its respective pressure. The resulting activated char was tested for SO_2 adsorption capacity. Each sample analyzed for SO_2 capacity was then analyzed for total sulfur content.

RESULTS AND DISCUSSION

The results of sieving the crushed dolomite and limestone samples are shown in Table 1. Over 75% of the limestone consisted of particles less than 75 microns in size compared with ~57% of the dolomite under the same crushing conditions.

From the results of the sieve fractions, it can be assumed that the limestone would have greater surface area, although not measured in this study, than that of the dolomite since it has a much larger fines fraction. Therefore, the former should have the greater capacity for SO_2 adsorption than the latter. However, from the results of SO_2 uptake in Table 2, it appears that that is not true. In addition, the rate of uptake of SO_2 should also be more rapid on that with the larger surface area, but instead the rates are nearly the same for the fully calcined samples and are identical for the half-calcined samples. If the difference between rates and capacities of the two samples were consistent, differential decrepitation of the materials might explain the apparent contradiction. However, this does not appear to be the case since the rates of uptake are the same while the capacities differ. The presence of the MgCO_3 in the dolomite may be the best explanation for the higher sorptive capacity of the dolomite. Assuming limestone to be CaCO_3 and dolomite to be $\text{CaCO}_3\text{-MgCO}_3$, there are more metal ions per unit mass in dolomite than in limestone resulting in the potential for more available SO_2 receptor sites. The presence of the MgCO_3 may catalyze the calcination and thus activate the surface more effectively. Additional data are needed to confirm this as a reason for the observed difference in SO_2 sorption between the dolomite and the limestone samples.

The SO_2 adsorbed on the activated char shown in Table 3 indicates that preparation of activated char from leonardite under pressure results in decreased activity toward SO_2 . This is supported by the total sulfur measurements made on the residual activated char after it has adsorbed the SO_2 . The decrease in SO_2 adsorption results from the loss of active sites on the char. The apparent pressure dependence may be due to heavy tar formation at the openings of pores resulting in a loss in total surface area and, consequently, the loss of active sites for SO_2 sorption.

CONCLUSIONS

- Both the fully calcined and half calcined dolomites tested were better SO₂ sorbers than the corresponding calcined forms of the limestone tested.
- Although their capacities for SO₂ differed, the rates at which the dolomite and limestone adsorbed were similar for the fully calcined forms and identical for the half-calcined forms.
- Crushing the stones resulted in a significantly different distribution of size fractions.
- Activated char produced from North Dakota Leonardite under increased pressure had lower activity toward SO₂ than that produced at ambient pressure, probably because of pore plugging by tar unable to boil away.

REFERENCES

1. *Keystone Coal Industry Manual*; Mining Information Services, Robert Dimond, Publishing Director, 1995, p S-2.
2. U.S. Department of Energy (DOE). "Clean Coal Technology: The Investment Pays Off," Report No. DOE/FE-0291 (Revised), July 1995.

ACKNOWLEDGMENTS

The authors wish to thank the U.S. DOE and the Morgantown Energy Technology Center for the support to carry out this work. This work was a small part of a much larger project.

TABLE 1
Sieve Fractions from Limestones and Dolomite

	Particle Size, μm				
	250-840	150-250	125-150	75-125	<75
Dolomite	0.1	0.7	10.3	31.4	56.8
Limestone	0.1	0.4	3.3	19.5	75.5

TABLE 2
Comparison of Fully Calcined and Half-Calcined Limestone
and Dolomite Toward SO₂ Adsorption

Abbr.	Calcination wt%	Ads. Total wt%	Ads. CO ₂ wt%	Ads. SO ₂ wt%	SO ₂ Ads. CO ₂ Eq. wt%	Ads. SO ₂ %/min.
Fully Calc.						
Doio.	-40.9	34.4	20.4	14.0	15.0	0.22
Lime	-32.6	39.5	31.0	8.5	8.0	0.19
Half-Calc.						
Doio.	-8.3	11.6	--	11.6	14.2	0.16
Lime	2.2	10.5	--	10.5	10.3	0.16

TABLE 3
Effect of Pressure on SO₂ Sorption by Activated Char
Prepared from North Dakota Lignite

pTGA, psig	SO ₂ Adsorbed on Activated Char, wt%	Total S in Spent Char, wt%
450	7.4	4.8
300	7.3	4.7
150	8.1	5.2
Ambient	8.7	6.0

RATES OF PYROLYSIS AND COMBUSTION OF BARK BY THERMOGRAVIMETRIC ANALYSIS

Wei-Yin Chen

Department of Chemical Engineering, Anderson Hall
University of Mississippi, University, MS 38677

Wood supplies approximately 3 percent of the U.S. energy consumption (Schreuder and Tillman, 1980). Bark represents about 10-15% of the weight of the trunk cut in the forest. Wood combustion phenomena has been extensively reviewed (e.g., Tillman *et al.*, 1981). Recent technological development is reflected in an article by Barsin *et al.* (1988), and a report published by the Electric Power Research Institute (Johnston *et al.*, 1993). Fundamental understanding of wood pyrolysis has also grown substantially in the last two decades. Shafizadeh (1982) reviewed the wood pyrolysis and combustion kinetics based on weight loss profiles. About the same time, Hajaligol *et al.* (1982) reported the kinetics of the individual product species for rapid pyrolysis of cellulose. Boroson *et al.* (1989) observed that heterogeneous cracking of wood pyrolysis tars takes place over flesh wood char surface. Pyrolysis kinetics of different lignocellulosic materials have been investigated by Bilbao *et al.* (1989, 1990). Heat and mass transfer limitations are inevitable during burning of large particles, and have been the target of a number of modeling efforts (e.g., Kanury, 1972; Maa and Bailie, 1973; Chan *et al.*, 1985; Ragland *et al.*, 1988; Bilbao *et al.*, 1993).

Due to its lower physical strength and less uniform structure than interior wood, bark is usually burned along with wood waste as a fuel, particularly by sawmills and pulp mills. Bark has the heating value of 8,000 to 10,000 Btu/lb, which is higher than that of wood (Wegner, 1991). The objective of this paper is to experimentally acquire information about the bark kinetics during pyrolysis and combustion conditions. A kinetic model is also developed for the comparison.

EXPERIMENTAL

Since weight loss is used as a measure of bark conversion in the present study, the design of experiments has some salient features of a thermal balance, Figure 1. The center piece of the reactor is a cylindrical sample basket of dimension 1 in \times 2 in in length, which is made of 40 mesh stainless steel screen. The reactor vessel is an alumina tube with inside diameter of 2.5 in, which is heated to the desired temperature by a Thermcraft furnace model 23-18-1ZH with dimensions 3 in \times 18 in long. The reactor is equipped with a distributor at about 6 in from the bottom end of the furnace, and a fluidized sand bed serving as a heat source of the gas stream.

Samples of pine bark, cut into 10mm spheres, were dried at 105°C for 24 hours before the experiment. Nitrogen and air were used as the fluidizing gas during pyrolysis and combustion, respectively. To begin a run, the sample basket containing a single particle of bark is lowering into the preheated fluidized sand bed. After a predetermined period of time, the basket was raised to a water-jacketed, reversed-nitrogen flow section for rapid quenching. Sample weight before and after the experiment were recorded. The ultimate analysis of the bark sample is shown in Table 1.

Experiments were conducted at sand temperatures 750, 800 and 850°C for pyrolysis; and 500, 600, 700 and 800°C for combustion. To achieve these temperatures, the furnace was set 90°C higher than the desired sand temperature. The gas flowrate, 15,000 ml/min, was chosen to ensure that it was three times higher than the theoretical air required at highest burning rate.

KINETIC MODEL

The bark combustion model under consideration contains three major components: bark pyrolysis, char combustion, and heat transfer.

During pyrolysis, the organic portion of the bark converts to volatiles and solid char, i.e.,



Here, the fraction of weight loss, V , is used as an index of bark conversion. The volatile compounds include the gaseous species and tarry species disengaged from the char. Similar to a number of coal pyrolysis studies (e.g., Howard, 1981), bark pyrolysis is treated as a first order reaction in the following form

$$\frac{dV}{dt} = k_1(V_\infty - V) \quad (2)$$

where V_∞ is the final volatile yield as time approaches infinity. The pyrolysis rate constant k_1 is assumed to follow the Arrhenius law

$$k_1 = k_{10} \exp\left(-\frac{E_1}{RT}\right) \quad (3)$$

where T_p is particle temperature, and E_1 is the pyrolysis activation energy.

Similar to coal pyrolysis (Howard, 1988), we observed temperature dependence of V_w during regression. Niksa (1988) proposed that phase equilibrium determines partitioning of tar in the gas and condensed phase, and the final volatile yield in the gas phase, V_w , depends on temperature as follows:

$$V_w(T_p) = V_{10} \theta^{\frac{E_3}{T_p}} \quad (4)$$

where V_{10} and E_3 are adjustable parameters.

In the presence of oxygen, oxidation of the organics in the char contributes to additional weight loss



Assuming char combustion is first order with respect to oxygen concentration and the weight of char, we obtain

$$\frac{dW}{dt} = -k_1(V_w - V) - k_2'W(\text{O}_2) \quad (6)$$

Since oxygen was continuously fed into the combustor at a rate four times that required for burning the volatile carbon, oxygen concentration is assumed to be constant during the combustion. Thus, we can combine k_2' and the oxygen concentration as a new constant k_2 and Eq. 6 becomes

$$\frac{dW}{dt} = -k_1(V_w - V) - k_2W \quad (7)$$

Assuming that the combustion rate constant, k_2 , follows the Arrhenius law,

$$k_2 = k_{20} \theta^{\frac{E_2}{RT_p}} \quad (8)$$

Mass transfer limitations, such as oxygen diffusion into the char, are usually involved in combustion of particles of 1 cm in diameter, thus the rate measured based on Eqs. 7 and 8 should be considered effective or global reaction rate (Carberry, 1976).

Combustion of volatiles generated in bark pyrolysis will also take place outside bark particles at the same time,



However, since this reaction does not contribute to the weight loss and it is not included in the present model.

Weight loss measurements indicate that devolatilization of bark particles takes place almost instantaneously at 800°C. However, at 500°C, devolatilization does not start until at about 20 s. These observations imply that heat transfer is a limiting factor in the range of our investigation, and an equation governing the temperature variation of the particle is required. Based on the published value of thermal conductivity of cellulosic materials, 0.12 W.m⁻¹.K⁻¹ (Reed, 1983), the estimated Nusselt number of heat transfer for a bark particle gives values in the range 0.8 to 1.8. Since this is not a large number, we assume that the temperature is uniform inside a bark particle during pyrolysis and combustion. It should be mentioned that there is evidently a radial temperature profile and diffusion limitations of volatiles inside the wood particles with diameter 56 mm (Bilbao *et al.*, 1993). Energy balance yields

$$\rho_p V_p C_p \frac{dT}{dt} = Ah(T - T_p) + \epsilon A \sigma (T_w^4 - T_p^4) + \Delta H_p r_p W_{p0} + \Delta H_c r_o W_{p0} \quad (10)$$

Equation 10 states that temperature rise of a bark particle is governed by convective heat transfer, radiative heat transfer, heat of pyrolysis, and heat of combustion. We assume that the heat of volatiles combustion is carried away by gas, and is not included in this equation. Our calculation reveals that convection contributes to less than 20% of radiative heat transfer. Furthermore, experiments indicate that char combustion is much slower than pyrolysis, and char combustion does not contribute significant weight loss and temperature rise during the heat-up period. Thus, the first and the fourth terms on the right hand side of Eq. 10 are eliminated in the regression process, i.e.,

$$\rho_p V_p C_p \frac{dT_p}{dt} - \epsilon A \sigma (T_w^4 - T_p^4) + \Delta H_p r_p W_{p0} \quad (11)$$

Again, due to the fact that significant char combustion does not take place during the heat-up period, the bark particle external surface area, A , in Eq. 11 is assumed to be a constant during the combustion process. The published value for heat capacity of bark, C_p , is 0.327 cal/g.°C (Reed, 1983), and the nominal density of bark particle, ρ_p , was experimentally determined, 0.42 kg/dm³.

The model discussed above has three dynamic equations, Eqs. 2, 7 and 11. Equations 3, 4 and 8 are also required for the integration of the three dynamic equations. The seven parameters, k_{10} , E_1 , k_{20} , E_2 , V_{10} , E_3 and ΔH_p are recovered from regression through comparison of the model with the data obtained from pyrolysis and combustion experiments. The optimization has been achieved by resorting to BCONF/DBCONF, a subroutine in the International Mathematical and Statistical Library which minimizes a multi-variable function subject to bounds on the variables using a quasi-Newton method and a finite-difference gradient. The integration of the large sets of differential equations has been carried out on a Cray X-MP2/216 supercomputer with LSODE, a software package based on Gear's method for solving stiff differential equations (Hindmarsh, 1982).

RESULTS AND DISCUSSION

The optimization procedure resulted in the following values of the seven system parameters:

$$\begin{aligned} k_{10} &= 1,557 \text{ s}^{-1} & E_1 &= 37,333 \text{ J/mol} \\ k_{20} &= 0.295 \text{ s}^{-1} & E_2 &= 22,028 \text{ J/mol} \\ V_{10} &= 0.862 & E_3 &= 228 \text{ K} \\ \Delta H_p &= 434 \text{ J/g of dry bark} \end{aligned}$$

The value of final volatile yield, V_{10} , is in good accord with the reported volatile matter for cedar bark, 0.869, moisture and ash free basis (Tillman *et al.*, 1981). The heat of pyrolysis, ΔH_p , is somewhat higher than that reported for cellulose, 274 J/g (Bilbao *et al.*, 1993), and that for cottonwood, 268 J/g (Pan, 1993). This discrepancy may be caused by the high heating rate, or the assumptions used in the present study. It has been demonstrated that high temperatures favor decomposition to volatiles, which require heat, while low temperatures favor char formation, which release heat (Shafizadeh and DeGroot, 1976). Bilbao *et al.* and Pan obtained their values through DSC analysis with a heating rate below 20 °C/min, and the heating rate in the present study is above 400°C/min. The activation energy of bark pyrolysis is consistent with those found by other researchers: 24,208 J/mol between 290 and 400°C (Bilbao *et al.*, 1993) and 52,900 J/mol above 325°C for pine wood (Bilbao *et al.*, 1991).

The experimental data in general are in good accord with the predictions of the model. Only part of our results are presented below. Figures 2 presents the comparisons of pyrolysis and combustion results from experiments at the sand temperatures 800°C. The predicted temperature profiles of bark particle during heating are also included in this Figure. Slower rise in temperature between 170 to 230°C indicates endothermic reaction of pyrolysis in this temperature range, which is somewhat narrower than that reported by Wegner, 100 to 450°C (1991). Note that char combustion does not contribute significant weight loss in the first 20s, while pyrolysis is essentially complete during this time. This observation is consistent with the assumption that heat of combustion of char does not play an important role during the heat-up period.

Figures 3 demonstrates the weight loss profiles during combustion at 600°C sand temperature. The data generally conform well with the model predictions. However, at 500°C, the pyrolysis is slower in the experiment than predicted by the model. This illustrates the limitations of the present phenomenological model. Bark is a complex material and its decomposition products contain numerous compounds, while the present model uses weight loss as an index of reaction conversion. The assumptions associated with heat transfer can also cause discrepancies. Furthermore, from thermodynamic principles and collision theory, both the frequency factor and the activation energy can be functions of temperature (Zellner, 1984).

Fragmentation of bark particles and volatiles ignition during combustion may be important to the future developments of phenomenological model. We observed fragmentation of bark particles at temperatures 600°C and above. Each bark particle breaks into 2 to 6 pieces along its geological planes after 15 to 25 seconds in the furnace, and higher temperatures cause more vigorous fragmentation. Fragmentation results in increase in larger surface areas and therefore reduced transfer limitations. Furnace temperature also affects ignition of volatiles. At 800 and 700°C, flame starts at about 2 s after the bark particle is lowered into the furnace. At 600°C, flame was observed at about 5s. At 500°C, ignition was delayed to 19s.

CONCLUSIONS

Bark from pine has been investigated in both pyrolysis and combustion environments. The experimental data are in good accord with a kinetic model which includes three dynamic equations: bark pyrolysis, char combustion, and heat transfer to the bark particle. Three of the seven parameters, final volatile yield, heat of pyrolysis, and activation energy of bark pyrolysis, are in good agreement with published values for similar species. These results suggest that the model is capable

of depicting the weight loss profiles in a furnace with a temperature in the range 500 to 850 °C.

Experiments also reveal that volatiles evolution and char combustion take place during two different periods of time during the thermal process. Furthermore, fragmentation of bark particles was also observed at temperatures above 600°C.

LITERATURE CITED

- Barsin, J.A., J. Pottera, and G. Stewart, "Conversion of A Recovery Boiler to Bark Burning," *Tappi Journal*, **71**, 107-113 (1988).
- Bilbao, R., A. Millera, and J. Arauzo, "Thermal Decomposition of Lignocellulosic Materials: Influence of the Chemical Composition," *Thermochemica*, **143**, 149-159 (1989).
- Bilbao, R., A. Millera, and J. Arauzo, "Kinetics of Weight Loss by Thermal Decomposition of Different Lignocellulosic Materials: Relation between the Results Obtained from Isothermal and Dynamic Experiments," *Thermochemica*, **165**, 103-112 (1990).
- Bilbao, R., M.B. Murillo, and A. Millera, "Thermal Decomposition of Lignocellulosic Materials: Comparison of the Results Obtained in Different Experimental Systems," *Thermochemica Acta*, **190**, 163-173 (1991).
- Bilbao, R., A. Millera, and M.B. Murillo, "Temperature Profiles and Weight Loss in the Thermal Decomposition of Large Spherical Wood Particles," *Ind. Eng. Chem. Res.*, **32**(9), 1811-1817 (1993).
- Bird, R.B., W.E. Stewart, and E.N. Lightfoot, "Transport Phenomena," John Wiley & Sons, New York, P.409, 1960.
- Boroson, M.L., J.B. Howard, J.P. Longwell, and W.A. Peters, "Heterogeneous Cracking of Wood Pyrolysis Tars over Fresh Wood Char Surfaces," *Energy & Fuels*, **3**, 735-740 (1989).
- Carberry, J.J., "Chemical and Catalytic Reaction Engineering," McGraw-Hill, New York, p.205, 1976.
- Chan, W.C.R., M. Kelbon, and B. Krieger, "Modeling and Experimental Verification of Physical and Chemical Processes during Pyrolysis of a Large Biomass Particle," *Fuel*, **64**, 1505-1513 (1985).
- Gray, R.L., and R.A. Parham, "A Good Look at Wood's Structure," *Chemtech*, **4**, 232-238 (1982).
- Hajaligol, M.R., J.B. Howard, J.P. Longwell, and W.A. Peter, "Product Compositions and Kinetics for Rapid Pyrolysis of Cellulose," *Ind. Eng. Chem. Proc. Des. Dev.*, **21**, 457-465 (1982).
- Hindmarsh, A.C., "ODEPACK, A Systematized Collection of ODE Solvers," Report UCRL-88007, Lawrence Livermore National Laboratory, August (1982).
- Howard, J.B., "Fundamentals of Coal Pyrolysis and Hydrolysis" in "Chemistry of Coal Utilization," second supplementary volume, edited by Elliott, M. A., Wiley Interscience, New York, pp.688-785, 1981.
- Johnston, S.A., J.G. Cleland, R.S. Truesdale, T.C. Clark, W.D. Stencil, L.D. Ostlie, and B. Weigel, "Whole Tree Energy™ Design - Volume 1: Engineering and Economic Evaluation," Final Report submitted to the Electric Power Research Institute, Report TR-101564 under Project 2612-15, Palo Alto, CA, December, 1993.
- Kanury, A.M. "Rate of Burning Wood: A Simple Thermal Model," *Combustion Science and Technology*, **5**, 135-146 (1972).
- Maa, P.S., and R.C. Bailie, "Influence of Particle Sizes and Environmental Conditions on High Temperature Pyrolysis of Cellulosic Material - I. Theoretical," *Combustion Science and Technology*, **7**, 257-269 (1973).
- Niksa, S., "Rapid Coal Devolatilization as an Equilibrium Flash Distillation," *AIChE J.*, **34**, 790-802 (1988).
- Pan, W.P., Western Kentucky University, Personal Communication, September 29, 1993.
- Ragland, K.W., J.C. Boerger, and A.J. Baker, "A Model of Chunkwood Combustion," *Forest Products Journal*, **38**(2), 27-32 (1988).
- Reed, R.J., North American Combustion Handbook, second edition, North American Mfg. Co, Cleveland, Ohio, 1983.
- Schreuder, G.F., and D.A. Tillman, "Wood Fuels Consumption Methodology and 1978 Results," in "Progress in Biomass Conversion," Vol. 2, K.V. Sarkanen and D.A. Tillman eds., pp.60-88, Academic Press, New York, 1980.
- Shafizadeh, F., "Introduction to Pyrolysis of Biomass," *Journal of Analytical and Applied Pyrolysis*, **3**, 283-305, 1982.
- Shafizadeh, F., and W.F. Degrade, "Thermal Analysis of Forest Fuels," in "Fuels and Energy from Renewable Resources," D.A. Tillman *et al.* ed., pp.93-114, 1977.
- Tillman, D.A., A.J. Rossi, and W.D. Kitto, "Wood Combustion - Principles, Processes, and Economics," Academic Press, New York, 1981.
- Wegner, T.H., "Wood" in "Encyclopedia of Polymer Science and Technology," edited by J. I. Kroschwitz, second edition, John Wiley & Sons, New York, **17**, pp. 843-887, 1991.
- Zellner, R., "Bimolecular Reaction Rate Coefficients," in "Combustion Chemistry," W.C. Gardiner ed., Springer-Verlag, New York, pp.129-134, 1984.

TABLE 1. Ultimate Analysis of Bark (Report by Huffman Laboratory)

dry-loss, %	4.92
ash, %	4.08
carbon, %	51.20
hydrogen, %	5.66
oxygen, %	40.67
nitrogen, %	0.21
sulphur, %	0.02

The sample was ground prior to analysis. Moisture was determined by loss on drying in air at 105°C to a constant weight and is on an as received basis. All other results are on a dried sample basis by weight.

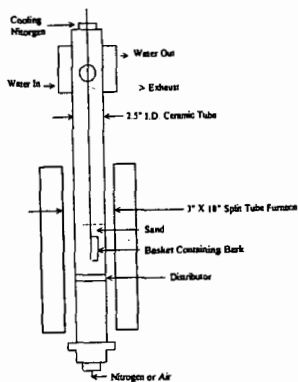


Figure 1. Experimental apparatus

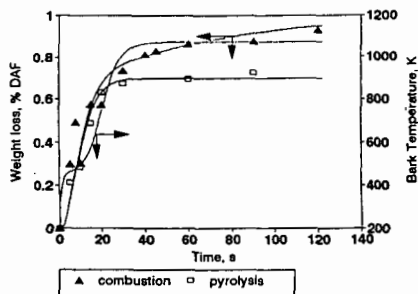


Figure 2. Experimentally observed and model predicted weight loss of bark during pyrolysis at 800°C sand temperature. Predicted bark particle temperature is also shown.

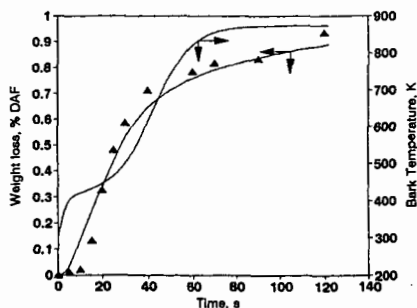


Figure 3. Experimentally observed and model predicted weight loss of bark during combustion at 600°C wall temperature. Predicted bark particle temperature is also shown.

A NOVEL SMOOTHING ROUTINE FOR THE DATA PROCESSING IN THERMOGRAVIMETRIC ANALYSIS

Keyu Wang, Shaojie Wang, He Huang, M. T. Klein and W.H. Calkins*
Dept of Chemical Engineering, University of Delaware, Newark, DE 19716

Key words: smoothing, differentiation, thermogravimetric analysis

INTRODUCTION

Thermogravimetric (TG) techniques have been used in characterizing fossil fuels (1-4) and in studying coal liquefaction kinetics, mechanisms, and processes (5,6). The TG techniques have been providing sensitive, rapid, and reproducible measurements for those purposes.

The primary output of thermogravimetric analysis (TGA) is in the form of a three-column matrix of time, temperature, and mass (or mass%). The first derivative of the TG (i.e. DTG) is capable of revealing fine details of the processes occurring more clearly for sample characterization (2,7) and/or as an input variable for further analysis, for example, in the SimDis (Simulated Distillation) TG technique (8).

There always is a limitation on the sensitivity of the TGA instrument. This is particularly true for those analyses run at either very low heating rates or very slow DTG decay experiments, where small changes in mass occur. Therefore, smoothing and filtering of these large data sets to obtain noise-free DTG curves are crucial in those TGA applications.

Several methods have been developed for smoothing and differentiation of experimental data (9-15). The objective of this paper is to present a novel and specific method for smoothing and differentiation of thermogravimetric data. The principle of the method is based on the characteristics of the TG data (e.g. time vs. mass). Linear regression and error analysis are used in the smoothing and filtering routine. The computer program required is simple and effective. The method used in the program promises auto-convergence. The reported technique in this paper could also be applied to other analytical instrumentation.

EXPERIMENTAL

The thermogravimetric analyzer (TGA) was a Model 51 TGA (TA Instruments, New Castle, Delaware). The program of manipulation of the TG variables, such as heating rate, type of purge gas and its flow rate, and final (or step) temperature, was determined by the objectives of the particular experiment. The output matrix of a TG scan (time, temperature, mass) was recorded by computer. The digitized data were then transferred into DOS (ASCII) format using a program provided by TA Instruments. The ASCII format data were loaded into MATLAB (The MathWorks, Inc.) and processed using a MATLAB routine.

METHOD OF SMOOTHING AND DIFFERENTIATION

The General Problem. The random errors which, regardless of their source, are characterized as noise are always present in the TGA measurements. This background noise reduces signal-to-noise ratio, resulting in decreasing sensitivity. This is particularly true when the DTG is the objective result of a TG scan. Figures 1 and 2 show the DTG plots for TG scans run at a very low heating rate (1°C/min) and a very slow DTG decay, respectively. These DTG plots were obtained from numerical differentiation of the original TG data. As shown in Figures 1 and 2, it is necessary for the investigator to remove the noise as much as possible without, at the same time, distorting the experimental data, especially for those processes where small changes in mass occur. Smoothing and filtering of these thermogravimetric data to obtain the noise-free differentiation (DTG curve), therefore, are required in the TGA applications.

The Characteristics of the TG Data (time vs. mass). A TG curve of the Illinois #6 coal at a heating rate of 1 °C/min in 100 cm³(STP)/min nitrogen is shown in Figure 3. Thirty one data points of (t,w) taken from Figure 3 are plotted in Figure 4. The plot shows a very good linearity between the mass and time. In general, this is always true for a certain short time interval of a TG scan. It is this characteristic that is used to develop a method for smoothing and differentiation of the TG data.

Smoothing and Differentiation by Linear Regression and Error Analysis. One of the simplest ways to smooth fluctuating data is by a n-point ($n=2k+1$; $k=1,2,3,\dots$) moving average procedure. In this method, a fixed odd number ($2k+1$) of data points are taken to obtain the average for the center point, $(k+1)$ th point, of the group. To move on, the first point in the group is dropped, the next point at the end of the group added, and the process is repeated. In statistics, noises in the data file are not filtered by this simple average procedure.

Consider a group of n (for example, $n = 11$) points of (t, m) taken from a TG file and plotted in Figure 5. Based on the characteristics of the TG data discussed in the previous section, a linear regression can be performed in this group by

$$m = a + b \times t \quad (1)$$

and represented by the solid line in Figure 5. The obtained linear regression parameters (i.e., a and b) can be used to estimate the m (mass) at each t (time) in the group. The errors (e) between the linear regression ($m_{cal}(i)$) and experimental data ($m_{exp}(i)$) in the group are defined as

$$e(i) = m_{cal}(i) - m_{exp}(i) \quad (2)$$

The statistical parameters of the errors for this group, e.g. mean (e_{mean}) and standard deviation (e_{std}) of the errors, are calculated by:

$$e_{mean} = \frac{\sum_{i=1}^{i=n} e(i)}{n} \quad (e.g. n = 11) \quad (3)$$

$$e_{std} = \sqrt{\frac{\sum_{i=1}^{i=n} (e(i) - e_{mean})^2}{n - 1}}$$

To eliminate the noise from this group, standard deviation of the errors can be used as a criterion to define the filter range. This is plotted as dashed-lines in Figure 5. In detail, if the experimental data point locates outside the filter range, i.e. $e_i > e_{std}$, it is considered as a noise in the group. To filter this noisy point, it is replaced by an estimated value of $m_{cal}(i)$ using the linear regression. This filter procedure can be used on each point in the group and a new data set can be formed. This new data set is plotted in Figure 6. The points with "x" in Figure 6 represent the filtered data. Linear regression can be again carried out in this new data group, followed with upgraded error analysis and filtering process. The linear regression, error analysis and the filter procedure are repeated until the standard deviation of the errors is below a predetermined value of $e_{std,0}$. In this study, a relative standard deviation of the errors, re_{std} , rather than e_{std} , has been used for evaluating the calculations. This relative standard deviation of the errors is defined as e_{std} times the absolute value of the slope (DTG) of the linear regression, i.e.,

$$re_{std} = abs(b) \times e_{std} \quad (4)$$

This relative standard deviation of the errors used as a criterion to evaluate calculations can insure the precision of very slow process (i.e., very low DTG scan). It has been found that $re_{std,0}$ set at 10^{-3} gives very satisfactory results. The final regression results are used to estimate the smoothed mass and differentiation for the center point of $t_{(k+1)}$, i.e.,

$$m_{k+1} = a + b \times t_{k+1} \quad (5)$$

Since the standard deviation of the errors constantly decreases with iterations, the computation method used in the program promises auto-convergence.

For a TG analysis, the n -point smoothing, filtering and differentiation routine has been moved in the data file similarly as the moving average method which has been described earlier. A scheme of the computation routine is illustrated in Figure 7. For the "end-points" (i.e., either the initial or the final k points in the data file), a different method has to be used to evaluate them. One of the simplest ways to handle this "end-points" problem is to throw them away, since these end-points usually are not important or not of interest. In this study, the end-points have been simply assigned by their original values. If the "end-points" become important, a much more sophisticated method developed by Leach et al. (10) could be used.

APPLICATIONS

SimDis TGA. A SimDis TGA method for determining the boiling point distribution of liquid fuels is reported elsewhere (8). Original DTG plot for a petroleum sample, light paraffinic vacuum distillate, is shown in Figure 2. To transfer the DTG decay into boiling point distribution, it is necessary to smooth the noisy DTG data. The results of $n = 0$ (i.e., original), 3-, 5-, 7-, 9-, and 11-point smoothing and filtering are illustrated in Figure 8. The

more the data points used for smoothing and filtering, the smoother the DTG curve. However, at the same time, the more CPU or the longer computing time are required. More importantly, a large data number n used in smoothing increases the risk of distorting the experimental data. Eleven-point smoothing and filtering has been found to give the optimized results for the cases studied thus far. Figures 9a and 9b show the comparison plot (i.e., a plot including both smoothed results and original experimental data) and 11-point smoothing plot, respectively. The results indicate the smoothing and filtering method used in this study is very effective.

Characterization of coal structure. A representative TG scan on the Argonne Premium Illinois #6 bituminous coal, which was dried in a vacuum oven with a nitrogen purge at 105 °C for 48 hours before use, is shown in Figure 10. The two phases, i.e., 1) the heating rate to 950°C in nitrogen and hold for 7 min; and 2) the oxidation at 950°C, provided measures of VM, FC, and Ash, respectively. The differential of the weight loss (DTG) curve highlights the various TG processes more clearly. This becomes even more distinct and complex if the heating rate is slowed down to about 1 °C/min (2). However, the original DTG plot for this low heating rate shown in Figure 1 is so noisy that the processes involved in the TG scan could not be distinguished. The comparison plot and the 11-point smoothing results for this low heating rate scan are shown in Figures 11a and 11b, respectively. The processes involved in the TG pyrolysis of the coal at this low heating rate, as shown in Figure 11b, are very clearly distinguished. The low temperature peak represents the loss of residual moisture below 200 °C. The main Volatile Matter peak starts at 350-400 °C and actually consists of three or perhaps four individual weight loss processes. The large peak is broad and probably consists of a number of pyrolysis processes. The well defined peak at 571 °C is tentatively identified as due to pyrite decomposition to pyrrhotite and sulfur because this peak is absent in coals containing little or no pyrite. Also, the decomposition temperature corresponds closely to that reported for pyrite (16). Two other small peaks are not yet identified but are fairly broad. They disappear gradually during coal liquefaction (5).

With this smoothing and filtered method, the sole function of the computation is to act as a filter to smooth the noise fluctuations and hopefully to introduce no distortions into the experimental data. The problem of distortion is quite difficult to assess. In Figures 1 and 2, there are small fluctuations in the raw data. Are these fluctuations real, or, as is more likely, are they just noise? The question can not be simply answered by taking just the data from a single run. However, if two or three runs were taken, they gave the same results or, more characteristically, in same patterns. These indicated that the fluctuations are due to the noise, since the random errors will not recur in exactly the same place in different runs. The results of duplicate tests on all samples inspected in this study suggest that the fluctuations are truly due to noise.

CONCLUSION

For a certain short interval of a TG scan, the correlation between the mass and time is linear. A smoothing and filtering routine based on the use of linear regression and error analysis has been developed and successfully applied in the thermogravimetric data processing. This method provides a filter to smooth the noise fluctuations and, at the same time, to introduce no distortions into the TGA experimental data. The computer program required is quite simple and effective. The method used in the program promises auto-convergence.

ACKNOWLEDGEMENTS

The support of this work by the subcontract from CONSOL under DOE Contract DE-AC22-94PC93054 and by the Department of Energy under DE22-93PC93205 is acknowledged. Additional funds for purchase of thermal analysis equipment was provided by the University of Delaware.

REFERENCES

1. Ottaway, M. *FUEL* **1982**, **61**, 713.
2. He Huang, Keyu Wang, M.T. Klein, and W.H. Calkins *ACS Fuel Chem Div Preprints* **40** (3), 465 (1995).
3. He Huang, Keyu Wang, W.H. Calkins and M.T. Klein *ACS Fuel Chem Div Preprints* **39** (3), 741 - 746 (1994).
4. He Huang, W.H. Calkins and M.T. Klein *I&EC Research* **33**, 2272-2279 (1994).
5. He Huang, Keyu Wang, M.T. Klein, and W.H. Calkins *ACS Fuel Chem Div Preprints* **40** (3), 550 (1995).
6. He Huang, Keyu Wang, M.T. Klein, and W.H. Calkins *Coal Science and Technology 24: Coal Science*, Eds J.A. Pajares and J.M.D. Tascon, Vol. II, p. 1207 (1995).
7. He Huang, D.M. Bodily, and V.J. Hucka *Proceedings 1993 International Conference*

- on *Coal Science* pp 411-414.
8. He Huang, Keyu Wang, M.T. Klein, and W.H. Calkins *ACS Fuel Chem Div Preprints* **40** (3), 485 (1995).
 9. Whitaker, S.; Pigford, R.L. *Ind. Eng. Chem.* **52**, 185 (1960).
 10. Leach, R.A.; Carter, C.A.; Harris, J.M. *Anal. Chem.* **56**, pp. 2304-2307 (1984)
 11. Baedecker, P.A. *Anal. Chem.* **57**, pp: 1477-1479 (1985)
 12. Khan, A. *Anal. Chem.* **60**, pp. 369-371 (1988)
 13. Guest, P.G. *Numerical Methods of Curve Fitting* University Press, Cambridge, England (1961).
 14. Hamming R.W. *Numerical Methods for Scientists and Engineers* McGraw-Hill Book Co., New York (1962).
 15. Ralston, A. *A First Course in Numerical Analysis* McGraw-Hill Book Co., New York (1965).
 16. Luganov, V.A.; Schebalin, V.I. *Can. Metall. Q.* **1982**, 21, 157.

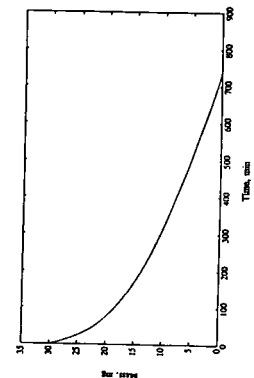


Figure 3 TG curve of Illinois #6 coal pyrolysis at 1 C/min (only volatile portion)

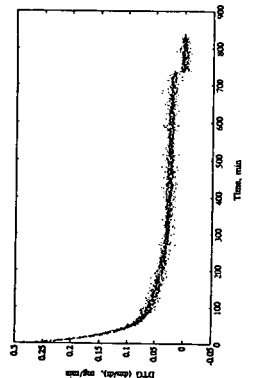


Figure 2 DTG decay of a SimDis TGA scan on a liquid fuel

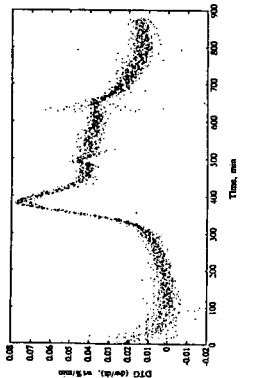


Figure 1 DTG of Illinois #6 coal pyrolysis at 1 C/min

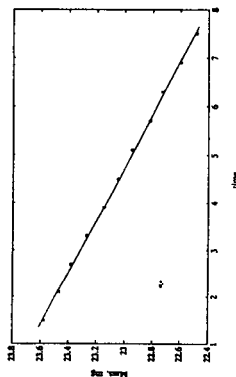


Figure 6 Mass vs time for a filtered n-point group

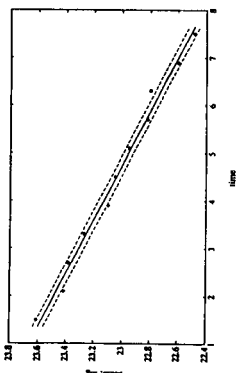


Figure 5 Mass vs time for a n-point group

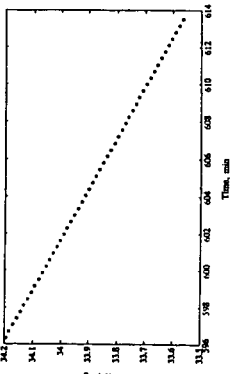


Figure 4 Characteristic of mass vs time in a TG scan (Thirty-one data points taken from Figure 3)

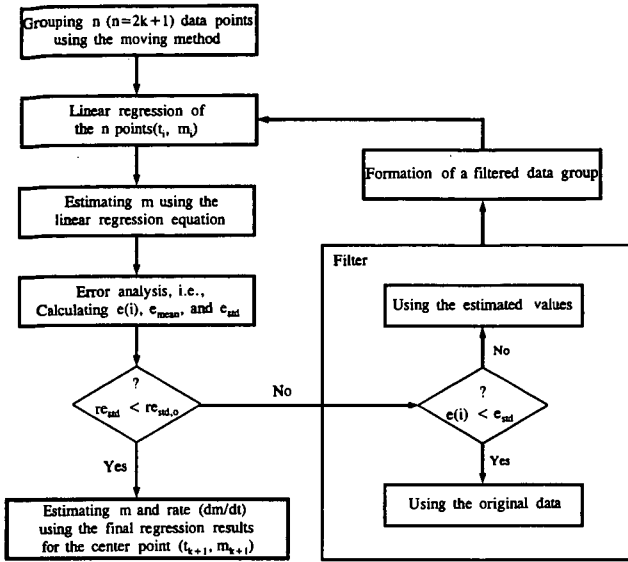


Figure 7 Flow-sheet of the n-point smoothing and filtering procedure

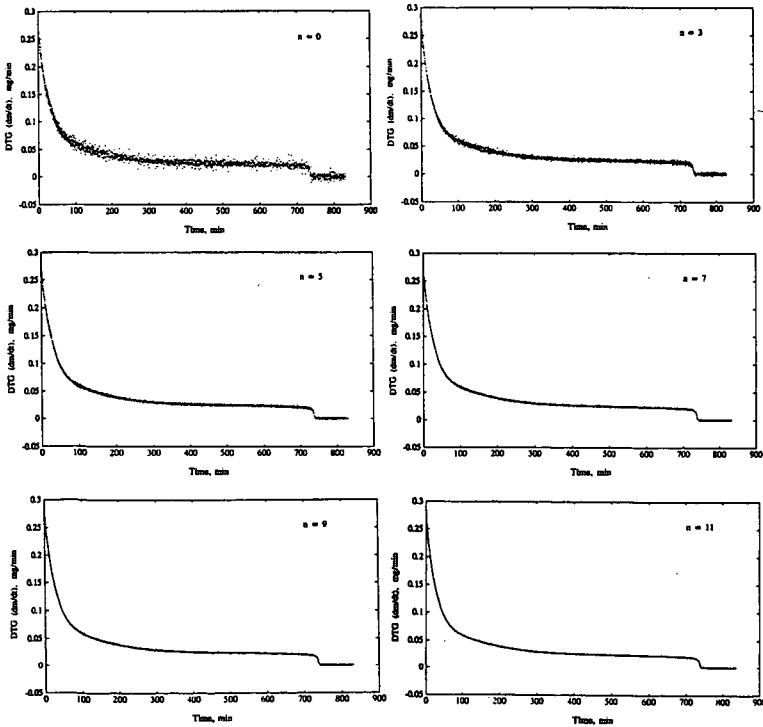


Figure 8 The results of n = 0-, 3-, 5-, 7-, 9-, 11-point smoothing and filtering

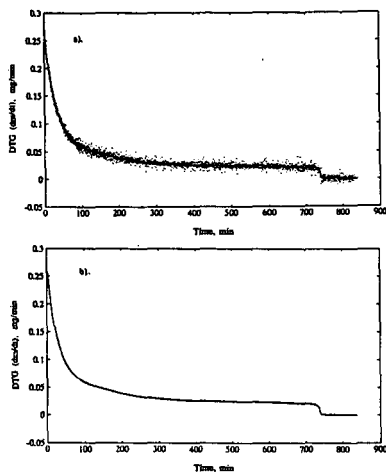


Figure 9 Visualization of n-point smoothing and filtering of the DTG at very slow heating rate shown in Figure 1: a). comparison plot; b). 11-point smoothing and filtering plot

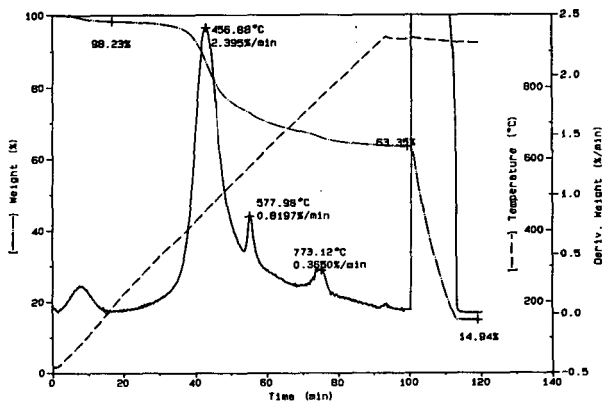


Figure 10 A TG scan of Illinois #6 coal at 10 C/min

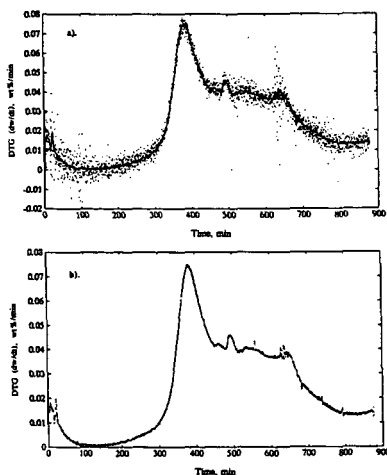


Figure 11 Visualization of n-point smoothing and filtering of the DTG decay shown in Figure 2: a). comparison plot; b). 11-point smoothing and filtering plot

ENERGY STORAGE MATERIALS AND COATINGS. DSC AND FLAMMABILITY STUDIES

Michael W. Babich and Ramazan Benrashid
Department of Chemistry
Florida Institute of Technology
150 West University Blvd.
Melbourne, Florida 32901-6988

Keywords: Energy Storage Materials, Phase Change Materials, Flammability

Introduction

For many years investigations into the thermal and moisture storage properties of materials undergoing reversible phase changes in the temperature range of interest for that particular application have been conducted. The prototypical material is, of course, water at 0°C or 100°C. The interest in these materials has arisen largely from the need to conserve fossil fuels and cut energy costs. Both reasons are still valid. (1-2)

These materials have been called phase change materials, (PCM's), Energy Storage Materials (ESM's) or enthalpy storage materials in the literature, and these terms are used interchangeably for the most part. They have been incorporated into a wide variety of components used in construction and fabrication of everything from buildings to packaging materials to space suits.

Interest has existed in phase change materials for thermal storage since the late 1940's largely due to the pioneering studies of M. Telkes using Glauber's Salt. (3,4) These studies set the tone and path for work to follow even through thermal storage using this salt was never widely commercially successful. The primary disadvantage of Glauber's Salt is phase segregation upon melting. Work prior to the latest ESM materials was reviewed by Lane in 1987. (5) The early work concentrated heavily on melting of salt hydrates and gave quite mixed results. Non-segregating hydrates (those with congruent melting) such as $MgCl_2 \cdot 6H_2O$ at 117° gave the best results, but are not always available for the temperature range of interest. Table 1 shows a selection of these types of materials which have been used commercially and their temperatures of transition.

One of the most novel approaches developed was to use the solid-solid transition in polyalcohols the temperature of which can be somewhat adjusted by blending. These materials include pentaerythritol and neopentyl glycol (6,7). These transitions have been studied from 25° to 140°C. The lower temperature cases have not proven very useful as yet in any actual application.

Our area of primary interest, of course, has been in the application of phase change materials for thermal storage. PCM's have been used supplementally in both passive heating and cooling applications. These PCM's incorporated into construction materials can function to limit the temperature variation in a commercial or residential structure over a twenty four hour cycle by releasing heat during cooler periods and absorbing heat during warmer periods. Energy savings of 30 - 70% have been projected and up to 90% of annual sensible cooling could be shifted to off-peak hours. Further, coupling enthalpy storage with moisture storage has been shown to control humidity as well.

Desired Properties

Lane has listed some of the following properties for phase change materials. (5) This list was modified by Babich and Hwang and is shown in Table 2. (8-9)

How the importance of the properties on this list are weighted depends entirely on the application intended. The optimum set of properties can be determined for each situation. The choice may be economics driven in one case or application driven in another. It is for this reason that we strongly feel no one material is likely to solve every problem. Instead a range of good phase change candidates must be available to fit the very many possible uses for these materials.

Methods of Study

These ESM materials have been evaluated by a wide variety of methods, but the most successfully used thus far is differential scanning calorimetry (DSC). This method works well for both neat and adsorbed materials and for both heating and cooling cycles. It has also been successfully demonstrated that the small sample size used in these studies gives totally reproducible results in large scale tests. (9) An actual DSC curve for undecylenic acid is shown in Figure 1.

From these curves one may readily obtain the heat of fusion or freezing and also the range of melting or freezing. Supercooling, if present, is obvious in these studies and the shape (width) of the transition is easily seen. These factors make this technique the method of choice. Differential Thermal Analysis (DTA) has also been used in some of the earlier work with some success. Actual bulk studies have been carried out utilizing structures ranging from passive test boxes to full scale room testing. These investigations have been described in detail in other work (10) In tests conducted at the Florida Solar Energy Center (FSEC) it has been shown conclusively that bulk tests agree very nicely with DSC studies conducted by Babich et al. (11)

The Current Situation

PCM's have now been developed which can be added to building materials e.g. wallboard, and which will contribute significantly to reduction of heating and cooling costs. There are three schools of thought with overlapping classes of compounds which presently represent the main efforts in low temperature thermal storage via energy storage materials. These areas can be subdivided by the approaches followed into the area of fatty acids and specifically blended mixtures thereof pioneered by Shapiro and coworkers, the long chain hydrocarbons developed by Salyer and coworkers and the more broad based search for new materials or the coating of older ones for specific uses by Babich et al.

Section I: Fatty Acids

Low melting fatty acids and blends of fatty acids have been considered as PCM's for several years. They have good properties in many respects. They are low-volatility, high boiling, low melting, organic materials which are readily imbibed by construction materials like gypsum wallboard. Further, many examples like coconut oil are very inexpensive making them very attractive as PCM's. Research by Shapiro and others has

been largely driven by economic considerations as well as properties (12-14). Some of the fatty acids and fatty acid mixtures studied early on are shown along with their thermal characteristics in table 3. Many of these mixtures are commercially available.

These materials are imbibed well into wallboard at very easily reproduced rates and with readily measured masses as shown in Figure 2. Further, they tend to be reasonably chemically stable and remain strongly absorbed indefinitely through many thermal cycles. They have normally been studied in the range of 20-30% absorption by mass. For these materials supercooling is not a problem at the rate of temperature change in normal structures. Actual room size structures using wallboard imbibed with fatty acid have been constructed and function well thermally.

The real drawbacks to the use these materials lay in two main areas. First they are aesthetically unappealing. They have odors which were not very evident in lab scale testing but become very strong in large scale testing precluding their use in many structures. They also discolor the wallboard slightly which can be overcome by painting. They contribute both to flame spread and smoke production in flammability tests as shown in Tables 3, (15,16). It has been stated that fatty acids may exhibit corrosivity in some applications though this has not been conclusively demonstrated, and also that they may promote mold growth.

Section 2: Long Chain Hydrocarbons

Low melting long chain hydrocarbons (sometimes called hydrocarbon waxes) have also been effectively utilized as PCM's absorbed into wallboard(17-19). They, like the fatty acids, also have good properties in several respects. These are also low volatility, high boiling, low melting organic materials which can be imbibed effectively by wallboard. A group of these materials studied and their thermal characteristics are shown in Table 5. Some of these are also available at very low cost. Witco Chemical Company for example can provide a predominantly n-octadecane (K-18) at ~\$0.50/lb/as apposed to 99% pure n-octadecane at ~\$10.00/lb. These hydrocarbons have also been effectively encapsulated and pelletized. (19)

These are used at approximately the same loading, 20-30% by mass, as the fatty acids and mixtures. The thermal characteristics are similar. These materials are chemically quite stable though some breakdown over extended times has been noticed. (20). Supercooling is also no problem in these materials at normal ambient thermal cycling rates.

Drawbacks, however, in these materials are quite similar to some of the fatty acids. The chief problem is once again flammability and smoke production. Again epoxy coatings can be effective reducing flammability in some cases to that of untreated wallboard. These PCM's do not support mold growth.

Section 3: Other Materials and Integrated Approaches.

Babich et. al. have taken the approach of ESM's tailored to specific purposes and/or controlling the disadvantages of materials discussed in sections 1 and 2. (8, 9, 11, 20) Many materials have been studied including inorganic materials and silicone waxes some of which show great promise. Work in the area of new materials is in its infancy and is just beginning to yield good results. Further coupling of PCM's with moisture storage coatings may be of even greater utility. (21) These workers have reexamined several organic PCM's and investigated several new ones as shown in Table 5. Many of these, especially hexadecane, 1-dodecanol and allyl palmitate work exceeding well. (9) Unfortunately, allyl palmitate is too expensive for routine commercial use unless a newer, less expensive source can be found.

Babich et al have also clearly demonstrated and discussed at length the effectiveness of coatings of epoxy paints with aluminum and magnesium hydroxides for control of flammability. (22,23) Rate of flame spread, rate of heat release and onset of smoke production have been greatly retarded. In many cases the treated material is as good as untreated wallboard. ASTM and NBS approved tests have been used and sample results are shown in Table 4 and Figure 3. In this figure the amount of control the coating yields is most obvious. The incremental cost increase for this method is very small as most commercial wallboard will have to be painted anyway. These coatings could be applied as the primer by wallboard manufacturers or in the structure after construction. Additionally this method may be successfully coupled with any of the materials discussed previously. Also a method has been developed with tremendous potential to couple ESM's with moisture storage systems. (21, 24) This approach, if further developed, could lead to new combinations of materials which will accomplish thermal storage with humidity control and be fire retardant as well. New congruent melting, salt hydrates are also currently under investigation both for ESM use and in coatings combining moisture exchange with ESM properties. Other desiccant materials are also being tested for use in coatings.

Summary

Tremendous potential exists in the area of ESM's for energy storage and in the area of moisture storage materials coupled with the ESM's. The efficacy of ESM materials for energy storage has clearly been demonstrated as has the utility of moisture storage agents for humidity control. The effectiveness of coatings in reduction of rate of flame spread, onset of smoke production and rate of heat release is indisputable. DSC is clearly the method of choice for preliminary studies of these systems.

References

1. J. Paris, M. Falardeau and C. Villeneuve, "Thermal Storage by Latent Heat: A Viable Option for Energy Conservation in Buildings," *Energy Sources*, 15, 85-93 (1993).
2. D. W. Hawes, D. Feldman and D. Banu, "Latent Heat Storage in Building Materials," *Energy and Building*, 20, 77-86 (1993).
3. M. Telkes, U. S. Patent 3,986,969 (1976).
4. M. Telkes, "Nucleation of Supersaturated Inorganic Salt Solutions," *Ind. Eng. Chem.*, 46, 1308 (1952).
5. G. A. Lane, "Phase-Change Thermal Storage Materials" in *The Handbook of Applied Thermal Design*, E. C. Guyer, ed. McGraw-Hill, New York (1987).
6. D. Chandra, C. S. Barrett and D. K. Benson, "Adjustment of Solid-Solid Phase Transition Temperature of Polyalcohols by the Use of Dopants," in *Advanced in X-ray Analysis*, vol. 22, ed. E. S. Barrett, Plenum, 350-313 (1986).
7. D. Chandra, J. Helms, and A. Mojumdar, *J. Electrochem Soc.*, 141, 1921-1927 (1994).
8. M. W. Babich, S. Hwang and R. D. Mounts, "The Search for Novel Energy Storage Materials Using Differential Scanning Calorimetry," *Thermochim. Acta*, 210, 83-88 (1992).

9. M. W. Babich, S. Hwang and R. D. Mounts, "DSC Studies of New Energy Storage Materials. Part 2. New Materials and Bulk Studies," *Thermochim. Acta*, 226, 163-168 (1993).
10. A. F. Rudd, "Phase-Change Material Wallboard for Distributed Thermal Storage in Buildings," *ASHRAE Transactions*, 99, Pt. 2, 339-346 (1993)
11. M. W. Babich S. Hwang and R. D. Mounts, "The Thermal Analysis of Energy Storage Materials by Differential Scanning Calorimetry," *Thermochim. Acta*, 210, 77-82 (1992).
12. M. Shapiro, D. Feldman, D. Hawes and D. Banu. "P.C.M. thermal storage in drywall using organic phase-change material." *Passive Solar Journal* 4(4): 419-438, (1987).
13. M. Shapiro and D. Feldman, "A Family of Thermal Ballast Building Bricks and Blocks," Proc. Ninth Biennial Congress ISES, Montreal, Canada, p. 853, June 23-39 (1985).
14. D. Feldman, M. Shapiro, D. Banu and C. J. Fuhs, *Sol. Energy Mater.*, 28(3-4) 201-216 (1989)
15. M. W. Babich, R. Benrashid and R. D. Mounts, "DSC Studies of New Energy Storage Materials, Part 3. Thermal and Flammability Studies," *Thermochim. Acta*, 243, 293-200 (1994).
16. M. W. Babich, R. Benrashid and R. D. Mounts, "New Energy Storage Materials: Thermal and Flammability Studies," *Proceedings of the 22nd North American Thermal Analysis Society Conference*, Denver, Colorado, 653-658 (1993).
17. I. O. Salyer, A. K. Sircar and R. P. Chartoff, "Advanced Phase Change Materials for Passive Solar Storage Application," *Proceedings of the Solar Buildings Conference*, Wash. D.C., March 18-20 (1985).
18. I. O. Salyer, A. K. Sircar, R. P. Chartoff and D. E. Miller, "Advanced Phase Change Materials for Passive Solar Storage Applications." *Proceedings of the 20th Intersociety Energy Conversion, Engineering Conference*, Miami Beach, Florida, August 18-23 (1985).
19. I. O. Salyer and A. K. Sircar, "Development of Phase Change Technology for Heating and Cooling of Residential Buildings and other Applications," *Proceedings of the 28th Intersociety Energy Conversion Engineering Conference*, Atlanta, Georgia (1993).
20. S. Hwang, M. S. Thesis, Florida Institute of Technology (1991).
21. A. F. Rudd, "Development of Moisture Storage Coatings for Enthalpy Storage Wallboard," *ASHRAE Transactions*, 100, 3744-3751 (1994).
22. M. W. Babich and R. Benrashid, "Energy Storage Materials Thermal and Flammability Studies," *Proceedings of the 23rd North American Thermal Analysis Society Conference*, 254-259 (1994).
23. M. W. Babich and R. Benrashid, "DSC and Flammability Studies of Organic and Inorganic Energy Storage Materials," *Thermochim. Acta*, In press (1995).
24. A. Kamel, M. Swami, S. Chandra and P. Fairey, "An Experimental Study of Building-Integrated Off-Peak Cooling Using Thermal and Moisture ("Enthalpy") Storage Systems," *ASHRAE Transactions*, 97, Part 2, 240-244, (1991).

Material Examples of Use	Transition Temp. °C	Heat of Fusion (J/g)	
$\text{CaCl}_2 \cdot 6\text{H}_2\text{O} - \text{CaBr}_2 \cdot \text{H}_2\text{O} - \text{KBr}$	15-34°C	121	Heat sink in heat pumps
$\text{CaCl}_2 \cdot 6\text{H}_2\text{O}$	27°	192	Passive solar panels Central solar Heat
Glauber's salt	32°	251	Greenhouse heating
$\text{MgCl}_2 \cdot \text{Mg}(\text{NO}_3)_2 \cdot 6\text{H}_2\text{O}$	58°	134	Hot water heating
$\text{Na}_2\text{C}_2\text{H}_3\text{O}_2 \cdot 3\text{H}_2\text{O}$	58°	225	Railway heating
$\text{Mg}(\text{NO}_3)_2 \cdot 6\text{H}_2\text{O}$	89°	163	Dishwashing systems
$\text{NH}_4\text{AlSO}_4 \cdot 12\text{H}_2\text{O}$	95°	267	Water heating
$\text{MgCl}_2 \cdot 6\text{H}_2\text{O}$	114°	167	Absorption AC

Table 1. Examples of Available Phase Change Materials - Salt Hydrates

Class	Specific Property
Thermal	Suitable phase transition temperature Reasonable phase transition range Large latent heat of transition High boiling point
Physical	Favorable type of phase transition Low vapor pressure High reproducibility Little change in volume
Chemical	Compatible with construction material Long term stability of materials Non-toxic Non-corrosive No additional fire hazard Low smoke production in fires No sensory irritation Good aesthetic qualities
Kinetic	No supercooling Sufficient crystallization rate
Economic	Cost Availability in marketplace

Table 2. Desirable Properties for Phase Change Materials

Material	mp (°C)	ΔH_m (J/g)	f_p (°C)	$-\Delta H_f$ (J/g)
EM625 Coconut Acid	25.0	107.1	15.8	110.1
EM626 Coconut Acid	25.4	119.1	17.5	119.6
EM627 Coconut Acid	30.0	117.2	26.2	147.1
EM659 Capric Acid	28.8	147.4	23.2	140.7
EM651 Lauric Acid	42.0	132.9	37.9	134.5
EM Methylpalmitate	26.8	104.3	20.0	94.1
EK Capric Acid	31.0	128.0	27.1	125.8
EK Lauric Acid	42.5	126.0	38.1	131.5
EK Methylpalmitate	28.8	163.2	23.3	180.9
EK Methylstearate	37.0	160.7	32.2	159.5
SG Undecylenic Acid	24.4	143.5	19.4	144.2
Capric Acid / Lauric Acid Ratio				
1/0	28.8	147.4	23.2	140.7
9/1	25.6	71.7	18.2	38.1
7/3	17.7	60.2	13.1	51.1
5/5	19.7	55.5	15.5	40.8
3/7	20.5	123.8	26.9	82.8
1/9	37.4	125.7	33.4	118.9
0/1	42.0	132.9	37.9	134.5

Table 3. Thermal Results for Fatty Acids and Fatty Acid Mixtures

EM = Emery Chemical Co., EK = Eastman Kodak Chemical Co.,
SG = Sigma Chemical Co.

Samples	# of Sample	D90	D240	D475	Dc	Corrected Dm	Dm/Wt G	Weight G	Sample Weight
α -Cellulose	5	5.4	92	158.6	8.9	195	71.5	1.95	2.7
Wallboard	3	1.4	19.5	35.3	0.8	35.4	0.8	6.3	49.2
FR Wallboard	3	0.8	16.2	38.2	0.2	37.8	0.7	6.1	53.7
S1	3	25.9	241.3	505.3	0.6	505.3	8.1	15.1	63.3
S1 Epoxy	3	2.3	101.6	390.5	4.5	477.8	3.0	12.6	70.4
S1 Al(OH) ₃	3	0.7	36.0	60.5	5.7	497.6	7.3	10.5	68.20
S1 Mg(OH) ₂	3	0.4	15.1	38.0	4.4	505	7.2	22.9	70.2

S2	3	27.7	237.8	496.8	31.5	479.7	7.8	13.2	59.7
S2F	3	25.9	219.5	466.2	31.3	463.7	7.5	10	62
S2 Epoxy	3	5.4	26.7	325	32	486.3	8.1	9.8	38.6
S2F Epoxy	3	3.3	24.9	376.8	29	480.7	7.2	10.9	55.4
S2 Al(OH) ₃	3	2.1	17.4	261	55	473.9	8	11.0	59.2
S2 Mg(OH) ₂	3	2.7	23.5	392	75.5	458.6	8	11.8	57.7
SF52 Al(OH) ₃	3	3.3	11.5	252.5	31	463.2	7.1	10.9	65.3
SF52 Mg(OH) ₂	3	0.9	10.7	248.4	27	390	6.1	12.2	64.3

S3	3	22.4	180.5	435	9.5	494	8.7	10.8	56.9
S3 Epoxy	3	25.8	160	489.5	5.8	496.9	8.1	9.3	61.3
S3 Al(OH) ₃	3	7.4	128.5	418.3	6.9	501.7	8	10.2	62.3
S3 Mg(OH) ₂	3	0.9	113.2	329.7	8.9	467.9	7.9	11.4	63.4

S4	3	10.4	104.6	499	13.3	487.6	8.6	12.1	56.9
S4 Epoxy	3	12.3	59.5	205.7	5	498.3	9.2	12.6	54.2
S4 Al(OH) ₃	3	15.5	59.2	201.5	4.2	494.7	9.3	11.7	53.6
S4 Mg(OH) ₂	3	0.6	13.1	121.1	2.5	427	7.6	10	56.6

S1=Hexadecane
S2=1-Dodecanol
S3=Undecylenic acid
S4=Coc-nut oil

Table 4. Results from Flame Spread Test.

Material	mp °C	ΔH_m (J/g)	f_p °C	ΔH_f (J/g)
n-Hexadecane b	20.0	216	10.4	220
n-Octadecane a	28.4	200	17.9	200
1-Dodecanol b	23.8	184	17.5	190
n-Heptadecane b	22.6	164	19.0	165
Allylpalmitate d	22.6	173	16.2	125
Undecylenic Acid e	24.8	141	18.1	143
1-Nonadecane b	23.2	131	20.1	134
1-Iodoheptadecane b	22.2	131	8.6	132
n-Octadecylacrylate c	25.7	115	22.1	99
Diphenyl ether b	27.2	97	-8.2	81
Diphenylmethane b	24.4	86	-3.3	75
Chlorobenzothiazole b	18.8	65		
3-Iodoaniline b	22.5	64		
Polytetrahydrofuran b	17.5	59	0.1	76.4
Trimethylcyclohexene b	24.1	47		
Phorone	25.8	124	11.2	3.7

Table 5. Thermal Results for New Enthalpy Storage Materials

*Average of three measurements. Average standard deviation for mp and f_p = 0.3°. Average standard deviation for H = 4 J/g. (a) Mainstream Engineering Co., (b) Aldrich Chemical Co., (c) Scientific Polymer Products, Inc., (d) Dajac Laboratories, Inc. (e) Sigma Chemical Co.

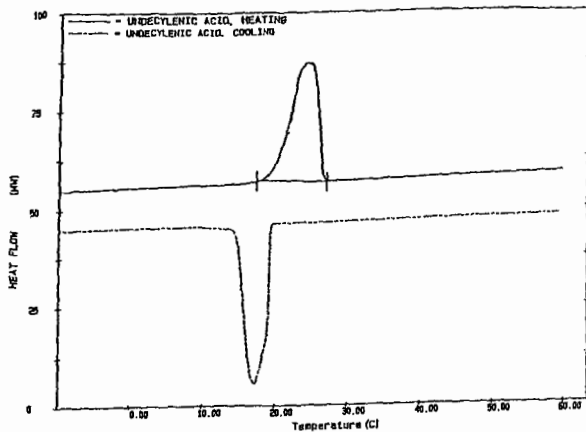


Figure 1. Sample DSC Curve for Undecylenic Acid (Heating and Cooling Curves)

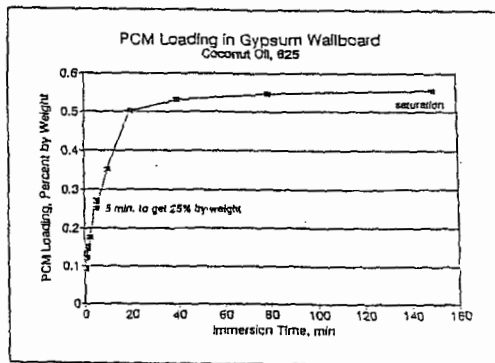


Figure 2. Sample ESM Loading in Gypsum Wallboard

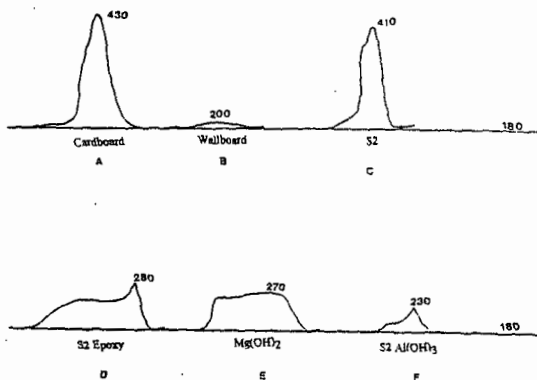


Figure 3. Comparison of maximum temperature in stack NBS Radiant Panel Tests for cardboard (A), wallboard (B) wallboard treated with 1-dodecanol S2 (C), epoxy coated S2 (D), $Mg(OH)_2$ /epoxy coated S2 (E), and $Al(OH)_3$ /epoxy coated S2 (F).

ANALYSIS OF ASPHALT-BASED ROOF SYSTEMS USING THERMAL ANALYSIS

Ralph M. Paroli and Ana H. Delgado

Institute for Research in Construction,
National Research Council of Canada
Ottawa, Ontario, Canada K1A 0R6

Keywords: Thermal analysis, roof membrane, asphalt, modified bitumen

INTRODUCTION

Asphalt has been used in the construction of roads and houses for thousands of years. The properties of asphalt has rendered it quite useful in roofing and waterproofing applications. The most popular use of asphalt in industrial roofing is in the form of a built-up roof or modified-bituminous sheet. This type of roof consists of asphalt, reinforcement and aggregate which is used to protect the asphalt from ultraviolet rays. All materials have their weaknesses and asphalt is no exception. A good asphalt (e.g., low asphaltene content) must be used to ensure the quality and low-temperature performance of roofing asphalts. Polymer additives can be added.

The criteria for choosing a polymer additive are: (a) the viscosity of the asphalt should not be significantly altered (b) It must be sufficiently compatible with the asphalt so as to avoid any phase separation during application (even at high temperatures). (c) It must improve some of the mechanical properties of the asphalt such as resistance to permanent deformation, fracture and high-temperature. In low-temperature environments, the polymer must be able to enhance the low-temperature flexibility and lower the glass-transition temperature (T_g) of the asphalt. Two commonly used polymer additives are styrene-butadiene-styrene block copolymer (SBS) and atactic polypropylene (APP). The exact amount of polymer added depends on the polymer and desired property. For example, 10-15% of SBS is sufficient to yield a continuous phase in the asphalt.

Roofing membranes have been used for many years. In the past, the testing of various roofing materials was simple because of the accumulated experience and also because of the lack of variety. Today, with the variety of additives, it is quite difficult to compare them solely on the basis of mechanical properties. This is especially true since the mechanical properties of these materials are not only related to macroscopic behaviour but also at the molecular level which is controlled by chemical composition and molecular arrangement.

Thermal analysis is a technique that can provide some insight as to why some roofing materials do not perform properly. In the past seven years, quite a few papers have been published using these techniques for roofing (see references 1-10 and references therein). Thermogravimetry (TG) can be used to monitor weight loss due to weathering and/or aging. Dynamic mechanical analysis (DMA) can be used routinely to determine the glass transition temperature. Together, DMA and TG can provide a measure of the degradative factors which can lead to the correlation between accelerated weathering and actual field performance. The objective of this study is to demonstrate the utility of TG and DMA in establishing the durability of modified-bituminous roof membranes.

EXPERIMENTAL

Composition of Modified Bitumen Membranes.

Four commercially-available, polymer-modified bituminous roofing membranes were obtained and labelled as SBS1, SBS2, SBS3 and APP1. A typical composition for the roofing membrane samples used in this study is given in Table I. The quantities will vary from product to product. It should be noted that the granules, reinforcement and

polyethylene account for between 36 and 40% of the total weight of a cap sheet but are excluded from the percentages listed in Table I.

Sample Preparation

Each material was cut into seven pieces of about 150 x 250 mm. One piece was used as a control, three were placed in an air-circulating oven preheated at 80 °C, and the remaining three were placed in an air-circulating oven set at 100 °C, for heat-aging. One piece of each material was removed from the oven, after 1, 7, and 28 days. Specimens were cut out for tensile testing and thermal analyses.

Thermogravimetry (TG)

The weight-loss of each roofing sample was monitored by thermogravimetric analysis using a Seiko Instruments Inc. STA 320 interfaced to a HP-900 Workstation. A piece of approximately 20 mg of sample was cut without including granules. The analyses were carried out at temperatures between 20 °C and 600 °C using a nitrogen gas flow of 150 mL min⁻¹ and from 600 °C to 1000 °C under air. The scanning rate was 20 °C min⁻¹. Throughout this study the derivative TG (DTG) curve was used as it provided the desired quantitative data (see Fig. 1). The data are tabulated in Table II as a function of heat-aging temperature and exposure-time.

Dynamic Mechanical Analysis (DMA)

The glass transition temperature of the membranes was obtained using a Rheometrics RSA II (software version 3.0.1) dynamic mechanical analyzer equipped with a mechanical cooling device. The following experimental profile was used for this study:

Geometry: 3-point bending
Sample width: 8 - 10.5 mm
Sample thickness: 3.5 - 4.0 mm
Sample length: 48.00 mm
Sweep type: Temp. steps
Frequency: 1 Hz (6.28 rad/sec)
Temperature Range: -100 °C to +30 °C
Heating Rate: 2.0 °C/min
Soak Time: 2.0 min
Strain: 2×10^{-2} %

Typical DMA curves are shown in Fig. 2. The glass transition temperature, T_g , (α -transition values) was obtained from the average of at least two and no more than four specimens from the same sample. The values are reported as the maximum in the loss modulus (E'') vs temperature curve. It is also possible to use the maximum of the $\tan \delta$ peak vs temperature curve, however, it was found that the E'' curve gave a better correlation with traditional mechanical data (e.g., tensile and elongation). The glass transition temperatures of the various samples are summarized in Table III.

RESULTS AND DISCUSSION

Three SBS (styrene butadiene styrene) modified membranes and one APP (atactic polypropylene) modified membrane were selected. The granules on the SBS modified membranes should be taken into account during analysis because they account for approximately one-third of the total weight and are not affected by high temperatures. Their presence minimizes the weight loss detected during the actual experiment. For this reason, the granules were removed from the SBS samples prior to testing. The APP modified membrane did not contain granules.

The results of the TG show that the polymer-modified bitumens are not affected by short term exposure to temperatures of 80 and 100 °C. But two samples show a large loss of weight after being heated in an oven for

28 days at 100 °C. The weight loss for SBS1 and SBS2, as determined by TG, is much less after 28 days of heating at 100 °C than it was at 7 days. Thus, weight was lost in the oven during the aging. This demonstrates that this technique can be useful in determining the relative stability of modified bituminous membranes. It is likely that changing the conditioning by heating the membrane in an oven for six months at 80 °C would provide a better reading on the long term durability of these membranes. In the field, loss of protective granules, which is a problem, will also expose the bitumen to UV radiation and accelerate the overall rate of deterioration of the membrane.

Generally, the glass transition temperature of control SBS modified membranes is in the -48 to -50 °C range. Heat aging, however, gradually raises the T_g to around -30 °C. On the other hand, the APP modified sample appears to be unaffected by heating as its T_g remains constant at -30 °C. Most samples also showed a another transition around -15 °C. While the component responsible for this transition is still unknown; its existence, however, might indicate that installing SBS-modified membranes in sub-zero temperature, using hot asphalt, as specified by the manufacturers could cause problems. It should be noted that all manufacturers call for their membranes to be unrolled and allowed to relax prior to installation.

CONCLUSIONS

The modified bituminous membranes, because of their low softening temperature and their complex chemical composition, provide results that are more difficult to interpret than the previously published EPDM and PVC membranes. The results, nevertheless, appear to be quite reliable when compared to the performance of these membranes in the field.

The results have shown that APP-modified material had a warmer glass transition temperature than the SBS-modified. The APP-modified bitumen, however, was more heat resistant than the SBS-modified ones.

The heating-aging temperature of 100 °C is not recommended because of the low softening point of the asphalt. A heat-aging temperature of 80 °C for six months could be preferable to assess the relative durability.

Loss of weight resulting from heat-aging affects the performance of modified bituminous membranes and appears to be an important factor in determining service-life. Little weight loss (~5%) after aging/weathering is indicative of stability to the aging program.

REFERENCES

1. C. G. Cash, *Single Ply Roofing Technology: ASTM STP 790*, pp. 55-64, (1982).
2. D. Backenstow and P. Flueller, *Proceedings, 9th Conference on Roofing Technology*, National Roofing Contractors Association, Rosemont, IL, pp. 54-68, April 1987.
3. R. M. Paroli, O. Dutt, A. H. Delgado, M. Mech, *Thermochimica Acta*, **182**, 303-317, (1991).
4. G. D. Gaddy, W. J. Rossiter, Jr., R. K. Eby, *Proceedings, 1991 International Symposium on Roofing Technology*, pp. 502-507, 1991, F. Kocich, editor, National Roofing Contractors Association, Rosemont, IL.
5. G. D. Gaddy, W. J. Rossiter, Jr., R. K. Eby, *ASTM STP 1136*, 168-175, (1991).
6. R. M. Paroli, O. Dutt, A. H. Delgado, H. K. Stenman, *Journal of Materials in Civil Engineering* **5**(1), 83-95, (1993).
7. K. Oba, and F. Björk, *Polymer Testing*, **12**, 35-56 (1993).
8. J. J. Penn, R. M. Paroli, *Thermochimica Acta*, **226**, 77-84 (1993).
9. I. S. Rodriguez, O. Dutt, R. M. Paroli, N.P. Mailvaganam, *Materials and Structures*, **26**(160), 355-361 (1993).

10. "Thermal Analysis Testing of Roofing Membrane Materials: Interim Report of the Thermal Analysis Task Group", *Conseil International du Batiment pour la Recherche l'Etude et la Documentation (CIB) W.83 and Réunion Internationale des Laboratoires d'Essai et de Recherche sur les Matériaux et les Constructions (RILEM) 120-MRS Joint Committee on Membrane Roofing Systems*, September 1993.
11. K. Oba, Flat roofs: Investigation of heat welding Techniques for polymer-modified bituminous roofing membranes. Dissertation, Royal Institute of Technology, Sweden (1994).
12. R. M. Paroli, O. Dutt, T. L. Smith, B. J. Whelan, Roofing Research and Standards Development: Volume 3, ASTM STP 1224, Thomas J. Wallace and Walter J. Rossiter, Jr., Eds., American Society for Testing and Materials, Philadelphia, 1994, pp.139-147.

Table I Typical matrix composition of SBS modified membranes

Ingredients	% by weight	Function
Bitumen	66 - 74	Waterproofing agent
Rubber modifier	11 - 16	Imparts elastomeric properties
Filler	11 - 18	Provides rigidity

Table II TG data for modified bituminous membranes

Heating Schedule		Weight Loss (%)			
Temp (°C)	Days	SBS1	SBS2	SBS3	SBS4
unheated		71.8	78.4	55.5	78.2
80	1	69.1	80.6	57.3	78.8
80	7	71.6	71.9	54.8	78.8
80	28	70.3	70.8	55.3	77.0
100	1	70.3	74.8	57.6	74.0
100	7	69.2	73.0	55.1	75.9
100	28	36.3	29.9	52.1	73.8

Table III Glass Transition Temperature (T_g) of Modified Bitumens

Heating Schedule		T_g (°C) for Samples			
Temp (°C)	Days	SBS1	SBS2	SBS3	APP1
Unheated		-50	-50	-48	-30
80	1	-50	-50	-46	-30
80	7	-40	-50	-46	-30
80	28	-40	-48	-50	-30
100	1	-40	-40	-50	-30
100	7	-40	-40	-48	-30
100	28	-30	-30	-30	-30

Figure 1. Typical TG/DTG curves for a polymer-modified bitumen roof membrane.

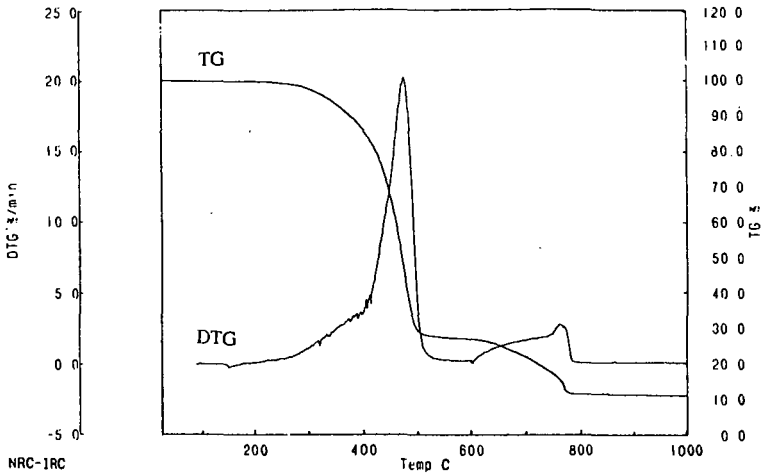
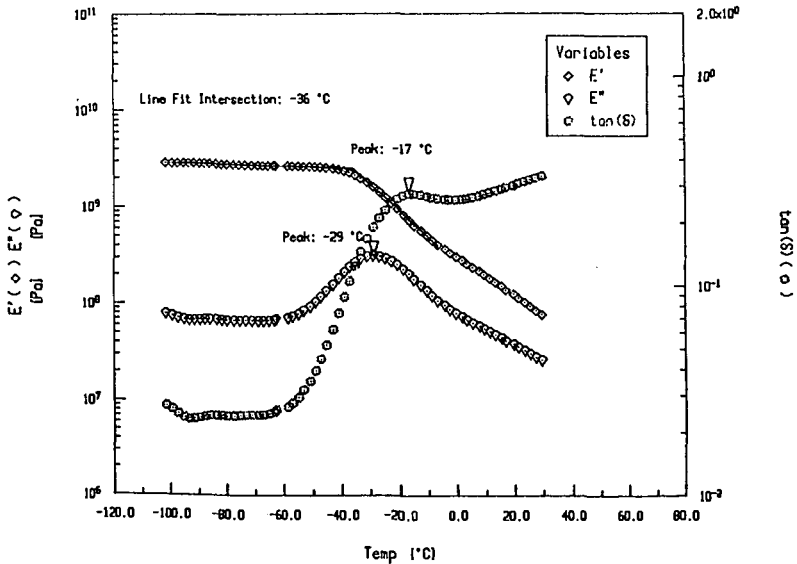


Figure 2. Typical DMA curves for a polymer-modified bitumen roof membrane.



USE OF TG-FTIR ANALYSIS FOR THE CHARACTERIZATION OF FUELS AND RESOURCES

Michael A. Serio, Rosemary Bassilakis and Peter R. Solomon

Advanced Fuel Research, Inc.
87 Church Street
East Hartford, CT 06108

Keywords: Thermal Analysis, FT-IR, Fuels

ABSTRACT

Thermogravimetric (TG) analysis combined with Fourier Transform Infrared (FT-IR) analysis of evolved products has proven to be a powerful technique for characterization of coal, source rock, heavy hydrocarbons, biomass, waste materials, and plastics. The TG-FTIR method can be used to determine the resource potential of a material, i.e., the types of products a material is likely to produce when subjected to processing by pyrolysis or combustion. It can also provide kinetic information for model validation or extrapolation and can provide the equivalent information to proximate and ultimate analysis. In addition, TG-FTIR analysis can be used to characterize the adsorbent potential and combustion reactivity of solids. The TG-FTIR method can provide this information in a more rapid, reproducible, and inexpensive way when compared to most other types of laboratory characterization methods such as drop tube reactors. This paper reviews the application of TG-FTIR analysis to hydrocarbon fuels and resources.

INTRODUCTION

Thermogravimetric analysis (TGA) has been employed in coal science to perform a number of characterizations including: proximate analysis,¹ kinetics of weight loss,² char reactivity,^{3,6} and gas adsorption measurements.⁷ A complementary technique, evolved product analysis, has been employed to study pyrolysis product distributions and kinetics,⁸⁻¹¹ functional group compositions,^{10,12,13} and temperature programmed desorption.¹⁴⁻¹⁵ A TG-FTIR instrument combines TGA with evolved product analysis by Fourier Transform Infrared (FT-IR) spectroscopy. FT-IR analysis of evolved products has advantages over mass spectroscopy in allowing analysis of very heavy products, and over gas chromatography in speed.

TG-FTIR instruments are available from several instrument manufacturers, including On-Line Technologies, Inc. (On-Line), an affiliate of Advanced Fuel Research, Inc. (AFR). In addition, Bio-Rad and Perkin-Elmer, among others, offer a TG-FTIR instrument. One of the differences among these instruments is the method used to analyze and quantitate the heavy liquid products from pyrolysis of the sample, which form an aerosol upon subsequent cooling prior to entry into the multi-pass FT-IR cell. These instruments have primarily been used for the analysis of polymers, pharmaceuticals, minerals, etc., including a limited amount of work done at AFR.^{17,36,37} Nearly all of the work on the application of TG-FTIR to hydrocarbon fuels and resources has been done at AFR or its collaborators. Consequently, the scope of this review will be limited to this body of work.

The application of TG-FTIR to coal analysis at AFR has been described in several publications.¹⁶⁻²⁵ To analyze coal, a sequence of drying, pyrolysis and combustion is employed to obtain: proximate analysis, volatiles composition, volatiles kinetics, and relative char reactivity. By using several different heating rates, kinetic rate constants for volatiles evolution have been obtained.^{17,21} TG-FTIR analysis has also been used at AFR to characterize other hydrocarbon materials such as modified coal samples,²⁶⁻²⁸ coal liquefaction resids,²⁹ petroleum source rocks,³⁰ lubricants,³¹ biomass,^{32,33} waste tires,^{34,35} and polymers.^{17,36,37} This paper will briefly review the use of the TG-FTIR technique at AFR for the characterization of hydrocarbon fuels and resources.

EXPERIMENTAL

Apparatus - A schematic of the AFR TG-FTIR instrument is presented in Fig. 1. Its components are as follows: a DuPont™ 951 TGA; a hardware interface (including a furnace power supply); an Infrared Analysis 16 pass gas cell with transfer optics; a Bomem 110 FT-IR; (Resolution: 4 cm⁻¹, Detector: MCT). A helium sweep gas (250 cc/sec) is employed to bring evolved products from the TGA directly into the gas cell. A window purge of 700 cc/sec is employed at each end of the cell. The system is operated at atmospheric pressure. This instrument package is available commercially as the *TG/plus* from On-Line Technologies, Inc. (East Hartford, CT).

The most difficult volatiles to analyze are the heavy decomposition products which condense at room temperature, such as tars from coal. In the *TG/plus*, the high conductivity helium sweep gas and the rapid cooling cause these products to form an aerosol which is fine enough to follow the gas through the analysis cell. The cell is connected without restrictions to the sample area. The aerosol is also fine enough that there is only a little scattering of the infrared beam and it is thus attenuated almost as though the tar was in the gas phase, as shown in Fig. 2. Based on the aerosol's Rayleigh scattering of infrared radiation, the diameter of the aerosol droplets in this case is less than 1.0 μm. As indicated above, the

technique for analysis of the heavy liquid aerosols is one of principal features that differentiate the various commercial TG-FTIR instruments.

Procedure - As an example of the analysis procedure, the pyrolysis and oxidation of a lignite is described. More detail can be found in Refs. 16 and 17. Figure 3a illustrates the weight loss from this sample and the temperature history. A 35 mg sample of Zap lignite, loaded in the sample basket of the DuPont™ 951, is taken on a 30 °C/min temperature excursion in the helium sweep gas, first to 150 °C to dry for 240 sec, then at 30 °C/min to 900°C for pyrolysis. Upon reaching 900 °C, the sample is immediately cooled to 250 °C over a twenty minute period. After cooling, a small flow of O₂ (0.3 cc/sec) is added to the helium sweep gas at the 57 minute mark and the temperature is ramped to 700 °C at 30 °C/min (or as high as 1000 °C) for oxidation.

During this excursion, infrared spectra are obtained once every thirty seconds. As shown in Fig. 2, the spectra show absorption bands for CO, CO₂, CH₄, H₂O, SO₂, COS, C₂H₄, and NH₃. The spectra above 250 °C also show aliphatic, aromatic, hydroxyl, carbonyl and ether bands from tar. The evolution of gases derived from the IR absorbance spectra are obtained by a quantitative analysis program which employs a database of integration regions and calibration spectra for different compounds^{16,17}. The routine employs regions of each calibration spectrum which permit the best quantitation with the least interferences. The routine is fast enough to allow the product analysis to be displayed on the computer screen during the actual experiment.

Figure 3b illustrates the integral of the evolution curves to obtain the cumulative evolved product amounts. Because the data are quantitative, the sum of these curves match the weight loss as determined by the TGA balance. Discrepancies occur in this match because of missing components such as H₂ which cannot be seen by IR. Also, when O₂ is introduced, the balance shows a net gain in weight due to O₂ chemisorption.

The TG-FTIR system provides all of the usual capabilities of a TGA for measurement of char reactivity or surface characterization by Temperature Programmed Desorption (TPD) with the additional advantage of measurement of the evolved products. A non-isothermal reactivity test developed at AFR using a conventional TGA system^{3,5} was later adapted to the TG-FTIR.³⁸ Studies of coal chars using TPD have also been made in this apparatus.²⁴

RESULTS AND DISCUSSION

Examples of analyses done with the TG-FTIR apparatus will be presented in detail for coal samples and selected examples will be given for lignin and polymers. The coal data included in this paper is primarily from samples from the Argonne Premium sample bank, which have been extensively characterized using this technique.^{18,19,21,24-26} Other characterizations of the Argonne samples have been summarized by Vorres.³⁹

Measurement of Char Properties - The results from the application of the TG-FTIR instrument to measurements of the critical temperature (T_c) (an index of reactivity that defines the temperature at which a small but measurable rate of weight loss occurs) and the oxygen chemisorption capacity (OCC) for the Argonne Premium coals are shown in Fig. 4. As expected, the values of T_c decrease with decreasing rank (increased oxygen content) which indicates that lower rank coals are more reactive. This variation in reactivity with rank is primarily due to mineral contributions to reactivity.^{2,5} The measurements of oxygen chemisorption capacity (OCC), which are related to the active site concentration, are inversely related to T_c , and are also shown in Fig. 4. In our work, we have found that the value of T_c is a more useful correlative parameter for reactivity than the OCC.³⁸

Measurement of Volatile Product Evolution - The TG-FTIR system has been used to conduct programmed pyrolysis experiments on the Argonne premium coals over a range of heating rates (3, 30, 50, 100 °C/min).^{18,19,21,24-26} The changes in the positions of the evolution curves with temperature for the various volatile components can be used to define the kinetic parameters. An example is shown in Fig. 5 where the temperature for the maximum tar evolution rate is plotted for the eight Argonne coals at two different heating rates. Similarly, the changes in the integrated amounts of each volatile product can be used to characterize the coal functional group composition, as shown in Fig. 6 for the evolution of NH₃.

An example of results from TG-FTIR analysis of eight lignin samples is shown in Fig. 7. This plot shows a summary of the gas, tar and char yields for a study where high tar yields were desired to allow subsequent processing of lignin into carbon materials.²² The tar yields from the eight lignin samples varied from ~10 wt% for the H₂SO₄ lignin to >50 wt.% for the Iotech lignin. Another feature of the use of TG-FTIR for the analysis of hydrocarbon materials is the ability to conduct an on-line spectroscopic analysis of the heavy liquid products. An example is shown in Fig. 8, which compares the spectrum obtained at the temperature of the maximum evolution rate for six polymers. The slope of the baseline indicates the degree of scattering and hence the size of the tar aerosols, as discussed above. This is a characteristic of the material which depends on the molecular weight distributions of the oligomers formed, the viscosity, and surface tension. Since the tar aerosol droplets are components of smoke and, ultimately of soot, the technique has the potential to provide information which correlates with these important combustion properties of polymers. Figure 8 indicates that the TG-FTIR method reveals

significant differences in the tar structure and in the size of the tar aerosols between these different polymers.

Relationships between Kinetic Rates of Different Volatile Species - It has been found that some pools in the different volatile species have peak evolution rates at the same temperature and those peaks have the same shifts when the heating rate changes. The Utah Blind Canyon coals provides a good example of this phenomenon^{19,24}. The TG-FTIR measurements indicate that the tar evolution, the CO₂-Loose, CO-Loose, and the H₂O-Loose pools all show very close peak evolution rate temperatures, at about 480 °C for 30 °C/min., at about 519 °C for 100 °C/min. and at about 430 °C for 3 °C/min. runs. This feature implies that these volatile pools can be fit with the same kinetic parameters. This may also imply that there is some common evolution chemistry.

Modeling of Devolatilization Processes - The kinetic parameters for the functional group pools from the eight Argonne premium coals and some additional coals have been determined using a set of rules that were developed to allow a systematic method of establishing the rank variations (e.g., the frequency factors were fixed at values of less than 10¹⁵/sec. and only the activation energies were allowed to vary with rank)²¹. The kinetic and compositional parameters obtained from TG-FTIR analysis are used along with other characterization information to calibrate our Functional Group - Depolymerization, Vaporization, Crosslinking (FG-DVC) model of coal devolatilization.²¹ A typical comparison of theory and TG-FTIR data is shown in Figs. 9 and 10. Figure 9 shows a comparison of theory and experiment for the weight loss and major volatile species for pyrolysis of a Consol #2 coal at 30 °C/min. Figure 10 shows a comparison of FG-DVC model predictions and experimental data for the tar evolution rate at 30 °C/min. from all eight Argonne Premium Coals. The agreement between the theory and experiment is generally quite good except for species where mineral contributions are important in Fig. 9 (CO₂, H₂O). The kinetic parameters obtained from the TG-FTIR method extrapolate well to very low heating rates, as in natural maturation processes,^{20,28} as well as to the high heating rates of importance in most coal gasification and combustion processes.^{18,21} Other versions of the FG-DVC model have been developed for lignin³³ and phenol-formaldehyde³⁶ using the same approach.

CONCLUSIONS

Thermogravimetric (TG) analysis combined with Fourier Transform Infrared (FT-IR) analysis of evolved products has proven to be a powerful technique for characterization of coal, source rock, heavy hydrocarbons, biomass, waste materials, and plastics. The TG-FTIR method can be used to determine the resource potential of a material, i.e., the types of products a material is likely to produce when subjected to processing by pyrolysis, or combustion. It can also provide kinetic information for model validation or extrapolation and can provide the equivalent information to proximate and ultimate analysis. In addition, TG-FTIR analysis can be used to characterize the adsorbent potential and combustion reactivity of solids.

ACKNOWLEDGEMENTS

This work was partly supported under a variety of federal government contracts and grants, primarily from the U.S. Department of Energy Morgantown Energy Technology Center, The National Science Foundation, and the U.S. Department of Defense. This support is gratefully acknowledged.

REFERENCES

1. Ottaway, W., *Fuel*, **61**, 713 (1982).
2. Ciuryla, V.T., Weimer, R.F., Bivans, A., and Motika, S.A., *Fuel*, **58**, 748 (1979).
3. Solomon, P.R., Serio, M.A., and Heninger, S.G., ACS Div. of Fuel Chem. Preprints, **31**, (3), 200 (1986).
4. Best, P.E., Solomon, P.R., Serio, M.A., Suuberg, E.M., Mott, W.R., Jr., and Bassilakis, R., ACS Div. of Fuel Chem. Preprints, **32**, (4), 138 (1987).
5. Serio, M.A., Solomon, P.R., Bassilakis, R., and Suuberg, E.M., ACS Div. of Fuel Chem. Preprints, **34**, (1), 9 (1989).
6. Mahajan, O.P., Yarzab, R., and Walker, Jr., P.L., *Fuel*, **57**, 643 (1978).
7. Suuberg, E.M., Calo, J.M., and Wojtowicz, W., ACS Div. of Fuel Chem. Preprints, **31**, (3), 186 (1986).
8. Winans, R.E., McBeth, R.L., and Neill, P.H., ACS Div. of Fuel Chem. Preprints, **33**, (3), 85 (1988).
9. Chakravarty, T., Windig, W., Hill, G.R., and Meuzelaar, H.L.C., *Energy & Fuels*, **2**, (4), 400 (1988).
10. Solomon, P.R. and Hamblen, D.G., *Progress in Energy and Combustion Science*, **9**, 323 (1983).
11. Burnham, A.K., Oh, M.S., Crawford, R.W., and Samoun, A.M., *Energy & Fuels*, **3**, 42 (1989).
12. Attar, A. and Hendrickson, G.G., *Coal Structure*, (R.A. Meyers, Ed.), Academic Press, NY, **5**, 131 (1982).
13. LaCount, R.B., Anderson, R.R., Friedman, S., and Blaustein, B.D., *Fuel*, **66**, 873 (1987).
14. Hall, P.J. and Calo, J.M., *Energy & Fuels*, **3**, 370 (1989).
15. Zhang, Z.G., Kyotani, T., and Tomita, A., *Energy & Fuels*, **3**, 566 (1989).
16. Carangelo, R.M., Solomon, P.R., and Gerson, D.G., *Fuel*, **66**, 960 (1987).
17. Carangelo, R.M., Solomon, P.R., Bassilakis, R., Gravel, D., Baillargeon, M., Baudais, F., and Vail,

- G., American Laboratory, p. 51, (1990).
18. Serio, M.A., Solomon, P.R., Charpenay, S., Yu, Z.Z., and Bassilakis, R., ACS Div. of Fuel Chem. Preprints, **35**, (3), 808 (1990).
 19. Solomon, P.R., Serio, M.A., Carangelo, R.M., Bassilakis, R., Gravel, D., Baillargeon, M., Baudais, F., and Vail, G., Energy & Fuels, **4**, (3), 319 (1990).
 20. Solomon, P.R., Serio, M.A., Carangelo, R.M., Bassilakis, R., Yu, Z.Z., Charpenay, S., and Whelan, J., Journal of Analytical and Applied Pyrolysis, **19**, 1 (1991).
 21. Solomon, P.R., Hamblen, D.G., Serio, M.A., Yu, Z.Z., and Charpenay, S., Fuel, **72**, (4), 489 (1993).
 22. Solomon, P.R., Serio, M.A., and Suuberg, E.M., Progress in Energy and Combustion Science, **18**, pp 133-220 (1992).
 23. Solomon, P.R., Serio, M.A., Carangelo, R.M., and Bassilakis, R., ACS Div. of Fuel Chem. Preprints, **35**, (2), 334 (1990).
 24. Carangelo, R.M., Serio, M.A., Solomon, P.R., Charpenay, S., Yu, Z.Z., and Bassilakis, R., ACS Div. of Fuel Chem. Preprints, **36** (2), 796 (1991).
 25. Bassilakis, R., Zhao, Y., Solomon, P.R. and Serio, M.A., Energy & Fuels, **7**, 710 (1993).
 26. Serio, M.A., Kroo, E., Charpenay, S., and Solomon, P.R., ACS Div. of Fuel Chem. Preprints, **37**, (4), 1681 (1992).
 27. Serio, M.A., Kroo, E., Teng, H., Solomon, P.R., ACS Div. of Fuel Chem. , Preprints, **38**, (2), 577 (1993).
 28. Charpenay, S., Serio, M.A., Bassilakis, R., and Solomon, P.R., "Influence of Maturation on the Pyrolysis Products from Coal and Kerogens, Part I: Experimental," Accepted in Energy & Fuels, (October 1995).
 29. Teng, H., Serio, M.A., Bassilakis, R., Knight, K.S., Bates, S.C., and Solomon, P.R., ACS Div. of Fuel Chem. Preprints, **37**, (4), 1903 (1992).
 30. Whelan, J.K., Solomon, P.R., Deshpande, G.V., and Carangelo, R.M., Energy and Fuels, **2**, 65 (1988).
 31. Bonanno, A.S., Bassilakis, R., and Serio, M.A., "TG-FTIR methods for the Evaluation of Lubricant Contamination," to be presented at ACS New Orleans meeting, March, 1996.
 32. Serio, M.A., Kroo, E., Bassilakis, R., Solomon, P.R., and Malhotra, R., ACS Div. of Fuel Chem. Preprints, **36**, (3), 1110 (1991).
 33. Serio, M.A., Charpenay, S., Bassilakis, R., and Solomon, P.R., Journal of Biomass & Bioenergy, **7**, (1-6), 104 (1994).
 34. Teng, H., Serio, M.A., Bassilakis, R., Morrison, P.W., Jr., and Solomon, P.R., ACS Div of Fuel Chemistry Preprints, **37**, (2), 533 (1992).
 35. Teng, H., Serio, M.A., Wojtowicz, M.A., Bassilakis, R., and Solomon, P.R., Industrial & Engineering Chemistry Research, **34**, 3102 (1995).
 36. Serio, M.A., Charpenay, S., Bassilakis, R., and Solomon, P.R., ACS Div. of Fuel Chem. Preprints, **36**, (2), 664 (1991).
 37. Serio, M.A., Bassilakis, R., McMillen, D.F., Satyam, A., and Malhotra, R., Intl. Conf. on Coal Science, Alberta, Canada, **II** (163) (1993).
 38. Serio, M.A., Solomon, P.R., Yang, Y.P., and Suuberg, E.M., "The Use of TG-FTIR Analysis to Determine Char Combustion Properties", presented at the AIChE Annual Meeting, Chicago, III, (Nov. 11-16, 1990).
 39. Vorres, K.S., Energy & Fuels, **4**, 420 (1990).

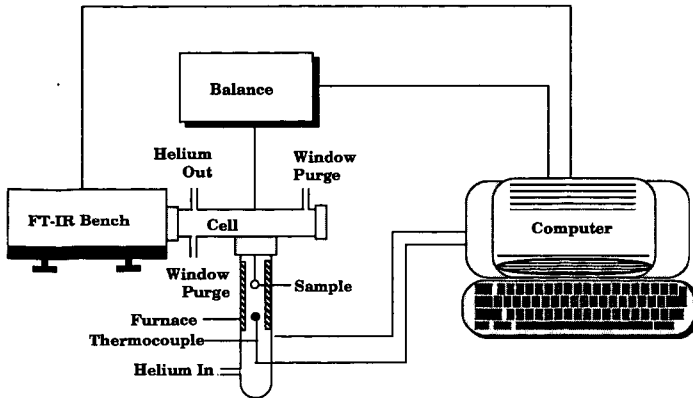


Figure 1. Schematic diagram of the standard TG/FT-IR instrument.

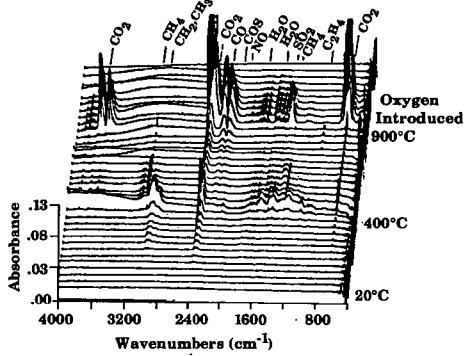


Figure 2. Spectra from TG/FT-IR of coal. Heating rate is 0.5°C/s^{-1} from 20 to 900°C . The remaining char is then burned at 700°C .

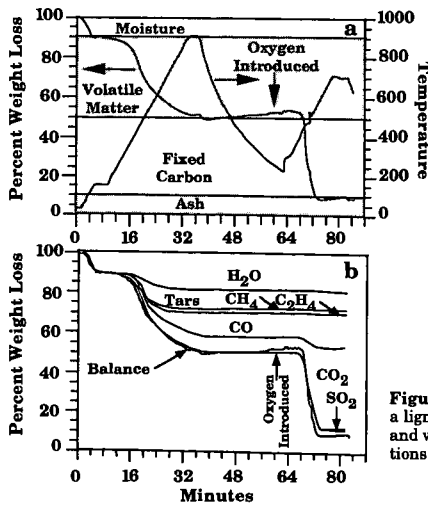


Figure 3. TG/FT-IR analysis of a lignite. a) Temperature history and weight loss; b) Species contributions to weight loss.

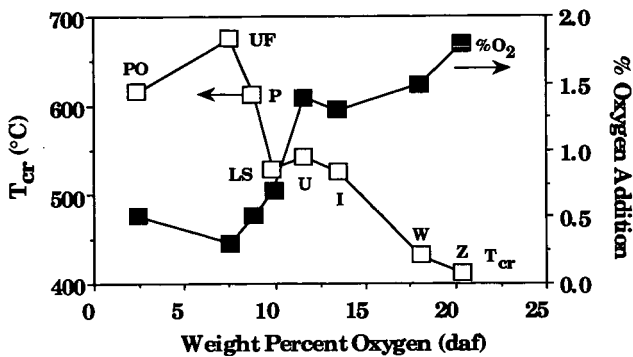


Figure 4. Rank variation of T_{cr} and oxygen chemisorption.

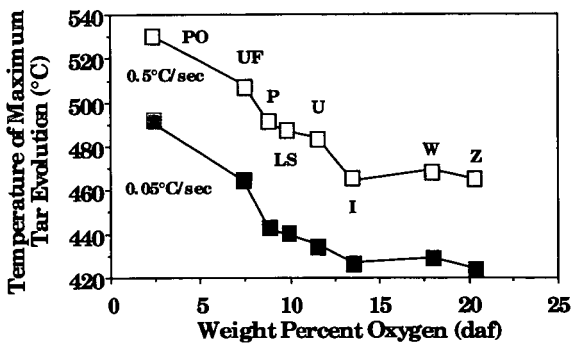


Figure 5. Rank variation of tar evolution temperature.

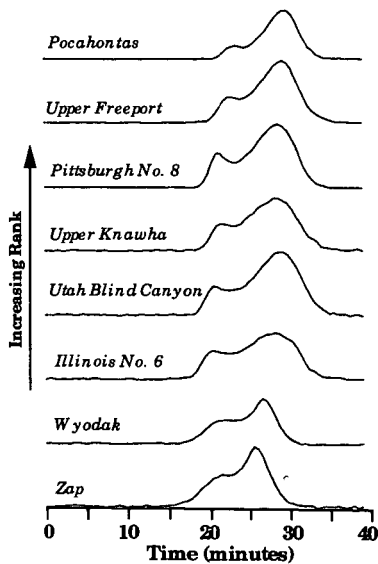


Figure 6. Evolution of NH_3 from programmed pyrolysis ($30^\circ C/min$) of the Argonne premium coals.

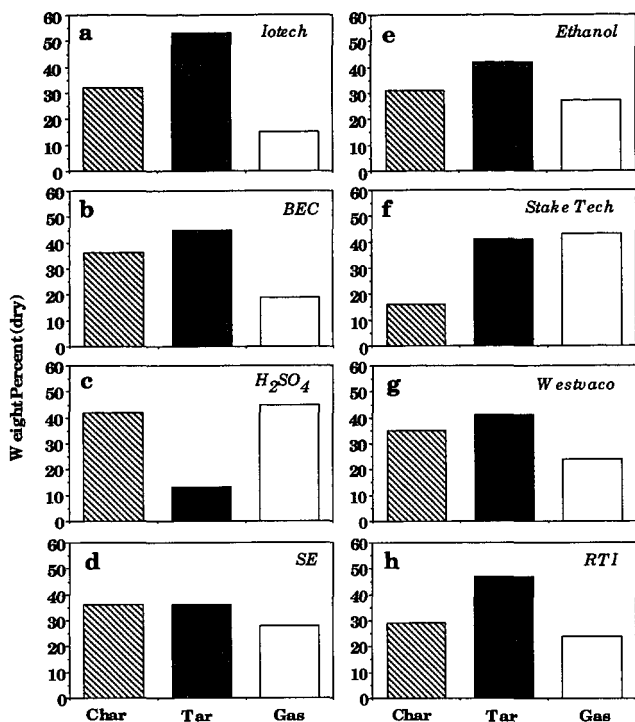


Figure 7. Comparison of char, tar and gas yields from programmed pyrolysis of eight lignins.

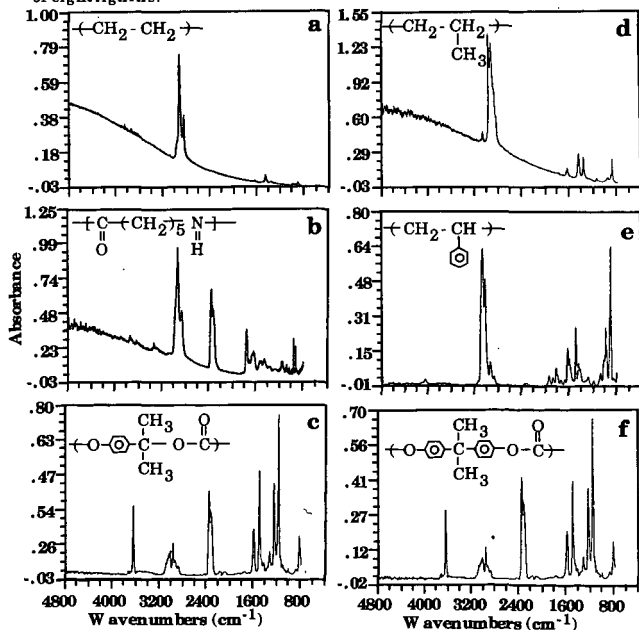


Figure 8. Comparison of IR spectra at peak temperature in tar evolution profile from TG/FT-IR analysis of several polymers. a) Polyethylene (PE); b) Nylon; c) Lexan (standard); d) Polypropylene (PP); e) Polystyrene (PS); f) Lexan (flame retardant).

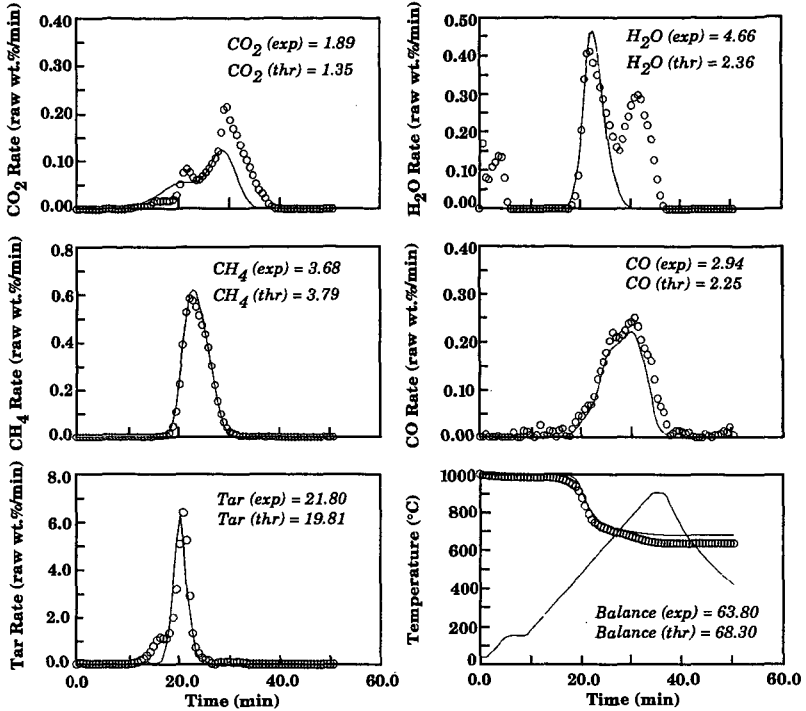


Figure 9. Comparison of TG/FT-IR data and FG-DVC model predictions for CONSOL #2 coal, pyrolyzed at 30°C/min.

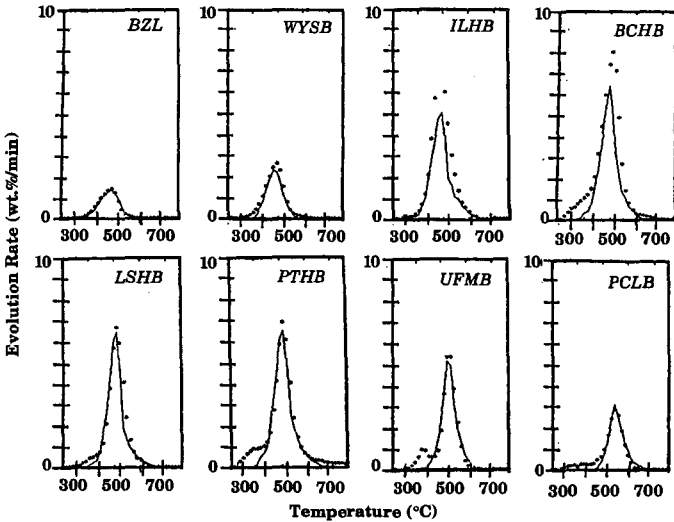


Figure 10. Comparison of measured and predicted tar evolution from pyrolysis of the eight Argonne premium coals.

A STUDY OF ON-LINE ANALYSIS OF CHLORINE DURING COAL COMBUSTION

John Napier, Jenny Heidbrink, Jennifer Keene, Hanxu Li, Wei-Ping Pan, and John T. Riley
Department of Chemistry and Materials Characterization Center
Western Kentucky University
Bowling Green, KY 42101

Keywords: Chlorine, coal, evolved gas analysis

ABSTRACT

The behavior of chlorine during the combustion of coal was studied using TG-FTIR and TG-MS systems. Parameters of the coal samples studied included variations in chlorine content, rank, and mesh size. The identification of evolved gases at different temperatures indicated three mechanisms of HCl release. The first evolution of HCl was due to thermal effects, and corresponds to the release of HCl absorbed on pore walls of the coal. The second evolution of HCl is a function of coal rank, and represents a more tightly bound chlorine associated with the hydrated coal matrix. The third evolution of HCl is a result of inorganic chlorides in the coal.

INTRODUCTION

The presence of chlorine in coal is a concern for end users of coal. This concern, if the chlorine in coals causes corrosion, has tremendous impact on the marketability of the coal. The extent of boiler corrosion due to chlorine may not be directly related to the amount of chlorine in the coal. However, it may be related to how the chlorine occurs in the coal or to other factors. During the combustion of coals of various types, the mechanisms of the release of chlorine species are influenced by many factors, such as the forms of chlorine in the coal, coal rank, and experimental conditions.

The main forms of chlorine present in coal that have been proposed are:¹

- inorganic chlorides
- chlorine ions in brine and other water associated with the coal.

Edgecomb² examined the release of chlorine as HCl in the heating of twenty-nine British coals (0.2-1.0% Cl) in dry air at 200°C for twenty-four hours. His studies showed that more than half of the chlorine is liberated as HCl at this temperature. However, Daybell suggested that chlorine in some British coals give off 97% of their chlorine as HCl in oxygen-free nitrogen at 258°C.³ Gibb observed that most of the chlorine in British coals evolved under mild conditions.⁴ Several Illinois coals were studied by Hackley and Chou using a high temperature furnace-quadrupole gas analyzer (HF-QGA) technique. They determined that the evolution of HCl from their coals began around 250°C, peaked at 495°C, and leveled off close to 600°C.⁵ Muchmore and coworkers investigated chlorine removal from an Illinois high-chlorine coal with thermal treatment followed by analysis using an electrode technique. It was concluded that 84.3% of the total chlorine in the coal was removed by preheating in nitrogen at a lower temperature prior to a six minute reaction at 385°C.⁶

These studies, reporting different coals having different chlorine release temperatures under different conditions, may provide some insight into the question concerning boiler corrosion and chlorine content. In the work reported in this paper the behavior of chlorine during combustion is investigated using relatively new techniques. The effect of chlorine content as well as rank and mesh size of coal on the evolution of chlorine species was investigated.

EXPERIMENTAL

This study used ten coal samples ranging in chlorine content (0.03-0.88%), mesh sizes (400, 200, and 60 mesh), and chemical composition as listed in Table 1. Combustion of the samples took place in an air atmosphere under either of two heating methods. The dynamic heating method, a steady increase in temperature with time, enables a view of the complete combustion process. The second, an isothermal heating method, allowed for the isolation and separation of HCl emission mechanisms. The isothermal method consists of steadily heating the sample to a certain temperature, holding at the temperature for a designated amount of time, followed by a continuation of the temperature increase.

Analyses of the combustion process and evolved gases were obtained utilizing TG-FTIR and TG-MS systems. The thermogravimetric (TG) studies gave combustion profiles in terms of weight loss and rate of weight loss and were done with either a DuPont 951 or a TA Hi-Res TGA 2950 thermogravimetric analyzer. By coupling the instruments with a VG Thermolab Quadrupole Mass Spectrometer (MS) one can identify and quantify evolved gases by their molecular weights. Interfacing a TG with a Perkin

Elmer 1650 Fourier Transform Infrared Spectrometer (FTIR) allows one to confirm the identified gases and distinguish between gases of the same molecular weights.

RESULTS AND DISCUSSION

Figure 1 is a typical thermogram showing the analysis of the combustion of a coal sample using the dynamic heating method. One can follow the transitions through the combustion process by noticing changes in both the TG curve showing weight loss and the DTG curve showing rate of weight loss. Points of interest on the DTG curve are the changes in weight loss rate at 300°C, 400°C, and 447°C. The region containing these points in order show: (1) a devolatilization zone, (2) an overlapping weight loss due to the initial combustion of the fixed carbon at the 400°C inflection point, and (3) a weight loss, due to combustion, with a maximum at 447°C (DTG peak maximum).

Mass spectroscopic profiles given in Figure 2 show the evolution of SO₂ (64), H₂O (18), CO₂ (44), HCl (36), and either acetic acid (60) or COS (60) during dynamic heating. The peak maximum for rate of weight loss in the TG curve corresponds to the peak maxima of CO₂ and SO₂ emissions at 447°C. The m/z = 60 peak follows the HCl and water curves by 10°C. FTIR on-line analysis shows the first peak in the m/z = 60 curve to be due to the evolution of acetic acid while the second peak is due to COS.

The emission of HCl and H₂O begins at 200°C, peaks at 300°C, and subsides. Their second peaks appear at 400°C with a maximum at 440°C before leveling off around 500°C. This indicates two mechanisms of chlorine release involving water. Expansion of the HCl curve shows a small third peak occurring at 700-800°C.

Employment of the isothermal heating method revealed HCl and water emissions as the temperature approached 300°C, as illustrated in Figure 3. At that point (30 min, 300°C) the temperature was held constant for one hour with no emissions occurring. Continuation of the temperature increase produced the second emission of HCl and water confirming two separate mechanisms, thus illustrating two different structures of chlorine bonding in the coal.

The first HCl peak is due to thermal effects and consistently peaks around 300°C for all coals. Due to the greater amount of energy needed to break the bonds, the second peak represents a more tightly bound chlorine released during the oxidation of the coal. The second peak is a function of coal rank due to its direct relationship with coal DTG maxima as is illustrated in Figure 4. DTG analyses of the coals indicate higher ranking coals having higher maximum rates of combustion. The higher temperature DTG peaks and higher ranking coals correspond to higher temperature maxima for the second HCl emissions.

A quantitative study of the evolution of HCl and SO₂ versus the content of the chlorine and sulfur in the coal was obtained by integrating the area under the HCl peaks in the mass spectra. A good agreement ($R^2 = 0.997$ for chloride and $R^2 = 0.942$ for sulfur) was obtained between the chlorine content and the total amount of HCl evolved, as is illustrated in Figure 5. This figure also provides evidence that most of chlorine in coal is released in the form of HCl during combustion. The slightly lower coefficient obtained for the sulfur is due to the limitation of TG systems. The TG system can only be heated to 1000°C. According to ASTM Method D 4239, the coal should be heated to 1400°C to identify the sulfate species. Thus, the temperature difference may cause the slightly lower correlation coefficient.

Mesh size also played a role in determining the temperature of HCl evolution. The smaller mesh coal produced emissions at a lower temperature. Smaller particle size, such as 400 mesh, has a higher surface-to-volume ratio allowing less hindrance to the devolatilization of the chlorine attached to the coal pores and surface.

CONCLUSIONS

Thermal analytical techniques reveal there are three HCl evolution peaks, indicating three different types of chlorine bonding to the coal. The first HCl evolution peak, due to thermal effects, is the release of HCl normally absorbed on pore walls. The second peak, a function of the coal rank, represents a more tightly bound chlorine associated with the hydrated coal matrix. A third peak is a result of inorganic chlorides in the coal.

Thermal analytical and mass spectral data indicate a good correlation between chlorine content in the coal and the total amount of HCl evolved. Results also show the smaller particle sizes of the coal cause HCl evolution to occur at a lower temperature.

ACKNOWLEDGEMENTS

The authors gratefully acknowledge the financial support of the Electric Power Research Institute, the National Science Foundation through the Research at Undergraduate Institutions Program, and a KY-USDOE/EPSCOR Traineeship.

REFERENCES

1. Sloss, L.L. "Halogen Emissions from Coal Combustion," IEACR/45, IEA Coal Research, London, February, 1992.
2. Edgecomb, L.J. *Fuel*, 1956, 35, 38.
3. Daybell, G. N. *Fuel*, 1958, 37, 283.
4. Gibb, W. H. "The Nature of Chlorine in Coal and Its Materials for Coal Conversion System," (Eds. Meadowcroft, D. B. and Manning, M. I.), Applied Science Pub., London, UK, Ch. 2, 1982, 25-45.
5. Chou, C.L.; Hackley, K.C.; Cao, J.; More, D.M.; Xu, J.; Rech, R.R.; Pan, W.-P.; Upchurch, M.L.; Cao, H.B. "Behavior of Sulfur and Chlorine in Coal During Combustion and Boiler Corrosion," Illinois Clean Coal Institute, Final Technical Report, Carterville, IL, August, 1993.
6. Muchmore, C. B.; Hesketh, H. E.; Chen, H.L. "Thermal Treatment for Chlorine Removal From Coal," Center for Research on Sulfur in Coal," Technical Report, Carterville, IL, July 1992.

Table 1. Ultimate Analysis Data (Dry Basis) for Coals Studied

Coal	Cl	C	H	O	N	S	Ash
A	0.88	79.75	5.37	8.20	1.55	0.94	3.23
B	0.39	63.95	4.21	6.31	1.29	1.31	22.24
C	0.38	70.34	4.25	6.55	1.54	1.02	16.10
D	0.26	75.40	4.92	6.70	1.50	2.94	8.17
E	0.16	72.29	4.99	7.13	1.27	4.47	9.71
F	0.20	86.71	4.23	2.17	1.27	0.66	4.77
G	0.13	66.20	4.21	7.10	1.25	0.71	19.84
H	0.04	65.85	4.36	18.19	1.25	0.80	9.72
I	0.03	68.43	4.88	16.24	1.02	0.63	8.77
J	0.03	76.89	5.49	10.76	1.50	0.62	4.71

Sample: COAL 33501 P-8#10-5
 Size: 20.4480 g
 Method: COAL
 Comment: IT-100C HT-15V HV-1638 MSFILE=ICCI607 70EV HT TEST

TGA

File: C:ICCI607
 Operator: PAN 10C/MIN TO 890
 Run Date: 28-Mar-95 02:55

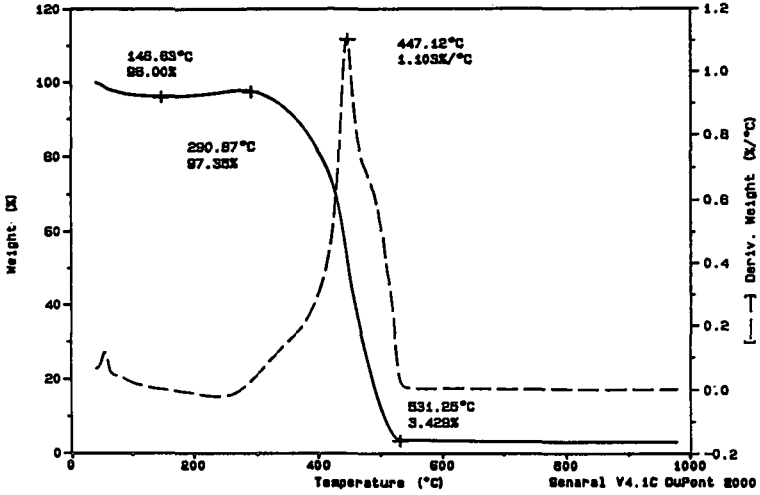


Figure 1. TG curve for the combustion of coal A in air.

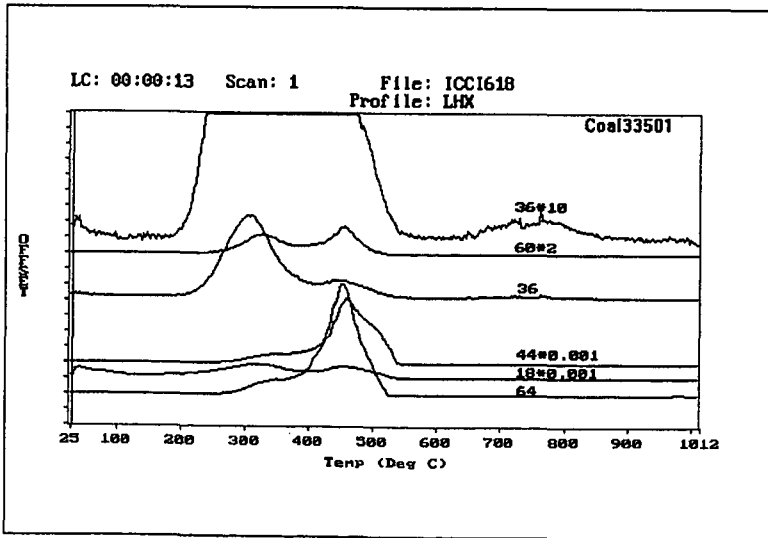


Figure 2. Mass spectrometric evolved gas profiles for the combustion of coal A.

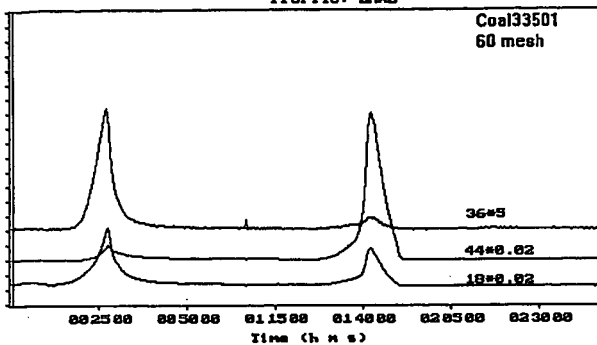


Figure 3. Mass spectrometric evolved gas profiles for combustion of coal A under isothermal conditions.

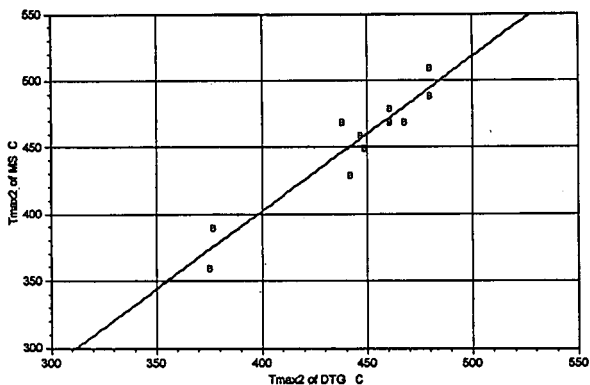


Figure 4. T_{max2} values from DTG curves versus T_{max2} values from mass spectra.

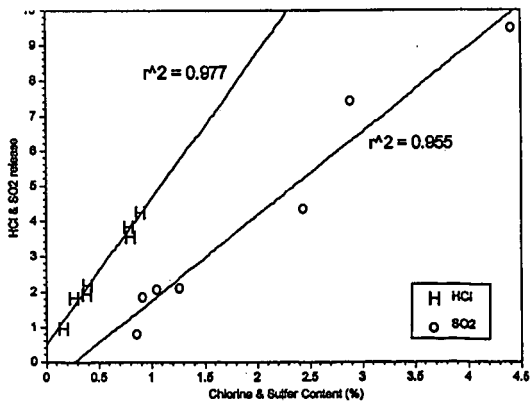


Figure 5. HCl and SO₂ release versus chlorine and sulfur content in coals.

TG/MS STUDY OF ORGANIC COMPOUNDS EVOLVED DURING THE CO-FIRING OF COAL AND REFUSE DERIVED FUELS

Shobha Purushothama, Richard Lu, Xiaodong Yang, John Hyatt,
Wei-Ping Pan, John T. Riley, and William G. Lloyd
Department of Chemistry and Materials Characterization Center
Western Kentucky University
Bowling Green, KY 42101

Key words: Evolved gas analysis, coal and RDF, co-firing

INTRODUCTION

The Environmental Protection Agency reported that the total municipal solid waste (MSW) produced in the U.S. increased from 179 million tons in 1988 to 195 million tons in 1990.¹ It is predicted that the country will produce about 216 million tons of garbage in the year 2000.² Waste-to-energy conversion of MSW appears to be most attractive because of the energy recovered, economic value of the recycled materials, and the cost saving derived from reduced landfill usage. However, extra care needs to be taken in burning MSW or Refuse Derived Fuel (RDF) to optimize the operating conditions of a combustor so that the combustion takes place in an environmentally acceptable manner. For instance, polychlorinated dibenzodioxins (PCDDs) and polychlorinated dibenzofurans (PCDFs) have been found in the precipitator fly ash and flue gas of a number of incinerator facilities in the United States and Europe. Though the amount of PCDDs and PCDFs is only in the parts-per-billion to parts-per-trillion range, these chlorinated organics exhibit very high toxicity ($LD_{50} < 10 \mu\text{g/Kg}$) and 2,3,7,8-tetrachlorodibenzodioxin has been found to be acenegenic, carcinogenic, and teratogenic. This has slowed or even stopped the construction and operation of waste-to-energy plants. In previous work,³ the study of single materials has given us a good understanding of the characteristics and thermal behavior of these materials, their relative thermal stability and temperature relationships, their decomposition products and the evolution profiles of different gaseous products. The formation of molecular chlorine during combustion processes could be a key step for the formation of chlorinated organic compounds. The production of phenol and furan during the combustion of newspaper and cellulose could provide the important precursors for the formation of polychlorinated dibenzodioxin (PCDD) and polychlorinated dibenzofuran (PCDF).

EXPERIMENTAL

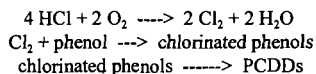
Materials used in this study include two coal samples (92073 - a KY #9 coal and 90003 - an IL #6 coal), PVC (OxyChem Corporation), cellulose (Whatman Corporation), and newspaper. The TG/MS system consists of a DuPont Instruments Model 951 Thermogravimetric Analyzer interfaced with a VG Thermolab Mass Spectrometer. The detection range of the TG/MS system is 1-300 atomic mass units (amu). Electron impact ionization energy is 70 eV. A sample size of ~20 mg was heated in air (50 mL/min) at a slow heating rate of 10°C/min to 700°C and a fast heating rate of 100°C/min to 900°C then held at the maximum temperature for five minutes. The MS system can automatically sample the gases evolved from the TG system, analyze them with its quadrupole analyzer, and save the spectra. The detailed experimental conditions are discussed in Lu's thesis.⁴

RESULTS AND DISCUSSION

Comparing the TG curves for the five raw materials (coals 92073 and 90003, PVC, cellulose, and newspaper) shows that the coals have a higher decomposition temperature and slower weight loss rates compared to the other materials. PVC, newspaper and cellulose show three distinct weight loss stages. At the fast heating rate similar results were obtained except that the weight loss shifts to higher temperatures (T_{max}) and the rate of maximum weight loss (R_{max}) increases. This indicates that the decomposition reactions of fuels occur much faster and at higher temperatures as the heating rate increases. The decomposition at the slow heating rate was studied in order to understand the mechanism of each stage. The study at the fast heating rate was done to approach the firing conditions of an atmospheric fluidized bed combustor (AFBC) unit. The heating rates in an AFBC system are much faster than those of the TGA experiments. Thus it is expected that the decomposition reactions occur at higher T_{max} and R_{max} values in the AFBC systems.

The evolved gases were identified using two analytical systems, TG/FTIR and TG/MS. The TG/FTIR system can be used to identify compounds with different functional groups and similar masses. The TG/MS can be used to identify species such as Cl_2 , O_2 , and N_2 which cannot be detected using FTIR techniques. The results show that at a fast heating rate the decomposition reactions are

compressed into a narrow time range. Hence the decomposition stages cannot be separated as is done with the slow heating rate. The FTIR data indicate that more hydrocarbons are produced at fast heating rates whereas more oxidation products are obtained at slow heating rates. Mass spectrometric results indicate that chlorine molecules are produced concurrently with HCl during the decomposition of PVC. The ratio of HCl/Cl₂ produced is around 150. This suggests that some of the abundant HCl could undergo a thermal Deacon reaction. This reaction is favored up to 600°C at atmospheric pressures. The Deacon reaction (given below) could provide a plausible starting point for the formation of chlorinated dioxins from the combustion of chlorine rich fuel mixtures.⁴ The suggested mechanism is as follows:



The study of single materials gives a good understanding of the characteristics and thermal behavior of these compounds, their relative thermal stability, and the evolution profiles of different gaseous decomposition products. This will help in the analysis of thermal decomposition products of blends and in the evaluation of their combustion kinetics and interactive mechanisms.

A series of experiments on blends (containing different amounts of coal, PVC, newspaper and cellulose) was conducted at both heating rates. PVC, which is a major source of chlorine, accounts for only 1% of MSW. A greater amount was used in these studies to investigate the conditions and mechanism for the formation of the chlorinated species. At a slow heating rate it is possible to evaluate kinetic and dynamic changes occurring during combustion. The studies at a fast heating rate will provide a better picture of combustion performance in an AFBC system.

The blends used in this study were manually prepared and labeled as follows:

- Blend 1: 03PVC is a mixture of coal 90003 and PVC (50% each);
- Blend 2: 03NEW is a mixture of coal 90003 and newspaper (50% each);
- Blend 3: 03Cell is a mixture of coal 90003 and cellulose (50% each);
- Blend 4: 03PN is a mixture of coal 90003 (50%), PVC (25%), and newspaper (25%);
- Blend 5: 035122 is a mixture of coal 90003 (50%), PVC (10%), newspaper (20%), and cellulose (20%);
- Blend 6: 73PVC is a mixture of coal 92073 and PVC (50% each);
- Blend 7: 73NEW is a mixture of coal 92073 and newspaper (50% each);
- Blend 8: 73Cell is a mixture of coal 92073 and cellulose (50% each);
- Blend 9: 73PN is a mixture of coal 92073 (50%), PVC (25%), and newspaper (25%);
- Blend 10: 735122 is a mixture of coal 92073 (50%), PVC (10%), newspaper (20%), and cellulose (20%).

1. TG/DTG Results

Table 1 is a summary of the TG/DTG results at both heating rates for all the blends. It can be seen that the maximum rates of major weight loss (R_{\max}) at the fast heating rate are much higher than those at the slow heating rate. For example, decomposition increases from 10%/min to 62%/min for blend #35122. This indicates that the decomposition reactions of fuels occur at a faster reaction rate as the heating rate increases. Since the heating rates in an AFBC system are much faster than those in TGA experiments it can be expected that decomposition reactions will occur at greater R_{\max} in AFBC systems.

On comparison with data for single materials, there is an important difference. For most blends, the combustion profiles are compressed into a continuous stage of weight loss at the fast heating rate. This means that the different decomposition stages for most blends can be separated from each other only at a slow heating rate. It is difficult to distinguish each decomposition stage in the combustion profiles at the fast heating rate, except for the moisture loss stage. Unlike those at the slow heating rate, the profiles of decomposition reactions for most blends display only one continuous weight loss at the fast heating rate. Also, the T_{\max} in the compressed profiles are in between the two T_{\max} values at the slow heating rate. For example, T_{\max} for H73PN is 344°C but T_{\max} for 73PN is 336°C and 432°C.

Figure 1 is a comparison of TG curves for blend 035122 and its components, coal 90003, PVC, cellulose, and newspaper; at the slow heating rate. The blend has a much lower decomposition temperature than the coal because of mixing with the easily decomposing components, (with high

volatile matter content), newspaper, cellulose, and PVC. This indicates that there are some mutual chemical interactions among the components during the combustion process. For the blend curve, the first weight loss is due to moisture. The second weight loss comes from the decomposition of PVC, newspaper and cellulose. The third weight loss is due to combustion of coal and carbon residues from PVC. It is possible that the combustion of newspaper, cellulose and PVC induce the shift of the coal combustion to a much lower temperature. The temperature at 50% weight loss ($T_{1/2}$) for coal is about 500°C and 370°C for the blends.

At the fast heating rate, the same trend is observed, the blend decomposes at much lower temperatures than the coal ($T_{1/2}$ for coal is ~750°C and ~450°C for blend). Compared with the blend curve at the slow heating rate the combustion profile of the blend becomes more continuous so that the second and third weight losses, which were clearly seen previously, cannot be definitely separated, indicating that combustion behavior is different at different heating rates.

2. Mass Spectrometry Results

Table 2 summarizes the tentative identification of some peaks in the MS spectra of blends 1 to 10 at the slow and fast (with a prefix "H-") heating rates. The compounds in bold type are also detected by the gas trap and GC/MS techniques. It is difficult to clearly interpret the complicated spectra obtained from the combustion of all the blends and attention was given to the sulfur and chlorine species in the evolved gases.

Figure 2 shows some mass profiles at the slow heating rate for blend 9(73PN). There are two major decomposition stages shown in this figure. The first stage occurs around 300°C. In this stage, HCl (36 and 38) and chlorine (70, 72 and 74) from PVC, furan (68) and furfural (96) from newspaper are major products. The second stage is at around 340°C. In this stage, larger molecules, toluene (92), methyl thiophene (98), xylene (106), chlorobenzene (112), and naphthalene (128) start evolving, which indicates that the coal begins to decompose. Phenol is also identified from the decomposition of newspaper. These two stages correspond to the second weight loss in the TGA curve.

There are similar results in Figure 3 (blend 5, file 035122). The peaks 60 (carbonyl sulfide) and 64 (sulfur dioxide) display the same changes as observed in coal 92073, i.e., sulfur dioxide has three decomposition phases and carbonyl sulfide has only two. In the profiles for HCl and molecular chlorine there are some differences. The HCl and molecular chlorine show two peaks at about 300°C and 340°C. The first peak may be attributed to the decomposition of PVC. The second peak is due to the decomposition of coal 90003 (high chlorine, low sulfur) and newspaper. An important fact is that molecular chlorine, phenol and furan are released at the same temperature range. This indicates that there is some possibility for the formation of chlorophenol at this temperature. However, it is difficult to identify chlorophenol from TG/MS studies due to two reasons. First, the amount of phenol ($m/z = 94$) present in the gas phase is very small. Secondly, chlorophenol has the same mass, 128, as naphthalene. These two species cannot be distinguished from each other in the TG/MS system. This problem can be resolved using a separation system. In tubular furnace studies more sample can be loaded, increasing the amount of phenol produced. Also the GC/MS system can separate the components prior to identification. The results from 10 grams of blend sample show that naphthalene is a major product and small amounts of chlorophenol is also identified. The results using 100 mg phenol as sample and 0.5% chlorine in nitrogen as purge gas and the same heating rate show that mono-, di-, and tri-chlorophenols can be formed. This indicates that during co-firing coal with MSW, either the amount of phenol produced is too small to form chlorophenol, or the amount of the produced chlorophenol is too small to be detected by the TG/MS system.

Comparison of the evolved gases at slow and fast heating rates show trends very similar to those of the individual raw materials. More hydrocarbons and chlorinated species are formed during the same time span at the fast heating rate whereas they evolve at different times at the slow heating rate.

CONCLUSIONS

- The TG/FTIR/MS system was used to identify molecular chlorine, furan, phenol and other aromatic compounds, along with HCl, CO, CO₂, and H₂O in the gaseous products of the combustion of coal, PVC resin, newspaper, and cellulose in air. This is a significant finding that will lead us to study this combustion step further to look for the formation of chlorinated organic compounds.
- The TG/MS techniques allow the study of reaction pathways for the formation of gaseous products during combustion.

ACKNOWLEDGMENTS

The authors gratefully acknowledge the financial support of the following agencies: The U.S. Department of Energy through the University Coal Research Program (DE-FFG-22-94 PC 94211), the National Science Foundation through the Research at Undergraduate Institutions Program (CHE-9320182), Huntsman Thermal Analysis Fellowship, and the U.S. Department of Energy University Coal Research Internship Program.

REFERENCES

1. Steuteville, R. "What is New in the Waste Stream," *Biorecycle*, **1992**, *33*, 10.
2. Dichristina, M. "How We Can Win the War Against Garbage," *Popular Science*, **1990**, *237(10)*, 57.
3. Lu, H.; Purushothama. S.; Yang, X.; Pan, W.P.; Flynn, J.; Gill, P. "Co-firing High Sulfur Coal with Refuse Derived Fuel," *Proceedings 24th NATAS Conference*, **1995**, 414-417.
4. Lu, H. "A Study of Combustion of Coal with RDF Using Thermal Analytical Techniques," M.S. Thesis, Western Kentucky University, **1995**.

Table 1. Summary of TG/DTG Results for Blends

Sample	$\Delta W_2(\%)$	T_{max}	R_{max}	$\Delta W_3(\%)$	T_{max}	R_{max}
03PVC	30	307	6	64	457	6
H03PVC	42	354	71	55	435	32
03New	30	340	19	59	463	8
H03New	93	349	41			
03Cell	43	341	17	48	442	18
H03Cell	92	361	67			
03PN	27	302	7	64	419	13
H03PN	94	345	81			
035122	49	300	10	44	444	7
H035122	51	324	62	39	595	13
73PVC	37	306	7	51	437	5
H73PVC	82	347	57			
73New	51	337	33	24	444	14
H73New	73	374	99			
73Cell	53	346	23	30	423	19
H73Cell	82	383	99			
73PN	52	336	31	29	432	12
H73PN	85	344	98			
735122	40	300	6	42	418	8
H735122	49	331	70	43	538	12

Note: R_{max} is maximum rate of weight loss, %/min; T_{max} is the temperature at R_{max} , °C; ΔW is the weight loss.

Table 2. Tentative Parent Structures of MS Peaks for Coal 92073 Blends

Name	B6	HB6	B8	HB8	B9	HB9	B10	HB10
dimethylnaphthalene		156						
vinyl naphthalene		154						
acenaphthene			154					
biphenyl			154					
methylbenzothiophene	148			148	148	148		
dichlorobenzene	146			146	146	146		
indan-1,3-dione	146			146	146	146		
methylnaphthalene		142		142	142	142		
decene		140		140	140	140		
ethylxylene		134	134		134	134	134	
tetrahydronaphthalene	132			132	132	132		
naphthalene		128	128		128	128	128	
chlorotoluene	126	126		126	126	126		
propylbenzene	120	120		120	120	120	120	
ethylmethylbenzene	120	120		120	120	120	120	
trimethylbenzene	120	120		120	120	120	120	
indene		116	116			116		116 116
chlorobenzene	112	112		112	112		112	112 112
octene	112	112		112	112		112	112 112
xylene	106	106	106	106	106		106	106 106
ethylbenzene	106	106	106	106	106		106	106
3-methyl-2-furanone	98	98	98	98	98		98	98 98
methylthiophene	98	98	98	98	98		98	98 98
furfural	96	96	96	96	96		96	96 96
phenol	94	94	94		94		94	94 94
toluene	92	92	92	92	92		92	92 92
thiophene	84	84	84	84	84		84	84 84
benzene	78	78	78	78	78		78	78 78
furan/1,3-pentadiene	68	68	68	68	68		68	68 68
SO ₂ /1,3-pentadiene	64	64	64	64	64		64	64 64

"H-" prefix means the fast heating rate was used. "B + number" means the blend + number. The compounds in bold type indicate those also detected by the GC/MS system.

COMPARISON FOR BLEND AND ITS COMPONENT TGA CURVES
 File: 035122.018 80003.006 PVC.002 NEWSPAPER.020 CELLULOSE.003

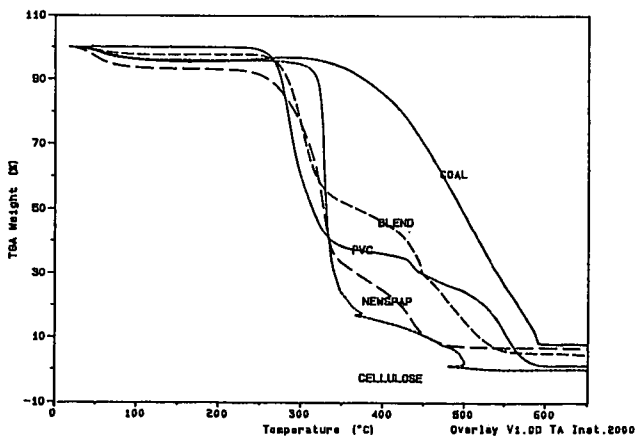


Figure 1. TG curves for blend 035122 and the four components of the blend.

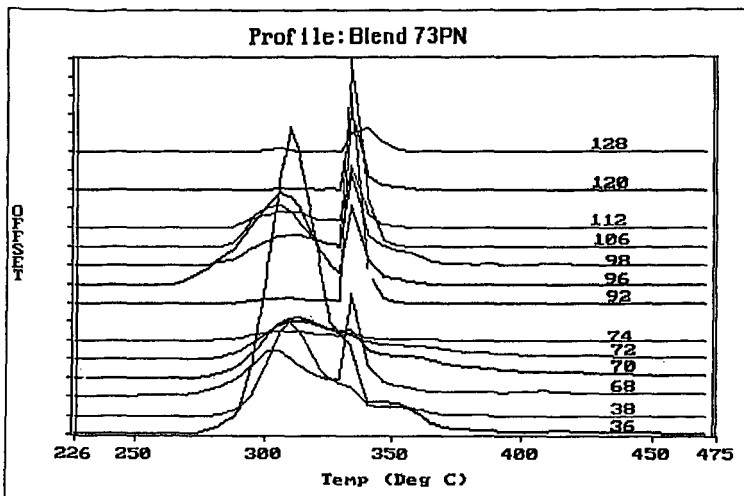


Figure 2. Profiles of m/z values for combustion products of blend 9(73PN).

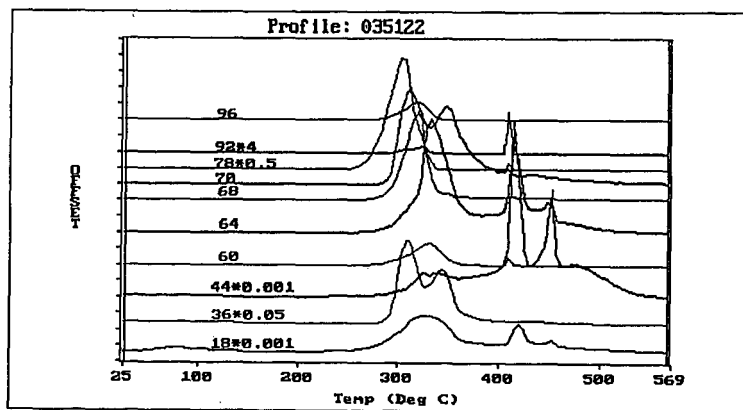


Figure 3. Profiles of m/z values for combustion products of blend 5(035122).

TG-FTIR METHODS FOR THE EVALUATION OF LUBRICANT CONTAMINATION

Anthony S. Bonanno, Rosemary Bassilakis and Michael A. Serio

Advanced Fuel Research, Inc.
87 Church Street
East Hartford, CT 06108

Keywords: Thermal Analysis, FT-IR Spectroscopy, Lubricants

ABSTRACT

A typical Air Force base will produce several thousand gallons per year of used turbine engine lubricants (1-5). The potential for contamination of the collected lubricants, particularly with halogenated compounds such as degreasing solvents and other fluids, reduces the effectiveness of a previously developed reclamation process. In this project, the feasibility of using two different thermal/FT-IR analysis methods in combination with advanced data analysis techniques to detect contamination in used turbine engine lubricants was investigated. The first method, TG/FT-IR combined with advanced data analysis routines, was shown to be capable of detecting the presence of several different types of contaminants in synthetic lubricants at concentrations of about 5%. It was demonstrated that data analysis routines based on factor analysis (SIMCA) and neural networks could be used for identifying the presence of a contaminant. The second method, TG/secondary oxidation/FT-IR, was developed specifically for detecting trace levels of chlorinated contaminants in lubricants. Optimization of this method using existing instrumentation led to a detection limit of about 300 ppm (w/w) organic chlorine in the lubricant. Further improvements in hardware and software components could lead to detection limits of <10 ppm. This instrumentation could also be used to characterize used motor oils, cooking oils or pyrolysis oils.

INTRODUCTION

The Dalton Process is a proprietary process for reclaiming synthetic ester based turbine lubricants (MIL-L-7808 and MIL-L-23699) for reuse (1,3,4). Under controlled collection of the used lubricants, this process has been shown to give as high as 95% yield of virgin lubricant (4). However, contamination of the used lubricants greatly reduces the yield of the reclamation process, and since supervised collection of used lubricants is not feasible, methods are required to rapidly determine the presence of unacceptable levels of contamination. Likely contaminants are volatile hydrocarbons in the form of kerosene type turbine fuels, domestic paraffins, petroleum naphthas, and chlorinated degreasing agents such as trichloroethylene. Previously used methods of identifying contaminated lubricant samples involved classifying the samples on the basis of appearance and odor (normal or abnormal), and subjecting the samples to a series of analytical tests in order to determine parameters such as volatile contaminant content, volatile hydrocarbon content, mineral oil content, and foaming propensity (3). The results of these analyses were used to specify whether a used lubricant sample was suitable for reclamation. A more rapid and objective method of classifying used lubricants and related materials is needed. Thermogravimetric (TG) analysis combined with Fourier Transform Infrared (FT-IR) analysis of evolved products has been used at Advanced Fuel Research, Inc. (AFR) and elsewhere for characterization of a variety of hydrocarbon materials (6,7). The objective of the current study was to investigate the application of TG-FTIR methods for the evaluation of lubricant contamination.

The successful development of a TG-FTIR based lubricant evaluation instrument would allow non-technical Air Force personnel to rapidly and reproducibly determine whether used lubricants are suitable for reclamation or reuse. This type of instrumentation would also find several uses in the commercial sector. These include analysis of used motor oils and of oils produced from post-consumer plastics. The processing of corn oil and cotton seed oil often results in the contamination of residual "soapstock" with chlorinated hydrocarbons, which prevents recovery of the useable oil through acidulation. The recovery of useable motor oil by supercritical fluid extraction is currently being evaluated. The value of the recovered oil is directly related to the amount of residual organochlorine in the extract.

EXPERIMENTAL

Sample Selection and Preparation

The Air Force provided two types of synthetic turbine lubricants (MIL-L-7808 and MIL-L-23699) from two different sources (Mobil and Hatco). The contaminants of primary interest were halogenated compounds, therefore, three chlorinated compounds were selected as representative contaminants for this work: trichloroethylene (TCE), dichloromethane, and *ortho*-dichlorobenzene (o-DCB). Other contaminants of interest included fluids that could routinely be found at an Air Force base and could potentially contaminate the used lubricants. A set of representative fluids was collected from commercial sources. These included methanol, motor oil (Castrol GTX 10W30), hydraulic jack oil (Gold Eagle),

brake fluid (Prestone), turbine fuel (Jet A), diffusion pump silicone oil, and Dow-Corning silicone oil (DC-200). The primary constituents of these fluids are given in Table 1.

Table 1. List of the lubricants and contaminants analyzed.

Type of Fluid	Primary Constituents
MIL-L-7808, MIL-L-23699	polyol esters
motor oil, hydraulic oil	mineral oils
brake fluid	polyalkylene glycol ethers
turbine fuel (Jet A)	aliphatic hydrocarbons
diffusion pump oil	poly(dimethyl/diphenyl siloxane)
DC-200 silicone oil	polydimethylsiloxane

A preliminary spectral analysis revealed that the MIL-L-7808 and MIL-L-23699 lubricants were quite similar. Consequently, further study was limited to the Mobil MIL-L-23699 lubricant. The samples analyzed included the pure lubricant, the pure "contaminants," and the lubricant spiked with a known amount of a given contaminant. The spiked samples were prepared by pipetting the required volume of the contaminant into a graduated cylinder and topping off with the lubricant. In order to minimize errors due to loss of volatile components, each sample was prepared immediately prior to analysis.

Lubricant Analysis Studies

TG/FT-IR Instrument - The combined thermal/FT-IR analysis technique is an extension of the TG/FT-IR (thermogravimetric analysis with FT-IR analysis of the evolved species) instrumentation developed by AFR and sold commercially by Bomem, Inc. as the "TG/Plus". The details of the TG/FT-IR method and instrumentation have been described previously in the literature (6-8), but a brief description will be given here. The apparatus, illustrated schematically in Figure 1, consists of a sample pan suspended from a balance within a furnace. As the sample is heated, the evolving volatile products are carried out of the furnace by an inert gas stream directly into a 5-cm diameter multi-pass gas cell (heated to 150 °C) for analysis by FT-IR. Spectra are obtained at specified time intervals in order to quantitatively determine the evolution rate and composition of the evolved products. The sample can be subjected to programmed temperature ramp rates between 3 °C/min and 100 °C/sec, with a temperature range of 20 to 1000 °C. The system monitors the time dependent evolution of specific gases, the heavy liquid evolution rate and its infrared spectrum with identifiable bands from the functional groups, the mass loss during the run, and the mass of the non-volatile residue remaining at the end of the run. An analysis of C, H, N and S in the residue can be obtained at the end of the pyrolysis experiment by introducing oxygen and analyzing the combustion products.

TG/FT-IR analysis of lubricant samples - Two specific problems were encountered during the initial TG/FT-IR analysis of the synthetic lubricant samples (9). It was found that the lubricant samples volatilized very rapidly, thus resulting in a high concentration of aerosol in the FT-IR gas cell. The high aerosol concentration resulted in significant scattering, and therefore the spectra appeared to be distorted. Additionally, the sample condensed on the quartz tube between the furnace and the flow cell, and then re-volatilized as the furnace reached a higher temperature. This limited the ability to correlate between the FT-IR data and the TG balance data. A method was developed that would result in slower evolution of the sample in order to improve the results. The lubricant was adsorbed onto pre-pyrolyzed sand and was crimped in a stainless steel boat. This was found to significantly slow the rate of evolution of the lubricant, and also limited the condensation of evolved products.

Using this sample introduction method, several samples were run in the standard TG/FT-IR mode using a temperature profile with a ramp rate of 30°C/min and a sample size of about 10 mg. The samples included the Mobil 23699 lubricant, the contaminants listed in Table 1, and the lubricant spiked with the contaminants (usually at a concentration of 5%). The spectra obtained during the runs were then converted to a format compatible with Spectra Calc data processing software (Galactic Industries, Salem, NH) for further analysis.

TG/secondary oxidation/FT-IR analysis of lubricant samples - TG/FT-IR with secondary oxidation or pyrolysis allows the evolved species to be oxidized or further pyrolyzed before passing into the FT-IR gas cell. The secondary oxidation unit consists of a quartz tube through which the evolved species flow prior to entering the gas cell. The tube houses a resistive platinum element which is used to heat the evolved species to 800-900 °C. A 15 mL/min flow of preheated gas is introduced just prior to the heater; helium is used for the secondary pyrolysis mode, and oxygen is used for the secondary oxidation mode.

RESULTS AND DISCUSSION

Detection of General Contamination in Synthetic Lubricants

SIMCA analysis for contaminants - In the development of a methodology to detect contamination in used turbine engine lubricants, the data analysis routine must be designed to answer specific questions. If specific contaminants are likely to be encountered, for example, silicone oil, then one could ask "Is there any silicone oil in the lubricant?" Then a spectral analysis routine could be developed to look for the IR bands characteristic of silicone. The question being asked in this case is more general; "Is there anything out of the ordinary in the lubricant?" In this case the spectral analysis routine must be more general, and should be capable of not only identifying IR bands that do not arise from the lubricant, but also differences in the relative intensities of bands that might also indicate the presence of a contaminant. A discriminant analysis technique based on principal components analysis (PCA) was applied to the data obtained in order to detect the presence of an unspecified contaminant.

Several studies have employed PCA, also known as factor analysis, in the development of discriminant algorithms. Although PCA and its applications have been thoroughly described in the literature (10,11), a brief discussion will be given with an emphasis on its role in discriminant analysis techniques. PCA involves decomposing the original data matrix of n spectra by m measurements (or wavelengths) into a matrix of scores, and a matrix of factors, as given by: $X = SF + E$; where X is the mean-centered data matrix, S is the n by a matrix of scores, F is the a by m matrix of factors, and the decomposition was carried out to a factors. E is an n by m matrix that contains the residual values for each spectrum at each measurement. The factors are linear combinations of the original measurements and are chosen sequentially to represent the directions of maximum variance in the data set. Each spectrum in the data matrix has a set of scores that indicate the amount of each factor required to represent the initial spectrum. Although the decomposition can be carried out to use all of the degrees of freedom available, usually the significant variance in the data set can be represented by a smaller number of factors, and any further factors represent only random variations (noise). After decomposition, each of the n spectra in the training set can be described by the set of a scores instead of m measurements (usually with $a < m$). This not only reduces the dimensionality of the data set, but also improves the quality of the data since some of the noise is excluded from the primary set of factors.

Malinowski has discussed the determination of the optimum number of factors, a , that are needed to accurately represent the data matrix (12,13). He showed that, for a data matrix that is factor analyzable, there exists a primary set of factors that consists of a mixture of meaningful information and error, and a secondary set of factors that consists of pure error, or noise. Since it is, the primary set that is of use in chemical analysis, rejection of the secondary set of factors will actually lead to an improvement of the raw data set. The problem lies in deciding where to separate the factors into primary and secondary sets. For multivariate quantitative calibration (e.g., partial least squares), the dependent variables can be used to monitor the progress of the decomposition. PCA decomposition, however, does not rely on dependent variables; the factors are selected solely on the basis of the variance within the data matrix. Malinowski derived several indicator functions which monitor the error via the eigenvalues associated with the factors (13). The eigenvalues give a measure of the amount of variance represented by each factor. The number of primary factors can be determined by starting with the least significant factor, and working backwards, until the point where the eigenvalues begin to represent more than the known experimental error. The factors beyond this point can be taken to be members of the primary set.

Once the training set data matrix has been decomposed by PCA, the scores can be used to develop a discriminant algorithm, similar to the way in which individual absorbance values can be used. Factorial discriminant analysis (FDA), which uses linear discriminating functions, has been demonstrated for several applications using NIR and mid-IR spectra (14-16). FDA uses the primary set of factors to define the space occupied by the training set. An alternative method, called soft independent modeling of class analogy (SIMCA), employs the information contained in the secondary set of factors (17). In SIMCA, the spectrum is reconstructed using the primary set of factors, and the residual spectrum is computed as the difference between the original and the reconstructed spectra. This is identical to computing the residual spectrum using the secondary set of factors but eliminates roundoff errors that can result from the small values in the secondary factors. The residual variance for a given spectrum is then computed as the sum of the squares of the values in the residual spectrum. An F -test can then be used to compare the residual variance for an unknown to the residual variances for the training set in order to statistically determine if the unknown is significantly different from the training set. Although FDA and SIMCA both employ PCA, the basic concept of the two techniques is quite different. FDA compares samples in a space that represents the significant variance of the training set, while SIMCA compares in the remaining orthogonal space. Van der Voet *et al.* have described these two spaces as inside-model space (IMS) and outside-model space (OMS), respectively (18). Both methods have certain merits, but the two are certainly suited to different types of applications. For example, FDA is best suited to an application that would discriminate against known sources of variation. This allows the PCA to accurately represent the space in which the variations will occur. SIMCA however is more suited to identify variations that are quite different from the inherent variance of the training set. The work of Gemperline *et al.* provides a

good example of this (19). Using SIMCA they successfully discriminated adulterated pharmaceutical raw materials from training sets of pure materials based on NIR reflectance spectra.

The data that are obtained during a TG/FT-IR run differ somewhat from the data typically used in discriminant analysis. FT-IR spectra are measured as the components of the sample evolve, and therefore spectra obtained during the run can vary widely. Therefore, discriminant analysis in the IMS will not be very useful since the variations in the factor space for an uncontaminated sample will be quite large. However, if the primary factors accurately represent the species evolving from the uncontaminated lubricant, then the presence of contaminants in a lubricant should result in evolving species that spectrally fall outside of the IMS defined for the uncontaminated lubricant. In this case, a discriminant analysis routine that analyzes the OMS (such as SIMCA) should be capable of detecting the presence of a contaminant. It is important to note that this approach requires that the contaminant produces evolving species that are spectrally different from the species evolving from the uncontaminated lubricant. The magnitude of required spectral difference is dependent upon the implementation of the discriminant algorithm, and spectral pretreatment will be particularly important.

SIMCA was evaluated as a method of detecting contamination in used synthetic lubricants on the basis of the data collected during a standard TG/FT-IR analysis (no postoxidizer). The spectra obtained during a run of an uncontaminated lubricant were used as the training set. First derivative spectra were used in order to eliminate the effects of baseline variations resulting from scattering. After selection of the spectral region of interest, the mean-centered training set was decomposed, and the number of factors in the primary set was determined using Malinowski's IND function (13). The residual variance was then computed for each spectrum in the training set and for all the spectra obtained from the runs of all the other samples, including the uncontaminated lubricant, various pure contaminants, and various "contaminated" lubricants. The residual variance for each spectrum, and the residual variance for the training set, were then used to compute the F -statistic using the approach outlined by Gemperline et al., (19). Gemperline classified samples as members if F was below the 95% level, as non-members if F was above the 99% level, and as undecided if F was between the 95% and 99% levels.

An example of the results of the factor analysis is shown in Figure 2. Figure 2a shows a plot of the spectra obtained for an uncontaminated lubricant and the residual spectra that result from projecting the spectra onto the primary set of factors. In Figure 2b, the spectra and residual spectra are shown for a lubricant sample contaminated with 5% polydimethylsiloxane. The large features present in the residuals result from spectral features due to the contaminant. Since these features are of larger magnitude than can be attributed to noise, this sample is identified as containing a contaminant. Several spectral regions were used to develop discriminant analysis routines, and the best general results were obtained using a region containing 4000-2450 and 2250-890 cm^{-1} . The 2450-2250 cm^{-1} region was excluded in order to reduce the effects of variable CO_2 evolution profiles, and the region below 890 cm^{-1} was excluded due to the presence of large noise spikes. These two regions were found to adversely affect the performance of the discriminant routines.

In Figure 3, the F -values are plotted for lubricant samples contaminated with several fluids. The samples with 5% silicone (PDMS) oil and 5% brake fluid are easily identified as contaminated, but the samples with 5% jet fuel, 5% motor oil, and 5% hydraulic oil all fell in the region where no decision can be made. This can be explained by the fact that the silicone oil and the brake fluid both have unique spectral bands that result in significant contributions to the residual spectrum, while the spectra of the other samples only exhibit bands due to C-H vibrational modes which are also present in the lubricant. Since these samples are only present at a concentration of 5% the contribution to the residual spectrum is small. This is verified by the fact that the sample with 30% hydraulic oil is identified as contaminated. In future work, additional spectral pretreatment methods will be investigated in order to magnify the spectral differences between the lubricant and these types of contaminants. It has been demonstrated by Hasenoerhl et al. (20) that pretreatment routines such as variance scaling and feature weighting can vastly improve the performance of PCA-based discriminant analysis routines.

The F -values were also plotted for another uncontaminated lubricant sample and samples contaminated with 5% methanol, 5% dichloromethane, and 5% trichloroethylene (TCE) (9). The discriminant analysis routine performed well for the uncontaminated sample and the methanol-contaminated sample. The two samples contaminated with chlorinated species were not detected as contaminated. This is due in part to the fact that the spectral region characteristic of C-Cl vibrational modes was excluded in order to limit the contribution of extraneous noise spikes. Results from analyses including this spectral region are poor due to the presence of these noise spikes, but do indicate that chlorinated contaminants can be detected at relatively high concentrations. As discussed below, much more sensitive detection of chlorinated contaminants can be achieved by using secondary oxidation to convert organic chlorine to HCl.

Artificial neural network analysis for contaminants - In the past decade, significant effort has been made to develop computing strategies that simulate biological systems. The resulting artificial neural networks (ANN) are grossly simple in comparison to biological networks, but are well suited for performing tasks such as pattern recognition, cost minimization, etc. (21). A typical ANN is made up

of three layers of processing units (nodes) and weighted connections between the layers of nodes. The input data is introduced at the input layer and is fed to the hidden layer through the weighted connections. Each node of the hidden layer sums its inputs and then applies an activation function to compute its output. The outputs of the hidden layer are then processed by the output layer, and their outputs are given as the output of the ANN. The function of the network is determined by the activation functions applied by the nodes and by the weights of the connections between the nodes. The weights can be strong or weak, and positive (excitatory) or negative (inhibitory). Typical activation functions are linear, step, and sigmoidal. Once the configuration of the ANN is defined for a given application, and the appropriate activation functions are selected, a network must be trained to perform the desired task. This is analogous to "learning" in a biological system. The usual method involves introducing training data to the ANN and comparing the output of the network to the correct or desired output. The error is then propagated back through the network in order to adjust the weights. This process is repeated until the error level falls below an acceptable level.

Recent applications of ANN technology to infrared spectral data fall into two primary classes: 1) multivariate quantitative analysis, and 2) classification. The primary advantage of ANNs for the development of quantitative models lies in the inherent capability to model nonlinearity. Classification networks applied to spectral data take advantage of the capability of ANNs to handle complex pattern recognition problems. Expert systems have been developed which employ ANNs to determine the functional groups present in a compound on the basis of its infrared spectrum (22). More specific classification networks have also been developed. Examples include sorting plastics encountered at a recycling plant based on their infrared spectra (23), and classifying woods as either hardwoods or softwoods on the basis of their FT-Raman spectra (24). These results are very promising and are indicative of the potential of using ANNs with spectral data to develop powerful classification techniques.

In order to investigate the potential of using a classification network to detect the presence of contaminants in synthetic lubricants, several networks were trained to recognize the presence of chlorinated solvents in the evolved species from a TG/FT-IR run. Training of the networks involved presenting examples of spectra from uncontaminated and contaminated runs. In order to provide a more general set of "contaminated" spectra, library spectra of dichloromethane and trichloroethylene (TCE) were added to the spectra obtained from the uncontaminated run.

Networks were developed and trained using the NeuralWorks ANN development package (NeuralWare, Pittsburgh, PA) in conjunction with custom C routines for data preprocessing and presentation. The network was trained using spectra from a TG/FT-IR run for an uncontaminated sample and spectra from the same run artificially spiked with library spectra. This was accomplished by writing a C program that presented either a spiked or unspiked spectrum to the network during training. The program was interfaced directly to the ANN development software in order to allow computation of new spiked spectra on the fly during training. At the beginning of each presentation, the program randomly chooses to present either a spiked or unspiked spectrum. If a spiked spectrum is to be presented, then a random fraction of a library spectrum is added to a randomly selected spectrum from the TG/FT-IR run. This presentation method allowed the training data to represent a large range of potential contamination conditions. Before presentation to the network, spectra were preprocessed with a Fourier filter routine to remove low frequency baseline variations and some of the high frequency noise, and the spectra were then normalized to unit vector length in order to give all spectra equal importance.

Figure 4 shows the prediction results from a network trained as described above. A network output of 1.0 indicates the evolution of a contaminant, and an output of -1.0 indicates that no contaminant is evolving. Figure 4a is the result for an uncontaminated lubricant run. While this result shows excellent prediction, this is the same data used to train the network, and therefore does not significantly demonstrate generalization. In Figure 4b, the result is shown for a TG/FT-IR run of a lubricant contaminated with TCE. The TCE evolving from 1-8 minutes is clearly identified as a contaminant, and the remainder of the run is accurately identified as uncontaminated. This result clearly demonstrates both the ability of the network to detect contamination and the ability of the network to generalize, i.e., accurately predict the uncontaminated portion of the run. The plot shown in Figure 4c shows the result for a TG/FT-IR run of a lubricant contaminated with dichloromethane. While the network clearly identified the contaminant evolving from 1-10 minutes, it did not successfully predict the absence of contaminant during the later part of the run (~45-70 minutes). This indicates that the network may produce false positives in the prediction of contamination.

Continuation of ANN development in future work will address the problem observed in Figure 4c. Further investigation of preprocessing routines should provide a solution to this problem. Additionally, other ANN architectures will be investigated. While the networks developed to date do not perform as well as desired, the results discussed above are promising, and indicate that further investigation may provide a powerful methodology for detecting contamination in synthetic lubricants.

Detection of Trace Chlorinated Contaminants in Synthetic Lubricants

While TG/FT-IR combined with the data analysis methods discussed above is well suited to identifying general contamination at relatively high concentrations, the detection of trace level contamination by chlorinated species is better accomplished using TG/FT-IR with secondary oxidation to convert the evolving organic chlorine to HCl. There are several factors that lead to greatly improved sensitivity for the detection of chlorinated species. Since the evolving species are converted to the gaseous combustion products (H₂O, CO₂, HCl), the quantitative analysis software can be vastly simplified. HCl can easily be measured by FT-IR in the presence of high concentrations of CO₂ and H₂O, since there is little spectral interference. Additionally, conversion of the evolving species to gaseous products eliminates the formation of aerosols in the gas cell, and therefore much larger samples of lubricant can be analyzed. This also allows for the use of a longer residence time in the gas cell and a faster temperature ramp in the furnace since there is less risk of condensation of heavy products on the gas cell mirrors and windows.

Two sets of samples contaminated with chlorinated compounds were run using the TG/FT-IR method with secondary oxidation. The first two samples were spiked with o-DCB and TCE, respectively, and ~45 mg samples were analyzed. The resulting spectra from the o-DCB contaminated sample are given in Figure 5. The spectra from this run shows the HCl evolving from 2-6 minutes into the run, along with high concentrations of H₂O evolving throughout the run. It is clear from the spectra that the relatively strong H₂O bands (4000-3000 cm⁻¹) will not obscure the weaker HCl bands between 3000 and 2600 cm⁻¹. As shown in Table 2, the measured HCl concentration agrees well with the expected concentration for the sample spiked with o-DCB, but is somewhat low for the sample spiked with TCE. It is believed that the bias observed for the TCE sample is a result of volatilization of the TCE during sample preparation.

Two ~200 mg samples contaminated with 1.3% and 0.13% o-DCB, respectively, were also run in order to increase the sensitivity of the method, and the quantitative analysis results are also summarized in Table 2. In the case of the ~200 mg samples, incomplete oxidation of the evolving lubricant led to the formation of significant amounts of methane, which can interfere with the quantitation of HCl. (Further tuning of the secondary oxidizer should allow for complete oxidation of samples of this size.) However, the HCl was still observed evolving from 2-6 minutes during the run (as was the case with the smaller samples), before the methane evolution becomes significant. It should be noted that a bias was observed for the 1.3% o-DCB sample, and it is believed that this is a result of an error in the preparation of the sample. The HCl concentration measured for the 0.13% o-DCB sample agrees well with the expected concentration of 0.065% HCl. This corresponds to 620 ppm (w/w) organic chlorine in the lubricant sample, and on the basis of the signal-to-noise ratio in the spectra, indicates a detection limit of about 300 ppm (w/w). On the basis of these results and projections of the gain that can be achieved with additional improvements the lower detection limit for organic chlorine in synthetic lubricant samples could be reduced to less than 10 ppm (9).

Table 2. Summary of the quantitative analysis results for the TG/secondary oxidation/FT-IR analysis of lubricant samples spiked with chlorinated contaminants.

contaminant	sample size (mg)	Cl conc. (wt %)	HCl conc. (wt %)	measured HCl (wt %)
0.65 wt% o-DCB	41.2	0.31	0.33	0.35
0.65 wt% TCE	46.9	0.53	0.54	0.37
1.3 wt% o-DCB	198.5	0.62	0.65	0.35
0.13 wt% o-DCB	208.2	0.062	0.065	0.059

SUMMARY AND CONCLUSIONS

In this work, the feasibility of using two novel thermal/FT-IR analysis methods in combination with advanced data analysis techniques to detect contamination in used turbine engine lubricants was demonstrated. The first method, TG/FT-IR combined with advanced data analysis routines, was shown to be capable of detecting the presence of different types of contaminants in synthetic lubricants at concentrations of about 5%, and this sensitivity could probably be increased to about 1% with software and hardware improvements. It was demonstrated that data analysis routines based on factor analysis (SIMCA) and neural networks could be used for identifying the presence of a contaminant. The second method, TG/secondary oxidation/FT-IR, was developed specifically for detecting trace levels of chlorinated contaminants in lubricants. Optimization of this technique using existing instrumentation led to a detection limit of about 300 ppm (w/w) organic chlorine in the lubricant. Further improvements in the hardware and software components could lead to detection limits of <10 ppm.

ACKNOWLEDGEMENTS

The authors gratefully acknowledge the support of this work by the U.S. Air Force under Contract No.

F33615-93-C-2328. The authors also wish to thank the Project Officer, Dr. Phillip Centers, for his help and support. The authors wish to acknowledge the contributions of Mr. Erik Kroo of Advanced Fuel Research, Inc. (AFR) to the experimental effort. The authors also wish to acknowledge helpful discussions with Dr. Chad Nelson and Dr. Peter Solomon of AFR, Mr. William Petrich of Independent Environmental Services (Homewood, IL) and Prof. Eric Suuberg of Brown University.

REFERENCES

1. Micallef, R.A., Squires, A.T.B.P., Technical Report AFWAL-TR-87-2067, Wright-Patterson AFB OH (November 1987).
2. Yoast, K.L., "Conservation of Petroleum Wastes at Red River Army Depot," Final Report No. USAMC-02-08-73-023, U.S. Army Material Command, Alexandria VA (March 1974).
3. Micallef, R.A., Squires, A.T.B.P., "Characterization of Used MIL-L-7808 Lubricants," Technical Report AFWAL-TR-85-2017, Wright-Patterson AFB OH (May 1985).
4. Micallef, R.A., Squires, A.T.B.P., "Reclamation of Synthetic Turbine Engine Lubricants," Technical Report AFWAL-TR-81-2072, Wright-Patterson AFB OH (August 1981).
5. Saba, C.S., Smith, H.A., Keller, M.A., Jain, V.K., Kauffman, R.E., "Lubricants Performance and Evaluation," Technical Report AFWAL-TR-87-2025, (June 1987).
6. Carangelo, R.M. Solomon, P.R., and D.G. Gerson, Fuel, 66, 960, (1987).
7. Whelan, J.K., Solomon, P.R., Deshpande, G.V., and Carangelo, R.M., Energy and Fuel, 2, 65, (1988).
8. Solomon, P.R., Serio, M.A., Carangelo, R.M., Bassilakis, R., Gravel, D., Baillargeon, M., Baudais, F., and Vail, G., Energy & Fuels, 4, (3), 319, (1990).
9. Serio, M.A., Bonanno, A.S., Bassilakis, R., Kroo, E., and Solomon, P.R., Final Report AFWAL-TR-93-2119 (November, 1993).
10. Malinowski, E.R., Howery, D.G., *Factor Analysis in Chemistry*, John Wiley & Sons, New York, 1980.
11. Jolliffe, I.T., *Principal Components Analysis*, Springer-Verlag, New York, 1986.
12. Malinowski, E.R., Anal. Chem., 49, 606 (1977).
13. Malinowski, E.R., Anal. Chem., 49, 612 (1977).
14. Devaux, M.F., Bertrand, D., Robert, P., Qannari, M., Appl. Spec., 42, 1015 (1988).
15. Devaux, M.F., Bertrand, D., Robert, P., Qannari, M., Appl. Spec., 42, 1020 (1988).
16. Downey, G., Robert, P., Bertrand, D., Kelly, P.M., Appl. Spec., 44, 150 (1990).
17. Wold, S., Sjostrom, M., in *Chemometrics: Theory and Application*, Ed. by B.R. Kowalski, American Chemical Society, Washington D.C., pp. 242-282 (1977).
18. Van Der Voet, H., Coenegracht, P.M.J., Hemel, J.B., Anal. Chim. Acta, 192, 63 (1987).
19. Gemperline, P.J., Webber, L.D., Cox, F.O., Anal. Chem., 61, 138 (1989).
20. Hasenoehrl, E.J., Perkins, J.H., Griffiths, P.R., Anal. Chem., 64, 656 (1992).
21. Kohonen, T., Neural Networks, 1, 3, (1988).
22. Wythoff, B.J., Levine, S.P., Tomellini, S.A., Anal. Chem., 62, 2702, (1990).
23. Alam, M.K., Stanton, S.L., Energy and the Environment, August, 4 (1992).
24. Personal communication with P.R. Griffiths, University of Idaho, October, 1993.

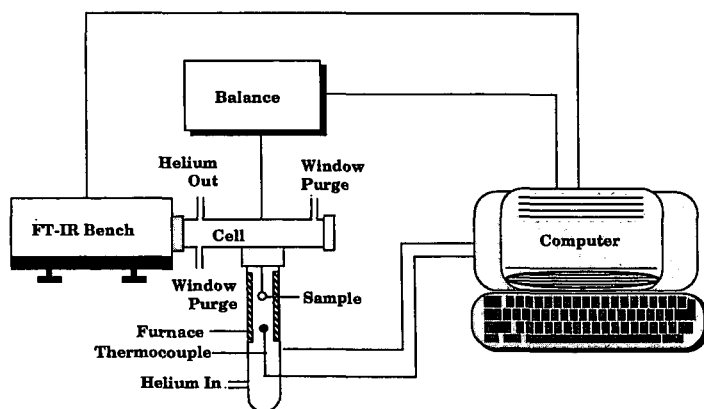


Figure 1. Schematic diagram of the standard TG/FT-IR instrument. The sample is suspended in the furnace, and, as the sample is pyrolyzed, the evolving species are swept into the FT-IR gas cell. The instrument was modified to include an oxidation zone before the gas cell.

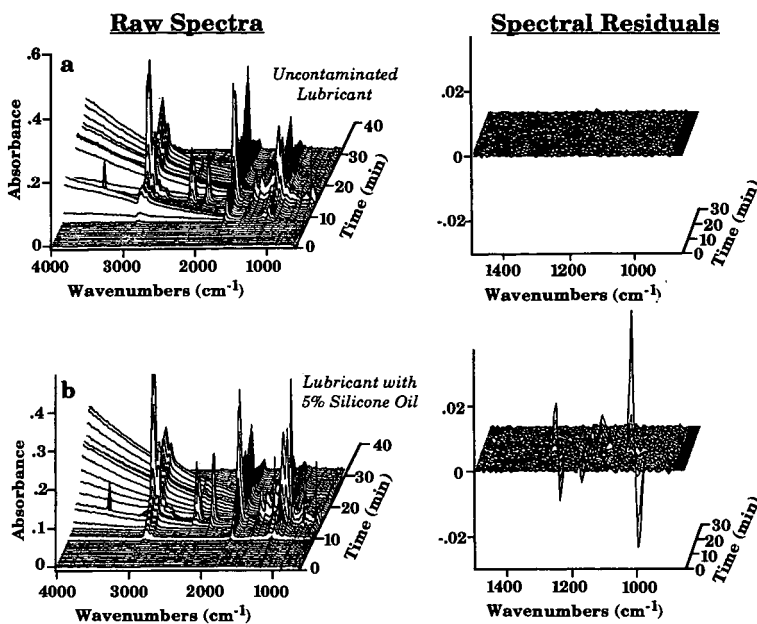


Figure 2. Examples of SIMCA analysis for TG/FT-IR runs of a) uncontaminated lubricant and b) lubricant with 5% polydimethyl siloxane. The raw spectra from the run are shown on the left, and the residual spectra resulting from projection onto the primary factors are shown on the right (note the expanded scale).

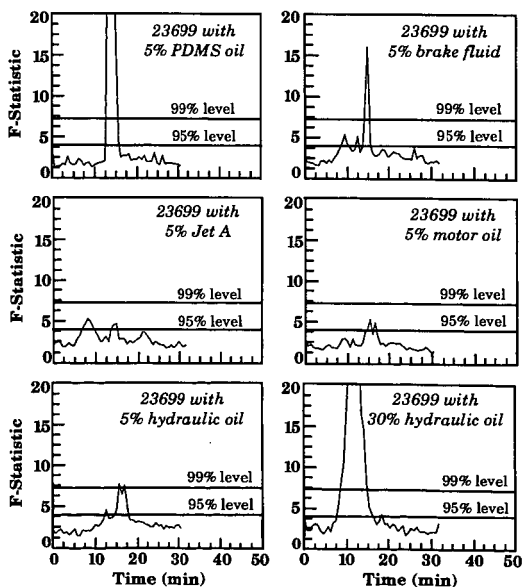


Figure 3. Results of SIMCA analysis for contamination in used synthetic lubricants. The F -values are plotted versus time for TG/FT-IR runs of lubricant samples contaminated with various fluids likely to be encountered at an Air Force base.

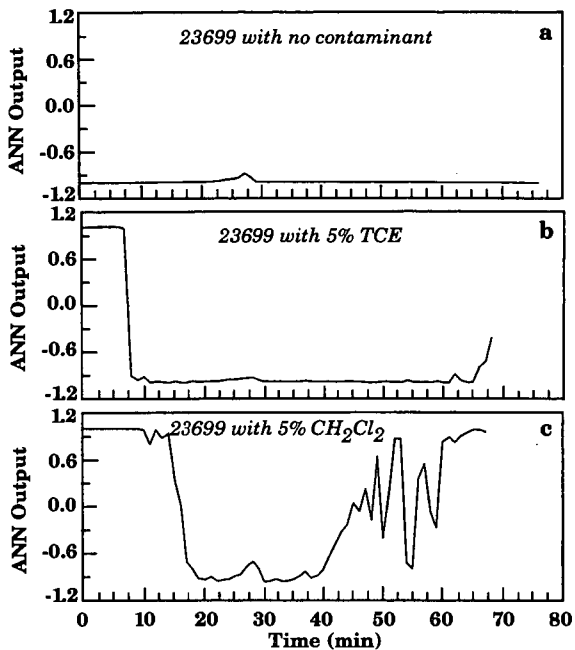


Figure 4. Neural network based prediction of chlorinated contaminants evolving during TG/FT-IR runs. A value of 1.0 indicates the presence of contaminant and -1.0 indicates the absence of contaminant. a) uncontaminated Mobil 23699; b) trichloroethylene contaminated Mobil 23699; c) dichloromethane contaminated Mobil 23699.

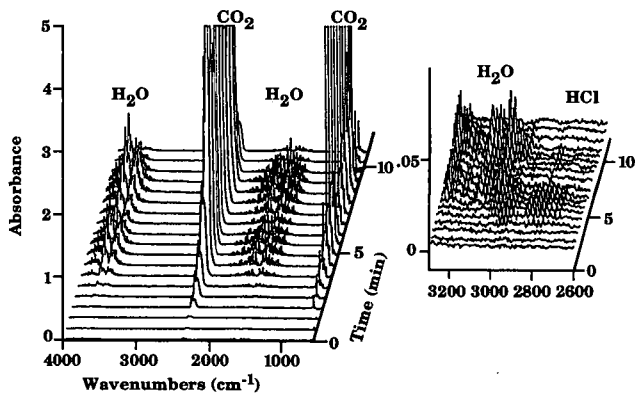


Figure 5. Spectra obtained during TG/secondary oxidation/FT-IR analysis of a 41.2 mg sample of lubricant spiked with 0.63% *o*-DCB. The scale is expanded in the plot on the right to show the evolution of HCl.

CHARACTERIZATION OF ACIDIC PROPERTIES OF MICROPOROUS AND MESOPOROUS ZEOLITE CATALYSTS USING TGA AND DSC

Chunshan SONG, Wei-Chuan LAI, Andrew D. SCHMITZ, and Kondam Madhusudan REDDY

Fuel Science Program, Department of Materials Science and Engineering, Pennsylvania State University 209 Academic Projects Building, University Park, PA 16802-2303

Keywords: Zeolites, Mesoporous zeolites, acidity, base, desorption, TGA, DSC

ABSTRACT

Thermal gravimetric analysis (TGA) and differential scanning calorimetry (DSC) were applied for characterizing the acidic properties of microporous and mesoporous zeolite catalysts through temperature-programmed desorption (TPD) of *n*-butylamine (*n*-BA) as a base probe molecule. A flow system was designed with heating and evacuation capability for preparing the *n*-BA adsorbed sample. In the TGA, *n*-BA desorption at different temperatures represents the interaction with surface acidic sites of different strength. The acid sites corresponding to base desorption at 100-240°C, 240-340°C, and 340-500°C, were classified as weak, intermediate, and strong acid sites, respectively. DSC indicates the endothermic nature of the differential thermogravimetric peaks (observed from TGA) in the above temperature regimes, confirming the TPD data. The microporous zeolites examined include three proton-form mordenites, three proton-form and metal-ion exchanged Y-zeolites, and four noble metal catalysts supported on mordenite and Y-zeolite. Four mesoporous zeolites were synthesized and examined by the same TPD method. Both the total acidity (mmol/g) and acid strength distribution depend on the zeolite type, Si/Al ratio, and metal loading. Ni and La ion-exchange decreased the strong acid sites. Pt and Pd loading on an HY decreased the strong acid sites but their loading on an H-mordenite had little effect on its strong acid sites. Mesoporous zeolites showed lower acidity and lower fraction of strong acid sites compared to HY and H-mordenites. However, the acidity of mesoporous zeolites strongly depends on the aluminum source compounds used in the hydrothermal synthesis of the zeolites.

INTRODUCTION

Recently, we have initiated a major effort in exploring microporous and mesoporous zeolite catalysts for conversion of polycyclic hydrocarbons related to fuel processing and shape-selective catalysis [Song and Kirby, 1994; Song and Moffatt, 1994; Schmitz and Song, 1994, 1995; Lai and Song, 1995; Reddy and Song, 1995a,b,c; Lai et al., 1995; Schmitz et al., 1995]. For a wide range of fuel processing reactions and shape-selective reactions, zeolite acidity is a key factor affecting activity and selectivity. In the present work, we attempt to characterize the acidic properties of mesoporous and microporous zeolites using thermogravimetric analysis (TGA) and differential scanning calorimetry (DSC).

Base molecules adsorb on Bronsted and Lewis acidic sites of solid surface, and can be removed by thermal desorption at elevated temperatures. The desorption temperature depends on the strength of the interaction between the base and the surface acidic sites. A widely used technique for characterizing the acidity of solid surface is temperature-programmed desorption of a base (e.g., ammonia) using thermal conductivity detector [Fernandes et al., 1994; Hunger and Szombathely, 1994]. However, acidity characterization can also be carried out using several other techniques, including infrared spectroscopy [Cannings, 1968; Lefrancois and Malbois, 1971; Ward, 1976; Makarova et al., 1994], nuclear magnetic resonance [Brunner et al., 1994], TGA [Ghosh and Curthoys, 1984], and calorimetry [Chen et al., 1992; Cardona-Martinez and Dumesic, 1992; Parrillo et al., 1994].

In this paper, we report acidity characterization of zeolites by temperature-programmed desorption of *n*-butylamine (*n*-BA) using TGA and DSC as detector. There are two advantages of using *n*-BA with TGA detection. The first one is that, compared to NH₃, *n*-BA is closer in size and length to hydrocarbon molecules, and the acid sites detected by *n*-BA desorption may be practically more useful. The second is that using a higher-molecular-weight base (relative to NH₃) can enhance the sensitivity of the TPD conducted on TGA, since TGA is not as sensitive as TCD. However, these advantages do not come without problems. Possible problems are *n*-BA decomposition at high temperatures [Ghosh and Curthoys, 1984] and likely slower diffusion compared to that of ammonia. Nonetheless, *n*-BA has been found to be a useful probe molecule for acidity characterization of zeolites.

EXPERIMENTAL

Microporous Zeolites

The microporous zeolites examined in this work include three hydrogen mordenites (HML8, HM20A, and HM30A), two noble metal loaded mordenites (Pt/HM30A and Pd/HM30A), and two sets of Y zeolite-based catalysts: the first set includes a hydrogen Y zeolite (HY-1 with SiO₂/Al₂O₃ molar ratio of 4.8) and two metal ion-exchanged Y zeolites (LaHY and NiHY); the second set includes another hydrogen Y-zeolite (HY-2 with SiO₂/Al₂O₃ molar ratio of 5.0) and two noble metal-loaded Y-zeolites (Pt/HY and Pd/HY). The three H-mordenites (HML8, HM20A, and HM30A) with different SiO₂/Al₂O₃ molar ratios (17, 21, and 38, respectively) were prepared by heat treatment of three commercial ammonium mordenite samples [Lai and Song, 1995; Schmitz et al., 1995]. The noble metal-loaded zeolites (Pt/HM30A, Pd/HM30A, Pt/HY, Pd/HY) were prepared by incipient wetness impregnation from aqueous solution of platinum and palladium salts: aqueous H₂PtCl₆ solution and aqueous PdCl₂ dissolved in hydrochloric acid (H₂PdCl₄). The noble metal loading on the support was nominally 6 wt%. The metal-loaded catalysts were calcined in air at 450 °C for 2 h after being dried in a vacuum oven. The three Y zeolites (HY, LaHY, and NiHY) were prepared according to the procedures described elsewhere [Song and Moffatt, 1994]. More details on the preparation and properties of the catalysts are described elsewhere [Song et al., 1991; Schmitz and Song, 1995].

Mesoporous Zeolites

The mesoporous materials were synthesized according to the procedure described elsewhere [Reddy and Song, 1995b]. Briefly, the mesoporous zeolites were synthesized from a mixture of reactants with the following composition: 50SiO₂·xAl₂O₃·4.32Na₂O·2.19(TMA)₂O·15.62(CTMA)Br·3165H₂O; where x=1.0 and 2.0. The organic template from the as-synthesized solids was removed by calcining the samples in a tubular furnace at 550 °C for one hour in

nitrogen and 6 hours in air flow. The calcined samples were ion-exchanged with ammonium nitrate (0.5M) at 90°C. The protonated form was then obtained by calcining these ammonium ion-exchanged samples at 480 °C for 3 hours. More details for synthesis and spectroscopic characterization may be found elsewhere [Reddy and Song, 1995b].

TGA and DSC of Base-Saturated Samples

The acidity of catalysts were characterized by the temperature-programmed desorption of a base using thermogravimetric analysis (TGA) in combination with differential scanning calorimetry (DSC). *n*-Butylamine (*n*-BA) was chosen as the base for adsorption-desorption study; it was obtained from Aldrich Chemical Company and was used as received with a purity of 99+%.

For the preparation of *n*-BA adsorbed samples, we have designed a flow system with heating and evacuation capability, where a given zeolite was degassed in vacuo at 400°C, cooled to room temperature, and then exposed to *n*-BA vapor in flowing ultra-high purity nitrogen for 1 hour; N₂ with a flow rate of about 100 cm³/min was used as a carrier gas. The base-saturated catalyst was then transferred to TGA or DSC for analysis.

The desorption experiments were carried out with base-saturated catalyst contained in an uncovered alumina crucible using Mettler TG50 thermogravimetric balance. Samples of about 10 mg were used in each measurement and a purge gas (N₂) flow of 200 cm³/min at room temperature was used. Before the thermal analysis was started, the base-saturated sample was kept at 30 °C for 30 minutes with purge flow to remove physisorbed *n*-BA. The desorption temperature was programmed from 30 to 600 °C at a heating rate of 10 °C/min, and the decrease in weight with increasing temperature was monitored. TGA and DTG (differential thermogravimetry) data were then obtained.

The desorption was also carried out in a differential scanning calorimeter using Mettler model DSC 27HP. About 7.5 mg of each of the catalysts was placed in an uncovered standard aluminum crucible (40 mL), and was heated from 30 to 600 °C at a rate of 10 °C/min with an initial isothermal time of 30 min. The system was continuously purged with 100 cm³/min of N₂.

RESULTS AND DISCUSSION

Figure 1 shows the TGA and DSC profiles of temperature-programmed desorption of *n*-BA from HY (HY-1). DSC curve shows only endothermic peaks: a low-temperature peak near 100 °C, a shallow peak near 200 °C, a large peak at 405 °C, and a shoulder near 440 °C. DTG shows similar results except that the peak near 100 °C is not as clear as that in DSC. It can be seen that for HY the results from DTG compared fairly well with that from DSC. The peak near 100 °C may be due to the desorption of physisorbed *n*-BA, and *n*-BA adsorbed on weak acid sites. As another possible contributing factor, trace amount of water might have re-adsorbed on the base-covered catalyst. However, prior to *n*-BA adsorption, the previously calcined catalysts were further thermally pretreated in situ under vacuum to remove moisture, then covered and saturated with base in situ, and transferred to TGA in a closed vial. Thus only the base-saturated sample is exposed to air during sample unloading from the adsorption apparatus and loading into the TGA cell. On the other hand, the high-temperature peaks above ca. 300 °C are attributed to *n*-BA desorption from acid sites. Stronger acid sites desorb the base (*n*-BA) at higher temperatures. Therefore, the *n*-BA desorption at different temperatures corresponds to the surface acidic sites with different acid strength.

The surface acidic sites corresponding to TGA-derived weight loss due to base desorption at 100-240°C, 240-340°C, and 340-500°C, were classified as weak, intermediate, and strong acid sites, respectively. DSC indicates the endothermic nature of the differential thermogravimetric (DTG) peaks, confirming the TPD data obtained using TGA. It was assumed that the weight loss below 100 °C (about 1-1.5 weight % of the saturated catalysts) was due to the desorption of physisorbed base, and thus only the amount of *n*-BA desorbed above 100 °C was considered in the calculation of acidity. The low temperature range of 100-240°C was chosen to represent weak acid sites based on the report of Ghosh and Curthoys [1984]. The temperature limit was set at 500 °C because it was suggested that the weight loss above 500 °C may also be due to the dehydroxylation of the catalysts [Ghosh and Curthoys, 1984].

Acidic Characteristics of Microporous Zeolites

The DSC and TGA curves of *n*-BA desorption are presented in Figure 2 for HY (HY-1) and metal-ion exchanged Y zeolites (and HM20A), and in Figure 3 for mordenites and noble metal-loaded mordenite catalysts. On the basis of Figures 2 and 3, the weight losses (due to *n*-BA desorption) from Y-zeolite catalysts are greater than those for the mordenites at all temperatures, indicating that the Y-zeolites have both more acid sites and higher acid strength than the mordenites.

Among the three Y-zeolites (HY, LaHY, NiHY), LaHY has slightly more weak sites than the other two, but it has fewer strong sites than HY. HY has more strong acid sites judged from the enormous endothermic heat flow (Figure 2, right) and sharp weight loss (Figure 2, left) in the 340-500 °C range. NiHY has similar amount of weaker sites but much fewer strong sites than HY and LaHY (Figure 2, left). Among the mordenite based catalysts, HML8 only possesses a small number of weak sites, in fact the least among the eight catalysts; however, it has similar amount of strong sites as HM30A has, although they have different SiO₂/Al₂O₃ ratio.

We also compared two sets of metal-loaded Y-zeolites prepared by impregnation. Their *n*-BA TPD profiles are presented in Figure 4. The metal loaded Y zeolites (Pt/HY, Pd/HY) give almost linear weight loss curves, devoid of the rapid weight loss at 340-500°C which is apparent with HY (HY-2, Figure 4, left). One explanation for this behavior is that the metal particles preferentially attach to the support at strong acid centers. Metal-support interactions of this nature may explain why Group VIII metals on acidic zeolites, especially on HY, are known to be electron-deficient [Stanislaus and Cooper, 1994]. A second possibility is that metal particles prevent *n*-BA from diffusing onto strong acid sites by blocking the channel.

Pd/HM38 (identical to Pd/HM30A in Figure 3) and Pt/HM38 (identical to Pt/HM30A in Figure 3) give TPD profiles that are similar to each other. In this case, the presence of metal does not significantly impede diffusion of *n*-BA. It is possible that a significant portion of the metals reside in the mordenite side-pocket channels (dimension 2.9 x 5.7 Å) that run perpendicular to the main channels. The two noble metal loaded mordenites have quite similar acidity, and they possess fewer strong sites than HM30A.

Tables 1-3 summarize the acidity of the microporous zeolite catalysts determined from the amount of *n*-BA desorbed (from the TGA measurements) at three temperature ranges (100-240, 240-340, and 340-500 °C). From Tables 1 and 2, the total acidity of the catalysts decrease in the following order: HY > LaHY > NiHY > Pt/HY = Pd/HY > HM20A >

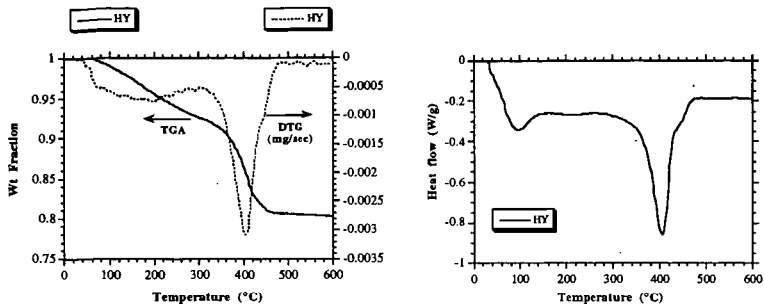


Figure 1. Temperature-programmed desorption of n-BA from HY zeolite (HY-1) conducted on TGA (left) and DSC (right).

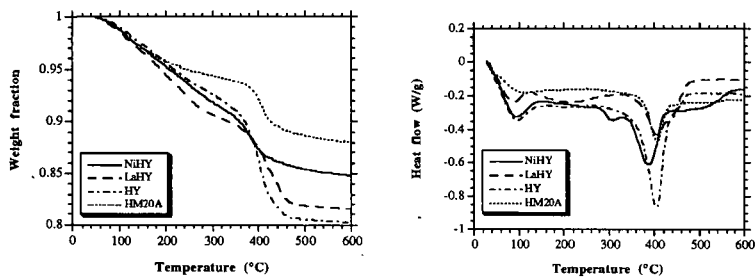


Figure 2. Temperature-programmed desorption of n-BA from proton-form zeolite catalysts conducted on TGA (left) and DSC (right).

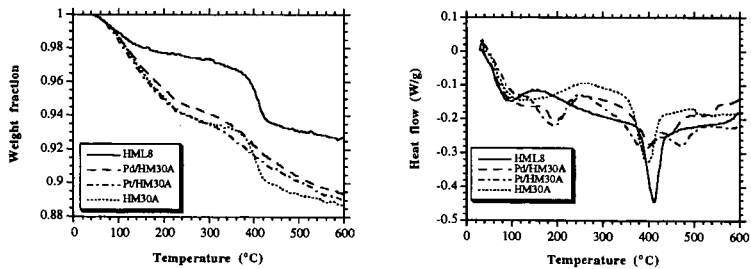


Figure 3. Temperature-programmed desorption of n-BA from mordenite-based catalysts conducted on TGA (left) and DSC (right).

HM30A > Pd/HM30A ≈ Pt/HM30A > HML8. Table 3 shows that the reproducibility of the TPD data is reasonably good.

Table 1. Acidity of Y-Zeolites from n-BA TPD (Acidity Unit: mmol/g)

Cat ID	HY (1)	LaHY	NiHY	HY (2)	Pt/HY	Pd/HY
Alt No.	HY-1	LaHY-1	NiHY-1	HY-2	Pt/HY-2	Pd/HY-2
T range, °C						
100 - 240	0.79	0.97	0.76	0.88	0.63	0.60
240 - 340	0.49	0.48	0.51	0.52	0.49	0.44
340 - 500	1.85	1.32	0.84	1.50	0.63	0.66
Total, mmol/g	3.12	2.77	2.11	2.90	1.75	1.71

Table 2. Acidity of Mordenites from n-BA TPD (Acidity Unit: mmol/g).

Cat ID	HML8	HM20A	HM30A	Pt/HM30A	Pd/HM30A
Alt No.	HM17 AS+WL	HM21 AS+WL	HM38 AS+WL	Pt/HM38	Pd/HM38
T range, °C					
100 - 240	0.19	0.56	0.75	0.68	0.62
240 - 340	0.10	0.17	0.15	0.18	0.17
340 - 500	0.57	0.80	0.61	0.44	0.51
Total, mmol/g	0.86	1.53	1.51	1.30	1.29

Table 3. Reproducibility of the Acidity Data (mmol/g) from n-BA TPD on TGA

Cat ID	HML8	HML8	HM20A	HM20A	HM30A	HM30A
Alt No.	HM17 WL	HM17 AS	HM21 WL	HM21 AS	HM38 WL	HM38 AS
T range, °C						
100 - 240	0.20	0.19	0.56	0.56	0.69	0.81
240 - 340	0.09	0.10	0.16	0.18	0.13	0.16
340 - 500	0.56	0.57	0.82	0.78	0.63	0.59
Total, mmol/g	0.86	0.86	1.54	1.52	1.45	1.56

Acid Characteristics of Mesoporous Zeolites

Mesoporous molecular sieves of MCM-41 type represent a new family of crystalline materials, and their synthesis has been made possible recently by Mobil researchers [Kresge et al., 1992; Beck et al., 1992]. The mesoporous zeolites (aluminosilicates) of MCM-41 type are of particular interest, because their uniform pores can be tuned in the range of 15 to 100 Å. Several research groups have reported the synthesis of mesoporous zeolites [Chen et al., 1993a,b; Corma et al., 1994; Borade and Clearfield, 1995; Reddy and Song, 1995a,b,c].

We have synthesized mesoporous zeolites, and found that the catalytic properties of the MCM-41 zeolites depend on the type of Al source compounds used for their synthesis [Reddy and Song, 1995b]. Here we compare the acidic properties of MCM-41 type mesoporous zeolites synthesized using alumina (pseudo boehmite), Al sulfate, Al isopropoxide, and sodium aluminate.

Figure 5 and Table 4 show the TGA results for TPD of n-BA from the mesoporous zeolites synthesized with feed SiO₂/Al₂O₃ molar ratio of 50 using four different Al source compounds. From the weight losses due to n-butylamine desorption, it is clear that MCM-41 samples prepared with aluminum isopropoxide and aluminum sulfate adsorbed more n-BA (about 18 wt%), whereas the sample prepared with pseudo boehmite adsorbed less n-butylamine (about 10 wt%). These results indicate that first two samples adsorbed more base, hence they are more acidic than the last one, which confirms that aluminum incorporation is better for the first two samples. The better Al incorporation was also verified by solid-state NMR and XRD, as reported elsewhere [Song and Reddy, 1995b]. The highest amount of n-BA was desorbed from the mesoporous zeolite prepared from sodium aluminate, in both the 100-240°C and the 340-500°C ranges. It seems that this mesoporous zeolite has the highest acidity among the four samples (synthesized with SiO₂/Al₂O₃ molar ratio of 50) examined.

Table 4. Acidity of Mesoporous Zeolites Determined from Desorption of n-Butylamine

n-Butylamine Desorption Temperature (°C)	Acid Strength	Acidity (mmol/g) of MCM-41			
		PB2(44) ^a	AS2(87) ^a	Al2(47) ^a	SA2(49) ^a
100-240	Weak ^b	0.81 ^b	1.27 ^b	0.84 ^b	1.84 ^b
240-340	Intermediate	0.06	0.17	0.25	0.16
340-500	Strong	0.10	0.29	0.32	0.42
Total acidity		0.97	1.73	1.41	2.42

^a Values in the parentheses indicate SiO₂/Al₂O₃ molar ratios of the samples synthesized using PB (pseudo boehmite), AS (Al sulfate), AI (Al isopropoxide) and SA (sodium aluminate).

^b A portion of the n-BA desorbed at 100-240°C may be due to physical adsorption.

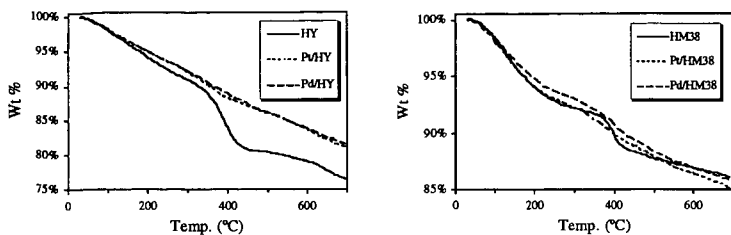


Figure 4. TGA-derived n-BA TPD from Pt- and Pd-loaded Y-zeolite (left, HY-2) and Pt- and Pd-loaded mordenite catalysts (right).

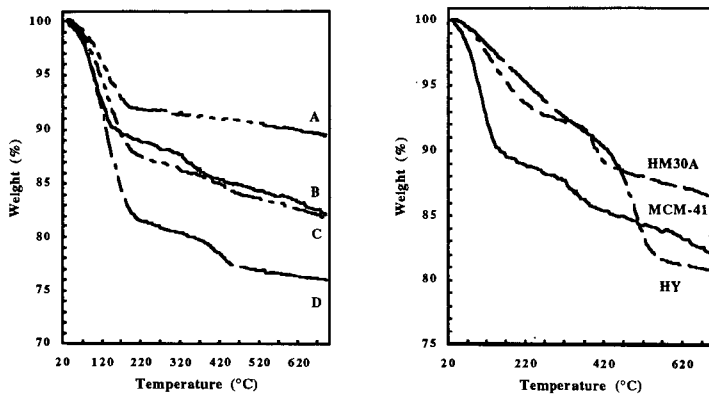


Figure 5 (Left). n-BA TPD from MCM-41 prepared using (A) pseudo boemite, (B) Al isopropoxide, (C) Al sulfate, and (D) sodium aluminate.

Figure 6 (Right). Comparison of n-BA TPD from MCM-41 prepared from Al isopropoxide and H-Y (HY) and H-mordenite (HM30A).

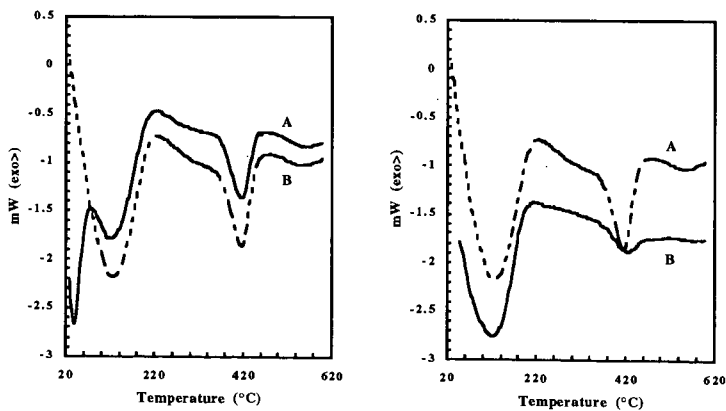


Figure 7 (Left). DSC for n-BA desorption from MCM-41 prepared from sodium aluminate ($\text{SiO}_2/\text{Al}_2\text{O}_3 = 25$) without (A) and with (B) initial N_2 flushing at room temperature for 30 min (DSC run started after the N_2 flushing).

Figure 8 (Right). DSC profiles of n-BA desorption from MCM-41 prepared from sodium aluminate with $\text{SiO}_2/\text{Al}_2\text{O}_3$ ratio of 25 (A) and 50 (B).

Figure 6 compares the n-BA TPD profile of a proton-form mesoporous zeolite (synthesized using Al isopropoxide with feed $\text{SiO}_2/\text{Al}_2\text{O}_3$ molar ratio of 50) with those of a H-Y zeolite (HY) and a H-mordenite (HM30A). Our preliminary TPD results indicate that compared to a hydrogen Y-zeolite ($\text{SiO}_2/\text{Al}_2\text{O}_3$: 5) and a hydrogen mordenite ($\text{SiO}_2/\text{Al}_2\text{O}_3$: 38), there are less number of strong acid sites in the MCM-41 samples. In terms of the relative amount of n-butylamine desorption in the temperature range of 340-500°C, the qualitative order of acidity is HY > HM > protonated MCM-41. From Figure 6, it appears that the amount of the n-BA desorbed from MCM-41 below 200 °C is much higher than that from either HY or HM. The higher amount of low temperature desorption compared to mordenite could be due to several factors: 1) larger number of acid sites with low acid strength, 2) larger pore volume and larger sorption capacity which lead to more n-BA physical adsorption, and 3) the easier out-of-pore diffusion of n-BA from mesopores which are not readily available in microporous zeolites.

On the basis of the above discussion, a question that arises is whether all the n-BA desorption at 100-240°C is really due to weak acid sites in the case of mesoporous zeolites. Figure 7 shows DSC profiles of a mesoporous zeolite (synthesized using sodium aluminate with feed $\text{SiO}_2/\text{Al}_2\text{O}_3$ molar ratio of 25) with and without initial N_2 flushing (purge flow). The initial N_2 flushing affects the n-BA desorption at low temperatures (<220°C), but does not affect the n-BA desorption at high temperatures. Figure 8 shows DSC profiles of two mesoporous zeolites (synthesized using sodium aluminate with feed $\text{SiO}_2/\text{Al}_2\text{O}_3$ molar ratios of 25 and 50). Since the acidity of zeolites is associated with Al in tetrahedral coordination, the zeolite with higher Si/Al ratio should have lower acidity. As shown in Figure 8, increasing Si/Al ratio decreased the high-temperature DSC peak, as expected. However, the effect of Si/Al ratio on the low-temperature peak appears to be significantly less compared to that on the high-temperature DSC peak. These results suggest that the low-temperature DSC peak with the mesoporous zeolites is partly due to physical sorption.

Summary

TGA and DSC are useful techniques for characterizing acidic properties of microporous and mesoporous zeolites by temperature-programmed desorption of n-BA. The desorption of n-BA at different temperatures represents its interaction with surface acidic sites of different acid strength. Base desorption at 100-240°C, 240-340°C, and 340-500°C, was classified as weak, intermediate, and strong acid sites, respectively. DSC indicates the endothermic nature of the DTG peaks (observed from TGA) in the above temperature regimes, confirming the TPD data. However, desorption of physisorbed n-BA may also contribute to the peak in the 100-240°C range.

For the microporous zeolites (Y and mordenites) examined, both the total acidity (mmol/g) and acid strength distribution depend on the zeolite type, Si/Al ratio, and metal loading. Among the three proton-form mordenites, no linear correlation between their acidity and their Si/Al ratio was observed. Ni and La ion-exchange of HY decreased the strong acid sites. Pt and Pd loading by impregnation on HY decreased the strong acid sites but their loading on an H-mordenite had little effect on its strong acid sites.

Mesoporous zeolite samples of MCM-41 type prepared using different aluminum sources do show acidity in their proton-form. Mesoporous zeolites show lower acidity and lower fraction of strong acid sites compared to HY and H-mordenites. However, the acidity of mesoporous zeolites strongly depends on the aluminum source compounds used in the hydrothermal synthesis of the zeolites. The acidity measured by n-BA desorption at 240-500°C decreases with respect to the Al source in the following order: sodium aluminate > Al isopropoxide > Al sulfate > pseudo boemite.

REFERENCES

- Beck, J. S.; Vartuli, J. C.; Roth, W. J.; Leonowicz, M. E.; Kresge, C. T.; Schmitt, K. D.; Chu, C. T. W.; Olson, D. H.; Sheppard, E. W.; McCullen, S. B.; Higgins, J. B.; Schlenker, J. C., *J. Am. Chem. Soc.*, 1992, 114, 10834.
- Borade, R. B.; Clearfield, A., *Catalysis Letters*, 1995, 31, 267.
- Brunner, E.; Beck, K.; Koch, M.; Pfeifer, H.; Staudte, B.; Zscherpel, D., *Stud. Surf. Sci. Catal.*, 1994, 84, 357.
- Cannings, F.R., *J. Phys. Chem.*, 1968, 72, 4691.
- Cardona-Martinez, N.; Dumesic, J.A., *Adv. Catal.*, 1992, 38, 149.
- Chen, C.-Y.; Burkett, S. L.; Li, H.-X.; Davis, M., *Microporous Mater.* 1993, 2, 17.
- Chen, C.-Y.; Li, H.-X.; Davis, M., *Microporous Mater.* 1993, 2, 27.
- Chen, D.T.; Sgarma, S.B.; Filimonov, I.; Dumesic, J.A., *Catal. Lett.*, 1992, 12, 201.
- Corra, A.; Fornes, V.; Navarro, M. T.; Perez-Pariente, J.; *J. Catal.* 1994, 148, 569.
- Fernandes, L. F.; Bartl, P.E.; Montero, J.L.F.; da Silva, J. G.; de Menezes, S.C.; Cardoso, M.J., *Zeolites*, 1994, 14, 533.
- Ghosh, A. K.; Curthoys, G., *J. Phys. Chem.*, 1984, 88, 1130.
- Hunger, B.; Szombathely, M.V. *Stud. Surf. Sci. Catal.*, 1994, 84, 669.
- Kresge, C. T.; Leonowicz, M. E.; Roth, W. J.; Vartuli, J. C.; Beck, J. S., *Nature*, 1992, 359, 710.
- Makarova, M.A.; Garforth, A.; Zholobenko, V.; Dwyer, J.; Earl, G.J.; Rawlence, D., *Stud. Surf. Sci. Catal.*, 1994, 84, 365.
- Lai, W.-C.; Song, C.; van Duin, A.; de Leeuw, and J.W., *Am. Chem. Soc. Div. Fuel Chem. Prepr.*, 1995, 40 (4), 1007.
- Lai, W.-C.; Song, C., *Am. Chem. Soc. Div. Fuel Chem. Prepr.*, 1995, 40 (4), 1018.
- Lefrancois, M.; Malbois, G., *J. Catal.*, 1971, 20, 350.
- Parrillo, D.J.; Biaglow, A.; Gorte, R.J.; White, D., *Stud. Surf. Sci. Catal.*, 1994, 84, 701.
- Reddy, K.M.; Song, C., *Am. Chem. Soc. Div. Fuel Chem. Prepr.*, 1995a, 40 (4), 1003.
- Reddy, K.M.; Song, C., *Catalysis Letters*, accepted for publication, 1995b.
- Reddy, K.M.; Song, C., *Catalysis Today*, accepted for publication, 1995c.
- Schmitz, A.D.; Song, C., *Am. Chem. Soc. Div. Fuel Chem. Prepr.*, 1994, 39 (4), 986.
- Schmitz, A.D.; Song, C., *Am. Chem. Soc. Div. Fuel Chem. Prepr.*, 1995, 40 (4), 918.
- Schmitz, A.D.; Bowers, G.; Song, C., *Am. Chem. Soc. Div. Fuel Chem. Prepr.*, 1995, 40 (4), 930.
- Song, C.; Kirby, S., *Microporous Materials*, Elsevier, 1994, 2 (5), 467.
- Song, C.; Moffatt, K., *Microporous Materials*, Elsevier, 1994, 2 (5), 459.
- Stanislaus, A.; Cooper, B.H., *Catal. Rev.-Sci. Eng.*, 1994, 36, 75.
- Ward, J.W. in "Zeolite Chemistry and Catalysis", ACS Monograph 171, J.A. Rabo Ed., ACS:Washington D.C., 1976, Chap. 3, pp. 118-284.

THERMAL STUDIES OF METAL PROMOTED SULFATED ZIRCONIA

Melody Bi, Hanxu Li, Wei-Ping Pan, William G. Lloyd, and Burtron H. Davis*
Department of Chemistry and Materials Characterization Center, Western Kentucky University,
Bowling Green, KY 42101, *Center for Applied Energy Research, University of Kentucky,
Lexington, KY 40506

KEY WORDS: Superacid, catalyst, evolved gas analysis

ABSTRACT

$\text{SO}_4^{2-}\text{-ZrO}_2$ is considered to be a superacid catalyst. The metal promotion on sulfated zirconia has been shown to enhance the stabilities of the catalysts. The activation of these catalysts involves complex chemical changes. In the present investigation, a simultaneous TG/MS technique was utilized to investigate the weight loss and to monitor the chemical compounds that evolve under controlled heating in different environments. Some insight of the activation mechanism of the catalysts was thus obtained. The evolution of HCl and Cl_2 were well identified according to the mass ratio of Cl isotopes. The evolution of SO_2 and SO showed a continuum beyond 900°C which corresponds to the TG results. This indicated SO_4^{2-} is present in the solid in a variety of structures. The samples were also analyzed in STD (TGA-DTA). The results show so far sulfate ion is the most efficient species to retard the phase transformation process of zirconia.

INTRODUCTION

Solid oxide catalysts have been widely used in petroleum refineries for skeletal isomerization of n-paraffins and to isomeric alkanes to produce oxygenates, which are important components of automobile fuels. Among the solid oxide catalysts, zirconium oxide (ZrO_2) is claimed to be the only oxide catalyst that has acidic, oxidizing and reducing properties. The discovery by Tanabe and Hattori of the superacidic properties of sulfuric acid treated zirconium oxide ($\text{ZrO}_2/\text{SO}_4^{2-}$), the acidity of which was estimated to be as high as $H_0 < -14.5$ by the adsorbed Hammett base technique, has given a new impulse to solid catalysis.¹ Sulfated zirconia was obtained by immersing hydrous ZrO_2 catalyst powders in a sulfuric acid solution. Such sulfated zirconia catalysts have exhibited superacidic properties and show high activity for isomerization of hydrocarbons.²⁻⁴ It was suggested that the superacid sites are generated by the interaction between the oxide and sulfate ions, and the presence of sulfate ion somehow inhibits the recrystallization of ZrO_2 , therefore the sulfated zirconia retained a much greater fraction of the initial surface area than the unsulfated catalysts.⁵ The addition of platinum to a sulfated zirconia catalyst has been shown to enhance the stability of the catalyst for the isomerization of butane and pentane at low temperatures, though the state of platinum in this type of platinum impregnated zirconia catalysts is still a matter of controversy.⁶ Recently, another class of solid superacid catalysts--sulfated zirconia oxide, containing Fe and Mn, have been shown to be active for the skeletal isomerization of n-butane at room temperature.⁷⁻⁹ Kinetic results indicated that this class of catalysts was about three orders of magnitude more active than a sulfated ZrO_2 . Though extensive characterization studies have been carried out on the sulfate modified zirconia, less has been reported for the metal promoted sulfated zirconia. Commonly, these catalysts are activated at temperatures in the region of $600\text{-}725^\circ\text{C}$ in air prior to use as catalysts for various reactions. The activation of these catalysts involves complex chemical changes. In the present investigation, simultaneous TG/MS and TG/DTA techniques were utilized to investigate the weight loss and the phase transformation of the solid and to monitor the chemical compounds that evolve under controlled heating in different environments.

EXPERIMENTAL

Zirconia was prepared by rapidly precipitating from a 0.3M solution prepared from anhydrous ZrCl_4 with an excess amount of NH_4OH to a final pH of 10.5. The resulting precipitate was washed thoroughly with deionized water until a negative test was obtained for the presence of chloride ions in the wash. The dried hydroxide gel was sulfated by immersing the powder in 0.5M H_2SO_4 and stirring for 2 hours. The precipitate was collected by filtration without further washing, and dried. $\text{Pt-SO}_4^{2-}\text{-ZrO}_2$ was obtained by impregnating sulfated zirconia powders with an aqueous solution of H_2PtCl_6 . The Fe/Mn promoted sulfated zirconia were prepared by dissolving appropriate amounts of Fe(III) and Mn(II) nitrate/sulfate salts in the amount of water needed to prepare a catalyst containing the desired amount of Fe and Mn using an incipient wetness impregnation technique. All catalysts, after impregnation, were dried at 120°C overnight and stored in a desiccator until used for thermal analysis. The samples thus prepared used in the present analysis include 1%(5%)Pt- $\text{SO}_4^{2-}\text{-ZrO}_2$ and 2%Fe/0.5%Mn (sulfate salt/nitrate salt)- $\text{SO}_4^{2-}\text{-ZrO}_2$.

The samples were analyzed in a TA TGA 2950 instrument which was coupled to a VG Mass Spectrometer (from ThermoLab), Figure 1. The MS spectrometer allows the determination of multiple gas components in the mass range of 1-300amu. It has a specially designed flexible capillary tube with a fused silica liner, which is heated to 170°C to avoid condensation of evolved gasses. It requires 60 milliseconds for gas transfer from the TGA to the MS. The mass spectrometer has a Nier type enclosed ion source, a triple mass filter, and two detectors (a Faraday cup and a secondary emission multiplier). The TG-MS system has an operating temperature range to 900°C. Data from the mass spectrometer was acquired using a log histogram mode scan (LHG) in which the intensities of all peaks in a specified mass range were monitored and stored repeatedly during the temperature program. A data conversion program was used to display the intensities of the desired ions as a function of temperature. The runs were conducted separately in a purge gas of helium or air at a flow rate of 50 ml/min. Heating rates were 20°C/min. The samples were also analyzed in a TA SDT 2960 instrument, which is an analysis module that is capable of performing both thermogravimetric analysis (TGA) and differential thermal analysis (DTA) at the same time in a temperature range from room temperature to 1500°C in a controlled atmosphere. While the physical measurement of weight loss is obtained by TGA, in the meantime, the thermal events occurring to the samples are recorded by DTA. An upward peak represents for an exothermic event while a downward peak represent for an endothermic event on a DTA curve. Platinum crucibles were used as sample holders, and Al₂O₃ was used as the reference material.

RESULT AND DISCUSSION

When 1%(5%)Pt-SO₄²⁻-ZrO₂ samples were heated in helium, two major weight loss regions are seen on TG curve, see Figure 2, curve (a), (b). According to the MS data, Figure 3, the first weight loss region is between room temperature to 620°C, which corresponds to the loss of water, carbon dioxide, hydrogen chloride and chlorine. The identification of HCl and Cl₂ is based upon the molar mass of the compounds as well as the mass ratio of the Cl isotopes. In the case of HCl evolved from 5%Pt-SO₄²⁻-ZrO₂ sample, the ratio of peak area integration of HCl(38)/HCl(36) is around 1:3, which meet very well with the theoretical data. The integration of Cl₂ peak area didn't give a good agreement with theoretical isotope ratio. This is because when only trace amount of chlorine is released from the sample, the magnitude of noise is comparable to the Cl₂ profile. In that case, the integration can not be precise to give the real isotope mass ratios. However, the trend does agree with that isotope peaks Cl(70)>Cl(72)>Cl(74). Water is lost during this temperature range. The long tail of water peak profile indicated most of water is present as adsorbate on the surface area, whereas some water exists in the deeper pores within the solid. The evolution of carbon dioxide at different temperature ranges is due to the coordination between carbon dioxide, which is a Lewis acid, and zirconia, which is a Lewis base, during sample preparation. The variation of weight loss at this temperature region depend upon the drying condition of the catalyst sample as well as the amount of sulfuric acid adsorbed on the sample. The second weight loss region is from 620°C to a temperature beyond 900°C, which corresponds to the decomposition of sulfate ion to give off sulfur oxides as well as a continuous evolution of HCl (MS data). The peak profiles of sulfur oxides show a continuum beyond 900°C since the profiles of SO₂ and SO didn't go back to the base line level. This can be evidenced by TG data which shows that the TG curve doesn't level off at this point. The results indicated that there could be different types of sulfate in zirconia. The evolution profile of HCl also shows 3 peak maxima which indicated several forms of bonding between Cl and zirconia. Thus, in the inert gas the heating events can be described as occurring in two temperature regions:

Region I (<620°C)



Region II (>620°C)

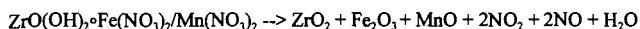


The evolution of oxygen coincides with the evolution of sulfur oxides as shown on the MS data and suggests that SO₃ might form prior to the evolution of SO₂ and SO. However, SO₃ was not identified by mass spectrometry. The results obtained when pretreating gas was air are similar to those of the runs in helium; however, when air is used it is not possible to measure the evolution of oxygen.

When 2%Fe/0.5%Mn(sulfate salt/nitrate salt)-SO₄²⁻-ZrO₂ samples were heated in helium to 900°C, there was also two major weight loss regions on the TG curve at the same temperature region as it for platinum sulfated zirconia. (see Figure 2, curve (c), (d). For Fe and Mn nitrate salt treated sulfated zirconia, the first major weight loss includes the decomposition of nitrate ion at around 300°C in addition to the other gas species as mentioned above for platinum sulfated zirconia sample (see Figure 4). Integration of peak area shows NO:NO₂ is 5:1, which agree with the fraction of nitrate ion that

evolves containing more NO than NO₂. Therefore, the heating events for this sample below 620°C can be described as follows:

Region I (<620°C)



The second major weight loss can be attributed to the decomposition of sulfate ion as seen in other sulfated zirconia samples in the second temperature region.

As for Fe/Mn sulfate salt treated sulfated zirconia, the result is similar to that of the platinum sulfated zirconia samples. It was shown that the existence of different metals or metal oxides does not affect the decomposition temperature of sulfate ion. Also, the results obtained when the pretreating gas was air are similar to those of the runs in helium, which indicate oxygen doesn't have any significant effect on the activation process.

When the platinum sulfated zirconia is analyzed in SDT at an air environment, we could see clearly the endothermic peak on DTA curve corresponding to the loss of gas species as water, carbon dioxide, hydrogen chloride and chlorine. There is a distinct exothermic peak on DTA curve occurring at 648°C which corresponds to the phase transformation of the solid from amorphous state to crystallite state. As a matter of fact, this exothermic event overlaps with an endothermic event which corresponds to the decomposition of the sulfate ion. Therefore, when heating the sample in air or an inert gas, the exothermic event is the result of an exothermic and an endothermic event so that the shape of the trace will depend upon the heat balance for these two events. For zirconia alone, this exotherm occurs at 450°C under the same heating condition, while in the presence of sulfate ion, the phase transformation process is retarded to a much higher temperature. It was found for sulfated zirconia samples, this exotherm occurs at 622°C under the same heating conditions. This indicates that the existence of metals on the sulfated zirconia doesn't have any significant effect on this exothermic event. When anions other than sulfate ion were used to treat sulfated zirconia, this exotherm occurs at 533°C for molybdate zirconia, 527°C for dichromate zirconia and 465°C for tungstate zirconia.¹⁰ It is found that sulfate ion is so far the most efficient species to retard phase transformation of the catalyst, thus permitting a high surface area to be maintained through a higher temperature range.

CONCLUSION

When catalyst samples of 1%(5%)Pt-SO₄²⁻-ZrO₂ and 2%Fe/0.5%Mn (sulfate salt/nitrate salt)-SO₄²⁻-ZrO₂ were heated in air or inert gas, online analysis by TG-MS shows different gas species evolved during different temperature regions. HCl and Cl₂ were identified even in trace amounts according to their isotope mass ratios. The existence of metals or metal oxides on the sulfated zirconia does not affect the decomposition of sulfate ion; neither does it affect significantly the phase transformation of the solid in air or inert gas environment. Sulfate ion was found so far to be the most efficient species to retard the phase transformation process of zirconia.

ACKNOWLEDGEMENT

The authors gratefully acknowledge the financial support of the Center for Applied Energy Research at University of Kentucky.

REFERENCES

1. Tanabe, K. and Hattori, H. *Chem.Lett.*, **1976**, 625.
2. Hini, M. and Arata, K. *J.Chem. Soc., Chem. Commun.*, **1980**, 851.
3. Arata, K.; Hino, M.; and Yamagata, N. *Bull. Chem. Soc. Jpn.*, **1990**, 63, 244.
4. Wen, M. Y.; Wender, I.; and Tierney, J.W. *Energy Fuels*, **1990**, 4, 372.
5. Scurrell, M. S. *Appl. Catal.*, **1987**, 34, 109.
6. Hosi, T.; Shimidzu, T.; Itoh, S.; Baba, S.; Takaoka, H. *Prepr.-Am. Chem. Soc., Div. Pet. Chem.* **1988**, 33(1), 562.
7. Hollstein, E.J.; Wei, J.T.; and Hsu, C.Y. US patents 4, 918, 041, 1990, and 4, 956, 519, 1990.

8. Hsu, C.Y.; Patel, V.K.; Vahlsing, D.H.; Wei, J.T.; and Myers, Jr., H.K. US Patents 5, 019, 617, 1991.
9. Lin, C.H. and Hsu, C.Y. *J. Chem. Soc., Chem. Commun.*, 1992, 20, 1479.
10. Bi, M.; Li, H.; Pan, W.P.; Lloyd, W.G.; and Davis, B.H. North American Thermal Analysis Society Conference, 1995, #76, 350.

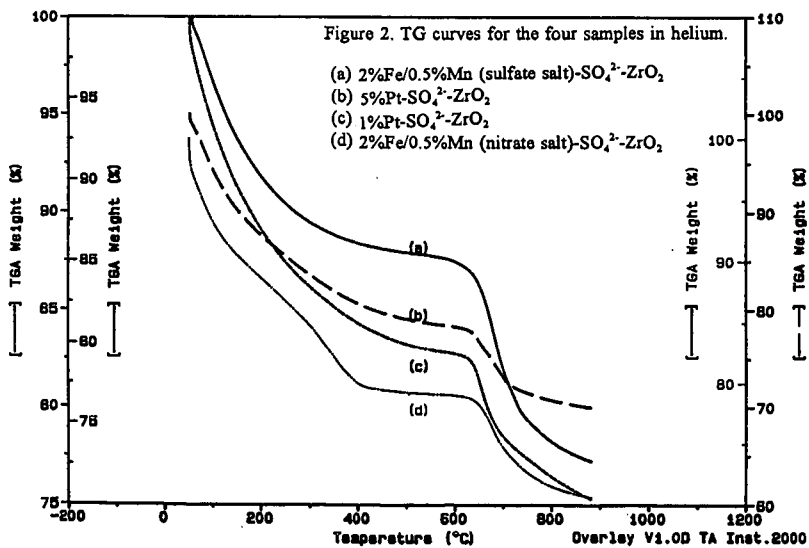
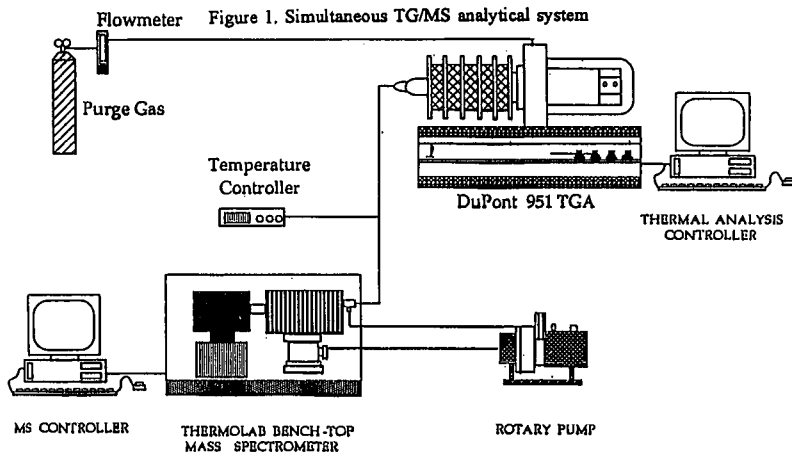


Figure 3. The MS data for 5%Pt-SO₄²⁻-ZrO₂ sample in helium.

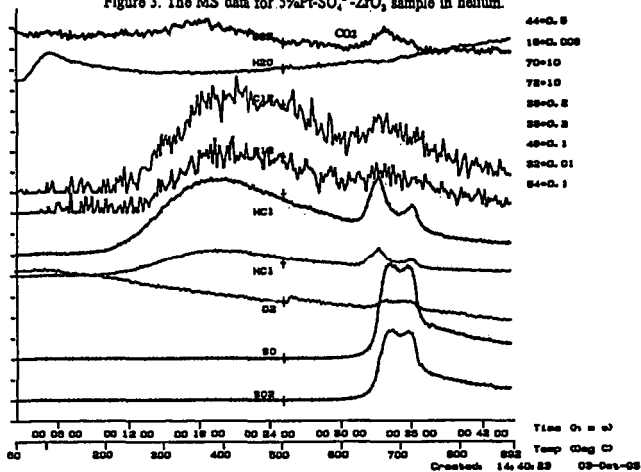


Figure 4. The MS data for 2%Fe/0.5%Mn (nitrate salt)-SO₄²⁻-ZrO₂ sample in helium.

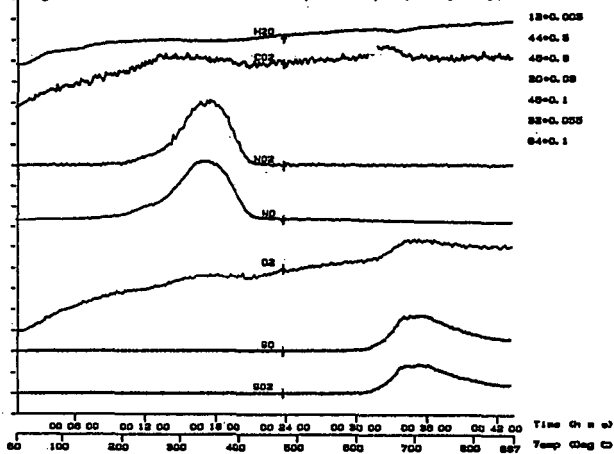
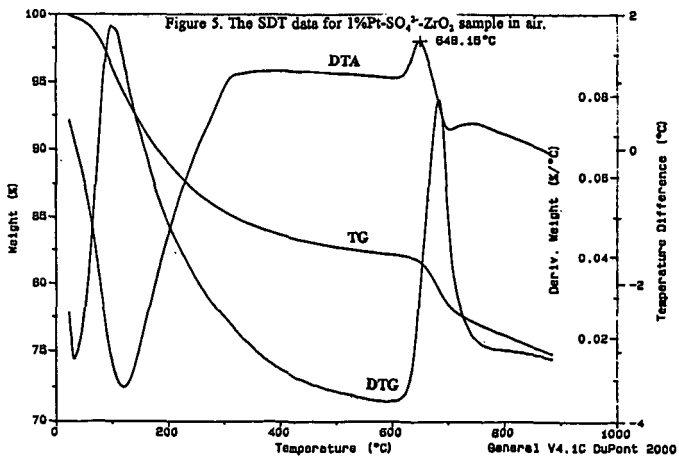


Figure 5. The SDT data for 1%Pt-SO₄²⁻-ZrO₂ sample in air.



MEASUREMENTS OF VAPOR PRESSURES OF HETEROATOM-CONTAINING PAH AND COAL-TAR MODEL MIXTURES

V. Oja and E.M. Suuberg
Division of Engineering
Brown University
Providence, RI 02912

Keywords: Coal Tar, Vapor Pressures, Polycyclic Aromatic Hydrocarbons

INTRODUCTION

This paper presents the results of measurements of the vapor pressures of large polycyclic aromatic hydrocarbons (PAH), including those containing heteroatoms, and some mixtures of these compounds. The work was motivated by the lack of vapor pressure data on coal tars, which tend to have a highly aromatic nature and which also contain significant numbers of heteroatoms. Relatively few data are available on the vapor pressures of large polycyclics containing heteroatoms. Knowledge of coal tar vapor pressures is important in predicting the pyrolysis behavior of coals, since most advanced models of coal pyrolysis utilize an evaporation step to describe the loss of tar from the particles [1-8].

There have been some efforts made at characterizing vapor pressures of coal liquids, as opposed to coal tars [9]. For the most part, that work was concerned with relatively lighter compounds than are of interest in pyrolysis (typically, four fused aromatic rings or less, with molecular weights of about 300 or less). Primary coal tars exhibit molecular weights that are well over 1000 [1,6]. In addition, there is a tendency in liquefaction to reduce the heteroatom content of the coal liquids, so the important role of heteroatoms in determining properties of coal tars might not be well modeled by coal liquids. The predictive methods seen to work reasonably well with hydrocarbon model compounds for coal liquids were often noted to work more poorly in heteroatomic systems [9].

There is little hope of characterizing materials as complex as coal tars in very great detail. There is strong incentive to keep the amount of data needed for prediction of vapor pressures of such mixtures to an absolute minimum. This issue has historically been addressed by the use of correlations based upon molecular weight distributions alone [1-8,10,11], since molecular weight and temperature are the two most important variables in determining vapor pressures. These correlations have been of one particular form, obtained from the Clausius-Clapeyron equation, assuming that the heat of vaporization is a function of the molecular weight and not a function of temperature. The resulting form of correlation developed by Suuberg et al. [10] is :

$$P = \alpha \exp\left(-\beta \frac{M^{\gamma}}{T}\right)$$

This is the simplest expression which appears to be consistent with the known thermodynamics of the situation and is used because of the lack of detailed chemical structure and vapor pressure data on coal tar. It should also be noted, consistent with this approach, that it has been shown possible to correlate molecular weight of coal liquids using only boiling point information, at least up to about 400 molecular weight [9].

Several workers have employed such a correlation, and values of the constants they have obtained by fitting the data to literature data on aromatic hydrocarbons are shown below:

	α	β	γ
Suuberg et al.[10]	1.23×10^5	236	0.654
Suuberg et al.[11]	5765	255	0.586
Niksa [3]	70.1	1.6	1.0
Niksa and Kerstein [4]	3.0×10^5	200	0.6
Fletcher et al. [5]	87060	299	0.59
Oh et al. [8]	6.23×10^5	561	0.474

In this expression, P is in atmospheres, T is in K, and M is in daltons. Comparisons of the predictions of several of these models have been offered elsewhere [5]. Wide variations were noted in the predictions, and there is a concern about adequacy of predictions of the vapor pressures under pyrolysis conditions. Nevertheless, it is clear that there is a general convergence of most of the values of α , β , and γ in the literature. A comparison of the predictions of boiling point with molecular weight is shown in Figure 1, for various models. The results of Tsonopoulos et al. [9] and Fletcher et al. [5] are seen to be in good agreement, but this is not surprising, since they involved regression of many of the same data on coal liquids. For reference, the measured

properties of anthracene are indicated.

Most of the experimental data in the literature on what might be considered model compounds for coal tars have been measured in a pressure range from 10^{-4} to 10 torr. A problem arises in extrapolating existing experimental data out of the temperature range in which it was obtained. Measurements of vapor pressures of high molecular weight materials requires high temperatures to obtain conveniently measurable pressures, but high temperatures cannot be employed because of the concern about thermal decomposition during measurement. This, then, requires the use of moderate temperatures ($<300^{\circ}\text{C}$) and sensitive, indirect vapor pressure measurement techniques. Yet it is the high temperature range ($>300^{\circ}\text{C}$) that is of practical interest for coal tars, since these materials are formed at those high temperatures. Thus the extrapolation to high temperatures is of great importance. Significant concerns arise because many of the measurements must be performed with the compounds of interest in the solid phase, as opposed to the liquid phase in which they might exist at the high temperatures of practical interest. Thus the measurements are being conducted under *sublimation* conditions, whereas in practice, true evaporation will be occurring. This makes the prediction of changes in vapor pressure with temperature very difficult. Not only is a correction required to correct for sublimation as opposed to evaporation (involving an enthalpy of fusion), but the enthalpy of evaporation itself is a decreasing function of temperature.

In sublimation work, it is not uncommon to find that the Clausius-Clapeyron equation, with a constant $\Delta H_{\text{sublimation}}$, fits vapor pressure data reasonably well, i.e., $d[\ln P^{\circ}]/d[1/T] = -\Delta H_{\text{subl}}/R$. The difficulty in developing reliable correlations of ΔH_{subl} with molecular weight is evident from the data of Figure 2, which shows data for high molecular weight aromatic hydrocarbons (a few containing heteroatoms). The poor correlation might be in part attributable to the difficulty of performing measurements by the indirect methods required. However, part of the difficulty might also be understood in terms of the enthalpy of sublimation consisting of contributions from the enthalpies of vaporization and fusion [12]. The enthalpies of vaporization of many compounds can be reasonably estimated by any number of means. The enthalpy of fusion, on the other hand, is very difficult to correlate with other properties [12]. For high molecular weight materials, the enthalpies of fusion can become comparable in magnitude to the enthalpies of vaporization. In this work, we are addressing this issue specifically, and will report on it separately.

EXPERIMENTAL

The vapor pressures of actual coal tars and model "tars", consisting of mixtures of PAH, are measured, using a molecular effusion/TGA technique. The various so-called "effusion" methods are based on the molecular effusion of a vapor from a surface, or through an orifice [13]. Of these methods, that which has been selected for use here is the Knudsen method [14,15], in which a substance of interest effuses through a small pinhole, of known area, in an otherwise sealed container or cell. The Knudsen method is used for the measurement of low vapor pressures in the range from 1 to 10^{-6} torr, under molecular flow conditions. This ideally requires that pressures inside and outside the sample cell are low enough that the frequency of collisions of vapor molecules with gas phase species are low in comparison with the frequency of collisions with the cell. The measurement of vapor pressure involves determining the rate of loss of molecules of the evaporating substance from the effusion cell under these conditions. Measurements are made under isothermal conditions, with weight loss from the cell being recorded as a function of time, generally in a TGA-type apparatus.

The basic theory of the effusion method has been often reviewed in the literature [14-16]. The theory of method is actually based upon the basic kinetic theory of gases. From these classical results, Knudsen derived an expression for the slow isothermal flow out of a cell with a small hole in it. The vapor pressure of a material in the cell can be calculated from Knudsen's original effusion rate result:

$$P_1 - P_2 = \frac{G}{t} \frac{w_1 + w_2}{\sqrt{\rho}}$$

where P_1 is the pressure of saturated vapor inside the cell, P_2 is the pressure outside of the effusion cell, w_1 is the resistance of hole in the cell, w_2 is the resistance of cell containing the sample, G is the mass lost by effusion, t is the effusion time, ρ is the density of the vapor at the temperature of experiment. The relation simplifies upon applying several simplifying assumptions, including the ideal gas law, that the pinhole leak is the main flow resistance, and assuming $P_1 \gg$

P_2 , yielding:

$$P = \frac{m}{t A_0} \left(\frac{2 \pi R T}{M} \right)^{1/2}$$

The above result is called the ideal Knudsen equation, in which P is the desired vapor pressure, m the mass loss during the effusion time interval, A_0 is orifice area, M the substance molecular weight, t the effusion time, and T the absolute temperature of the experiment. It is further assumed when applying this equation to the effusion process that the equilibrium vapor pressure of the effusing species obtains within the cell, that the orifice walls do not intercept and return into the cell an appreciable fraction of molecular current entering the hole, that there is no back flux into the orifice exit and the number of intermolecular collisions in the vapor phase occurring within the orifice is negligible.

In our implementation, the mass loss rate was continuously recorded, using a Cahn 2000 recording electrobalance. The cell containing the pinhole leak was suspended on one arm of the balance, which has nominal sensitivity in the μg level. The backpressure in the TGA system was maintained at 10^{-7} torr, which has been noted to be sufficient so as to provide accuracy in the 10^{-6} torr range of vapor pressures. The cell itself was maintained inside of a black capsule within the TGA, and was in close proximity to a thermocouple within the capsule. This was necessary in order to achieve the 0.1°K accuracy in temperature measurement required in vapor pressure work at low temperatures.

RESULTS AND DISCUSSION

Variation of Vapor Pressure with Temperature

Typical results are shown in Figure 3, for anthracene between 47 and 75°C . The anthracene was of 99+% purity, purchased from Sigma Chemical Company, and used without further purification. Comparison is shown with other sources of data on this compound [17-21]. Again, the spread of the data is indicative of the difficulty in performing such measurements, on even relatively "easy" low molecular weight aromatics. The other feature which is clear from Fig. 3 is that the assumption that the enthalpy of sublimation is reasonable. Our results provide an enthalpy of sublimation of 101.6 kJ/mol. By way of comparison, the enthalpy of vaporization of anthracene, at its normal boiling point of 340°C , is 56.5 kJ/mol [12]. The melting point of anthracene is 216°C , so our experiments were performed much below the melting point. This is, again, very clear indication of the danger in blindly extrapolating vapor pressure data over a wide range of temperatures. The actual extrapolation is shown in Figure 4. It is seen that the extrapolation leads to a reasonable prediction of the first reported point in the liquid region, since this was very close to the melting point of the anthracene. As one extrapolates into the liquid region, the comparison becomes progressively poorer, because $\Delta H_{\text{subl}} \neq \Delta H_{\text{vap}}$. If one considers the earlier suggested correction of the enthalpy of sublimation to the enthalpy of vaporization, the enthalpy of fusion would be around 45 kJ/mol. The ratio of the enthalpy of fusion to the enthalpy of vaporization is roughly 0.8 , which is quite close to the the same ratio for *n*-dodecane (0.84 [12]), the normal alkane with a molecular weight closest to that of anthracene.

Mixture Models

It is unclear what mixture models can be used to describe vapor-liquid equilibrium for tars, which are obviously multicomponent mixtures. Typically, the most common assumption is Raoult's Law, in which the tar mixture is assumed ideal. There have been no attempts to establish how reasonable this assumption might be. Nearly ideal mixing behavior was seen for aromatic hydrocarbon mixtures (e.g. anthracene and perylene). An example of how a simple mixture model might badly fail is provided in Figure 5, for a mixture of phenanthridine and 1-hydroxypyrene. Aromatics containing such functional groups would be expected in coal tars. It would be anticipated that there would be strong acid-base interaction in this case, and this is clearly shown by the fact that the vapor pressure is far lower than predicted by Raoult's Law. Clearly more work is needed to establish how closely Raoult's Law might be followed in real tars.

ACKNOWLEDGMENT

The financial support of the U.S. Department of Energy, under grant DE-FG22-92PC92544, is gratefully acknowledged.

REFERENCES

1. Suuberg, E.M., in *Chemistry of Coal Conversion* (R. Schlosberg, Ed.), Plenum, 1985.
2. Unger, P.E., Suuberg, E.M., *18th Symp. (Int.) on Comb.*, The Comb. Inst., p. 1203, 1981.
3. Niksa, S. *AIChE J*, **34**, 790 (1988).
4. Niksa, S. and Kerstein, A., *Energy Fuels*, **5**, 647 (1991).
5. Fletcher, T., Kerstein, A., Pugmire, R., Solum, M., Grant, D. *Energy Fuels*, **6**, 414 (1992).
6. Solomon, P.R., Serio, M.A., and Suuberg, E.M., *Prog. Energy Comb. Sci.*, **18**, 133 (1992).
7. Solomon, P.R., Hamblen, D.G., Carangelo, R.M., Serio, M.A., Deshpande, G.V., *Energy Fuels*, **2**, 405 (1988).
8. Oh, M.S., Peters, W.A., and Howard, J.B., *AIChEJ*, **35**, 776 (1989).
9. Tsonopoulos, C., Heidman, J., and Hwang, S.-C., *Thermodynamic and Transport Properties of Coal Liquids*, Wiley, 1986.
10. Suuberg, E.M., Peters, W.A. and Howard, J.B., *17th Symp. (Int.) on Comb.*, The

- Combustion Institute, p. 117, 1979.
11. Suuberg, E.M., Unger, P.E., and Lilly, W.D., *Fuel*, 64, 956 (1985).
 12. Reid, R.C., Prausnitz, J.M., and Poling, B., *The Properties of Gases and Liquids*, 4th Ed. McGraw-Hill, 1987.
 13. Dushman, S., *Scientific Foundations of Vacuum Technique*, Wiley, 2nd edition, 1962.
 14. Knudsen, M., *Ann. Physik.*, 28, 999, 1909.
 15. Knudsen, M., *Ann. Physik.*, 29, 179, 1909.
 16. Hollahan, J., *J. Chem. Educ.*, 39, 23, 1962.
 17. Hansen, P.C and Eckert, C. A., *J. Chem. Eng. Data*, 31, 1 (1986)
 18. DeKruif, C.G., *J. Chem. Thermodynamics*, 12, 243 (1980).
 19. Kelley, J.D. and Rice, F.O., *J. Phys. Chem.*, 68, 3794 (1964).
 20. Macknick, A.B. and Prausnitz, J.M., *J. Chem. Eng. Data*, 24, 176 (1979).
 21. Sonnefeld, W.J., *Anal. Chem.*, 55, 275 (1983).

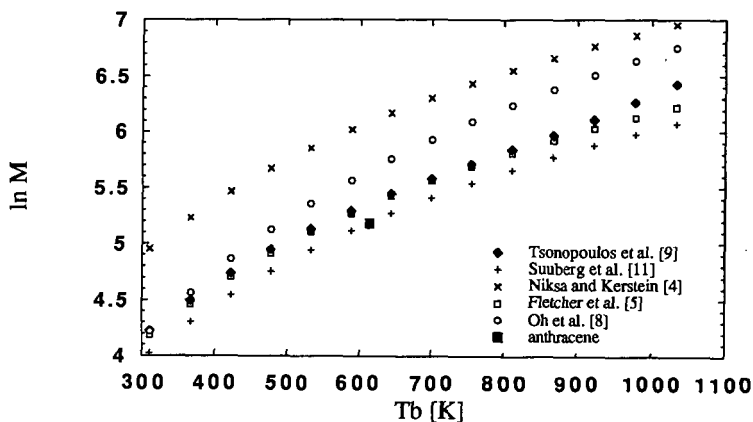


Figure 1. Predicted variation of boiling point with molecular weight, for low molecular weight aromatics.

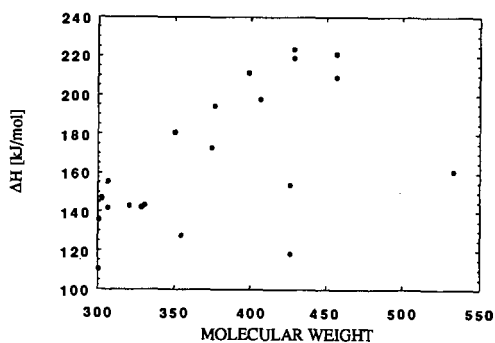


Figure 2. Variation of enthalpies of sublimation with molecular weight of aromatics. Data from *Handbook of the Thermodynamics of Organic Compounds*, by R.M. Stephenson and S. Malanowski, Elsevier, 1987.

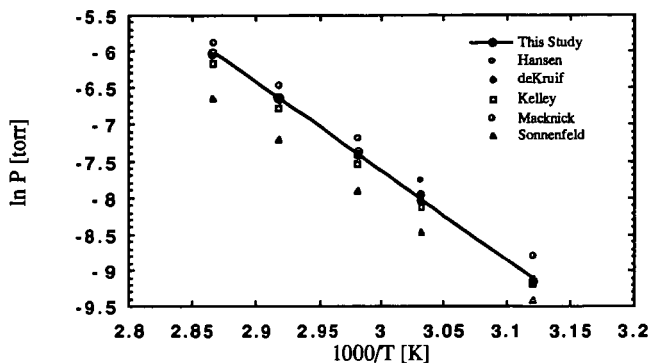


Figure 3. Vapor pressures of solid anthracene, from this study and the literature.

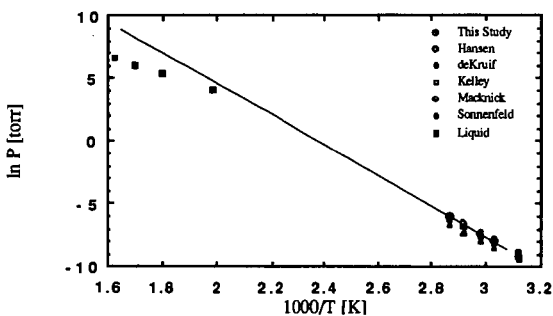


Figure 4. Vapor pressures of solid and liquid anthracene. Liquid data from Stephenson and Malanowski.

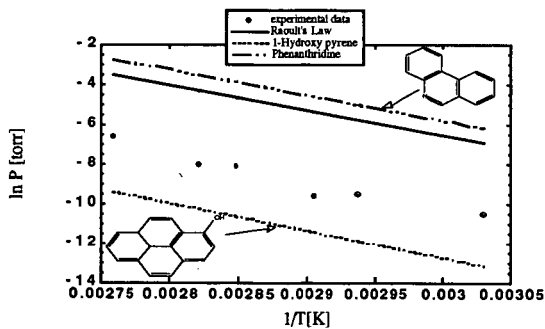


Figure 5. Vapor pressures of 1-hydroxypyrene, phenanthridine, and a mixture of 54 mol% 1-hydroxypyrene, 46% phenanthridine. The Raoult's Law prediction for the mixture is also shown.

DISTILLATION OF LIQUID FUELS BY THERMOGRAVIMETRY

He Huang, Keyu Wang, Shaojie Wang, M. T. Klein and W.H. Calkins*
Dept of Chemical Engineering, University of Delaware, Newark, DE 19716

Key words: thermogravimetric analysis, distillation, liquid fuels

INTRODUCTION

The most widely used separation technique in the petroleum industry and other liquid fuel production processes as well as in much of the chemical industry is distillation. To design and operate an appropriate commercial and laboratory distillation unit requires a knowledge of the boiling point distribution of the materials to be separated. In recognition of these needs, the ASTM developed the distillation procedures of D86, D216, D447, D850, and D1078. They are widely used in laboratories for the purposes of sample characterization, product and quality control, and distillation column design. However, the significant drawbacks of these ASTM methods include 1). close monitoring of the distillation is required. This is particularly difficult for those samples which are very toxic and/or cause any other safety problems; 2). the sample under test must be transparent and free of separated water (1); and 3). results obtained by these methods are not particularly precise. This motivated the development of a novel automatic distillation system based on the use of a custom-built thermogravimetric apparatus.

Thermogravimetry (TG) can be used to determine variation in mass as a function of temperature and/or time. Thus, thermogravimetric techniques, in principle, could be used in study of any physical and chemical processes where changes in mass are function of temperature and/or time. Hence, either commercial or custom-built thermogravimetric apparatus provides flexible means and unique features for study of various physical processes and chemical reactions. In the state-of-the-art custom-built thermogravimetric system, a computer is generally used for data acquisition of time, temperature and mass.

Massoth and Cowley (2) utilized a stirred flow thermogravimetric reactor for catalytic studies of hydrogenation of 1-butene under steady-state conditions. Sears et al. (3) reported a pressurized thermogravimetric equipment for use in oxidizing atmospheres at high temperatures. Dean and Dadyburjor (4) used a continuous thermogravimetric technique, combined with a pulse microreactor and on-line gas chromatograph, to study deactivation of cracking catalysts by coking.

In this paper, design and operation of a custom-built thermogravimetric apparatus for the distillation of liquid fuels are reported. Using a sensitive balance with scale of 0.001 g and ASTM distillation glassware, several petroleum and petroleum-derived samples have been analyzed by the thermogravimetric distillation method. When the ASTM distillation glassware is replaced by a micro-scale unit, sample size could be reduced from 100 g to 5-10 g. A computer program has been developed to transfer the data into a distillation plot, e.g. Weight Percent Distilled vs. Boiling Point. It also generate a report on the characteristic distillation parameters, such as, IBP (Initial Boiling Point), FBP (Final Boiling Point), and boiling point at 50 wt% distilled. Comparison of the boiling point distributions determined by TG (thermogravimetry) with those by SimDis GC (Simulated-Distillation Gas Chromatography) on two liquid fuel samples (i.e. a decanted oil and a filtered crude oil) are also discussed in this paper.

EXPERIMENTAL

Apparatus. A schematic diagram of the thermogravimetric apparatus for distillation is shown in Figure 1. A K-type thermocouple was used to measure the boiling temperature. The thermocouple was supported by a tight bevel-seal (Kontes, Vineland, New Jersey) with the thermocouple vertical and centered in the tube of the distillation head and in such a position that the thermocouple end-point (i.e. thermocouple joint) is level with the lowest point of junction between head tube and head neck (see Figure 1). The signal from the thermocouple was first processed by a DIN Rail Thermocouple Transmitter (MCR-TC Series, Omega Engineering, Inc.). A Mettler PK300 Balance with precision of 0.001 g was used to monitor the mass change in the distillate receiver. A Mettler GC47 D/A Converter was used to transfer the digital signals from the balance to analog signals for data acquisition. Asystant+ data acquisition system with DT2805 A/D board (Asyst Software Technologies, Inc.) was installed in a IBM computer and used for data acquisition. Both temperature and mass signals were sampled at 1 Hz. A ASTM distillation head and 250-ml flask (Kontes) and an electric heater were used for distillation.

Distillation. For each distillation, about 100-g liquid fuel was transferred into the distillation flask. Both the empty flask (W_{flask}) and initial distilland liquid fuel ($W_{initial}$) were weighed using the balance. Adjust the electric heater referring to the instructions given in ASTM D1078 and record the temperature and distillate mass by the computer. After the

condenser tube has drained, the total mass of distillate weighed by the balance was recorded as recovery (W_{recovery}). Cooling the distillation flask to room temperature, the distillate left plus the flask ($W_{\text{left+flask}}$) was weighed by the balance. The amount of residue (W_{residue}) was obtained by the subtraction of W_{flask} from $W_{\text{left+flask}}$. The amount of distillation loss (W_{loss}), due to surface wetting, was estimated by subtracting W_{initial} and the sum of W_{recovery} and W_{residue} .

Cleaning System. The apparatus system is cleaned in place by a series of suitable low-boiling solvent distillation. The number of cleaning distillations and type of solvent used are selected based on the distilland being studied. The effectiveness of cleaning can be monitored by analysis of the distillate streams (e.g. by GC analysis). After cleaning, the distillation glassware are placed into an oven and the temperature set above the boiling point of the solvent used.

Data Processing. The collected mass data were processed using an 11-point smoothing filter of the Linear Regression & Error Analysis procedure (5).

Materials Studied. A decanted oil and a filtered crude oil, together with seven other liquid fuels (designated as Samples A, B, C, etc.), have been studied using the thermogravimetric distillation apparatus. Pure organic compounds from low boiling point to high boiling point, such as methylene chloride (99.9+%), tetralin (1,2,3,4-tetrahydronaphthalene, 99%), and 1-methylnaphthalene (98%) from Aldrich Chemical Co., have been used for testing and calibrating the apparatus.

RESULTS AND DISCUSSION

Calibration of the Apparatus System Using Pure Organic Compounds. Several pure organic compounds have been used to test and calibrate the thermogravimetric apparatus. In theory, transfer time of distillate through the condenser, as a delay effect, should be corrected for accurately determining the boiling point distribution (i.e. Weight Percent Distilled vs Boiling Point) and characteristic distillation parameters, such as Initial Boiling Point (IBP), Final Boiling Point (FBP) (or Decomposition Point, DP). Results of the tetralin distillation using the TG method are shown in Figure 2. Surprisingly, there was no distillate-transfer time observed (see Figure 2). The dashed-line in Figure 2 defines the time required by the distillate being transferred through the condenser. The results shown in Figure 2 indicate no delay effect, i.e. as soon as the temperature reaches the tetralin boiling point, the first drop of tetralin falls into the distillate receiver. The same results were obtained in distillations of methylene chloride and 1-methylnaphthalene. The reason of these phenomena may be due to that the condenser surface was wetted by the vapor of the sample before its boiling point was reached. The Weight Percent Distilled vs. Boiling Point for the tetralin is shown in Figure 3. That the boiling point was increased after 95 wt% distilled is apparently due to impurities in the tetralin. The results of duplicate tetralin distillations are summarized in Table I. Weight percent distillation recoveries, residues, and losses, plus the boiling points observed, together with the literature value (6), are also given in Table I.

Distillation of Liquid Fuels. Plots of the Weight Percent Distilled vs. Boiling Point for the seven liquid fuels using the TG method are shown in Figures 4-10. Based on ASTM definition (7), the IBP (Initial Boiling Point) is the temperature detected as the first drop of condensate falls into the distillate receiver. Thus, in this TG method, the Initial Boiling Point was the temperature recorded at which the distillate mass is above zero. The mass of the first drop of the distillate recorded for these liquid fuels was in the range of 0.005 to 0.02 g. The Final Boiling Point (FBP) (i.e., the end point or decomposition point) was the maximum temperature recorded during the test. If no residue was left in the distillation flask, the dry point, instead of FBP, was reported. Characteristic distillation parameters (e.g. IBP, FBP, BP @50 wt%), together with the weight percent distillation recoveries, residues, and losses, of the seven liquid fuels are summarized in Table II.

The first derivative of TG distillation (i.e. $d(\text{wt}\%)/dt$) vs boiling point for Sample A is shown in Figure 11. This plot indicates the density function of distillate against boiling point. It can be used as additional information for characterizing the boiling property of liquid fuels.

Comparison of TG Distillation with SimDis GC. Plots of the Weight Percent Distilled vs. Boiling Point using the TG method (solid line) and SimDis GC technique (dashed line) for a filtered crude petroleum and a decanted oil are shown in Figures 12 and 13. The results show significant differences. It is more evidenced when the characteristic distillation parameters (e.g. IBC, FBP, BP @50 wt%) of the two samples determined by the both methods are summarized in Table III. These deviations of the SimDis GC method from the distillation may be resulted by the interactions between the tested sample and the selected column packing and by the differences in properties and distillation characteristics between the calibration standards and tested samples. The weight percent distillation recoveries, residues, and losses are also included in Table III. Compared to the SimDis GC

method, the TG technique, when operated under atmospheric pressure, is limited to measuring the boiling point up to about 380 °C.

CONCLUSION

The custom built thermogravimetric apparatus for distillation provides an accurate, convenient, and simple determination of boiling point distribution of liquid fuels. It has potential as a modified method to replace the widely used ASTM distillation methods. Boiling point distributions of two oil samples determined by the thermogravimetric method and SimDis GC technique show significant differences. These deviations of the SimDis GC method from distillation may be due to sample-GC column packing interactions and differences between the calibration standards and tested samples.

ACKNOWLEDGMENTS

The support of this work by the subcontract from CONSOL under DOE Contract DE-AC22-94PC93054 and by the Department of Energy under DE22-93PC93205 is acknowledged.

REFERENCES

1. Distillation of Industrial Aromatic Hydrocarbons and Related Materials *ASTM D 850*, 1991.
2. Massoth, F.E. *Chem. Tech.* 1972, May, 285.
3. Sears, J.T.; Maxfield, E.A.; Tamhankar, S.S. *Ind. Eng. Chem. Fundam.* 1982, 21, 474.
4. Dean, J.W.; Dadyburjor, D.B. *Ind. Eng. Chem. Res.* 1988, 27, 1754.
5. Wang, Keyu; Wang, Shaojie; Huang, He; Klein, M.T.; Calkins, W.H.; paper to be presented in the *Symp. on the Thermal Analytical Techniques*, March 24-29, 1996, in New Orleans.
6. Lide, D.R. *CRC Handbook of Chemistry and Physics*, 72nd ed.; CRC Press, Inc., Boca Raton, FL, 1991.
7. Distillation of Petroleum Products *ASTM D 86*, 1990.

Table I Results of tetralin distillation

Distillation Run No.	Boiling Point °C	Recovery wt%	Residue wt%	Loss wt%
1	207.8	98.7%	0.7%	0.6%
2	207.7	99.1%	0.5%	0.4%
3	207.8	98.9%	0.5%	0.6%
Literature value	207.6	-	-	-

Table II Results of the seven liquid fuel distillations

Sample	IBP °C	BP @50wt% °C	FBP °C	Recovery wt%	Residue wt%	Loss wt%
A	206.1	278.5	316.4	95.3%	3.2%	1.5%
B	169.4	285.6	334.9	90.5%	8.6%	0.9%
C	84.3	285.6	346.2	89.7%	9.8%	0.5%
D	194.1	272.7	350.8	96.1%	3.5%	0.4%
E	105.1	365.7	378.2	59.9%	35.1%	5.0%
F	209.6	342.0	353.8	71.9%	23.3%	4.8%
G	198.1	280.6	348.5	95.5%	3.9%	0.6%

Table III Comparison of SimDis GC with TG

Distillation Method	IBP °C	BP @40wt% °C	BP @50wt% °C	FBP °C	Recovery wt%	Residue wt%	Loss wt%
Sample: Crude oil							
TG (1st)	56.3	-	301.5	314.7	71.9%	22.0%	6.1%
TG (2nd)	55.8	-	297.6	314.9	72.6%	21.1%	6.3%
SimDis GC	95.6	-	431.1	720.0	91.0%	-	-
Sample: Decanted oil							
TG (1st)	244.1	363.7	-	364.6	42.5%	50.2%	7.3%
TG (2nd)	244.9	368.7	-	373.6	46.8%	45.5%	7.7%
SimDis GC	215.6	383.9	-	705.0	99.5%	-	-

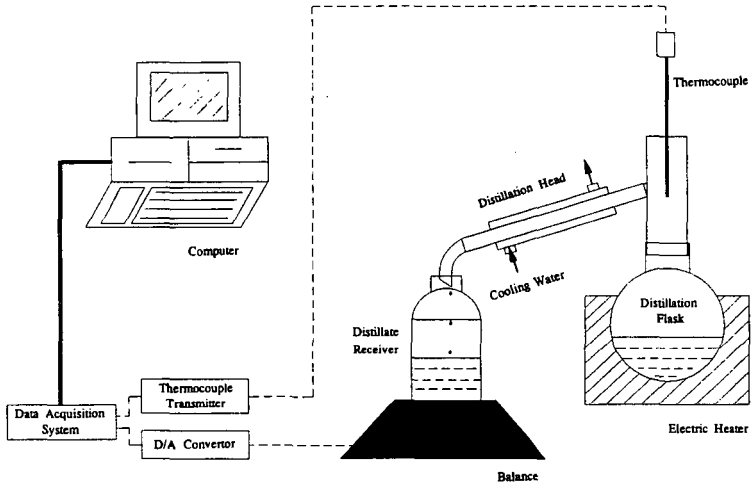


Figure 1 Schematic diagram of a custom built TG for distillation

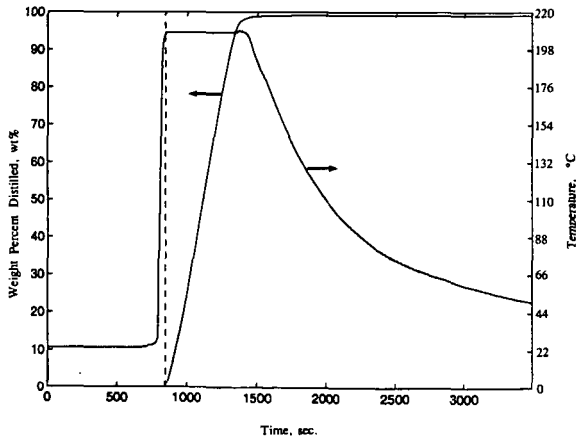


Figure 2 Temperature-mass-time plot for tetralin distillation

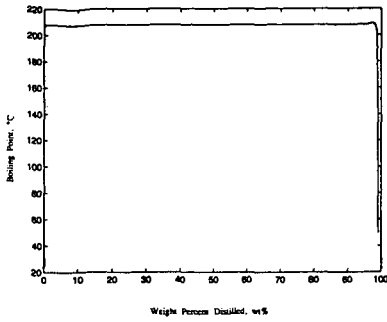


Figure 3 wt% vs T_b of tetralin

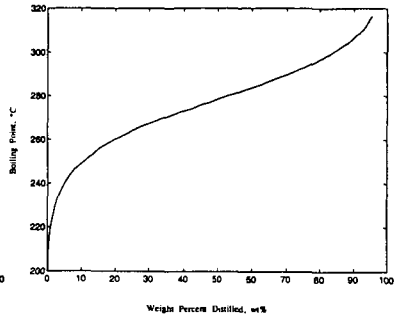


Figure 4 wt% vs T_b of Sample A

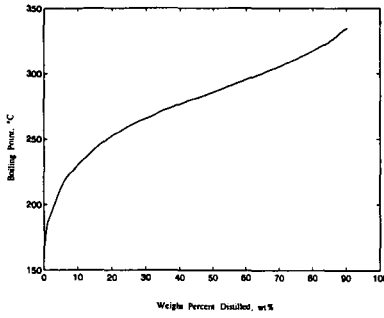


Figure 5 wt% vs T_b of Sample B

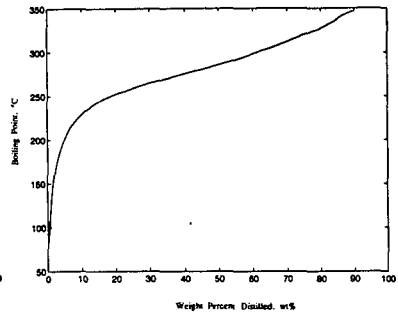


Figure 6 wt% vs T_b of Sample C

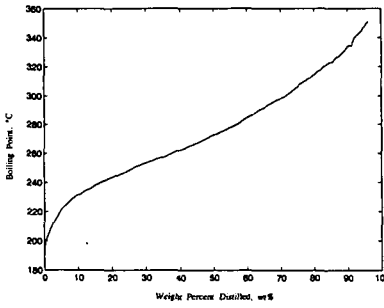


Figure 7 wt% vs T_b of Sample D

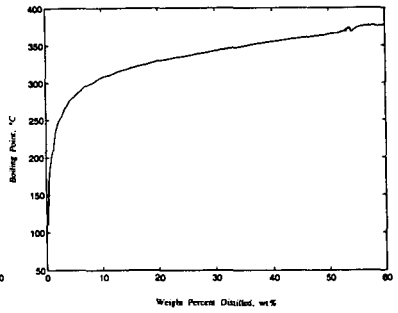


Figure 8 wt% vs T_b of Sample E

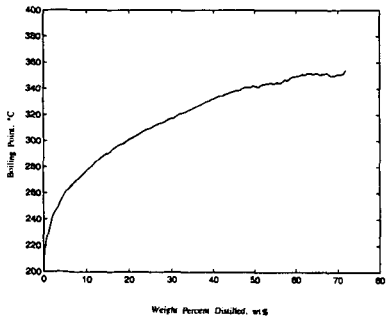


Figure 9 wt% vs T_b of Sample F

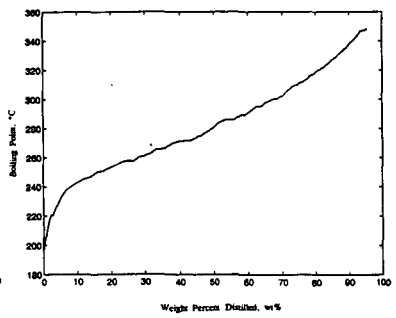


Figure 10 wt% vs T_b of Sample G

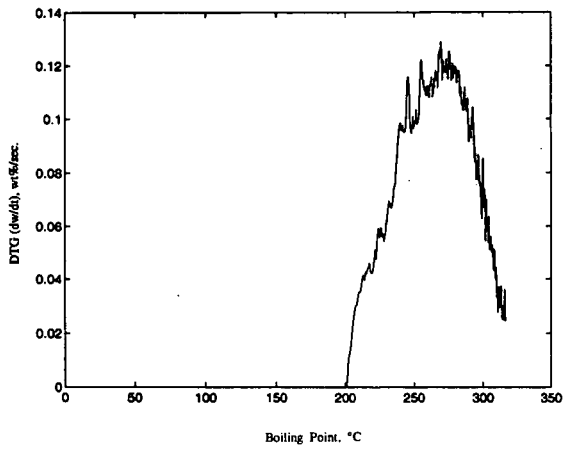


Figure 11 DTG vs T_b of Sample A

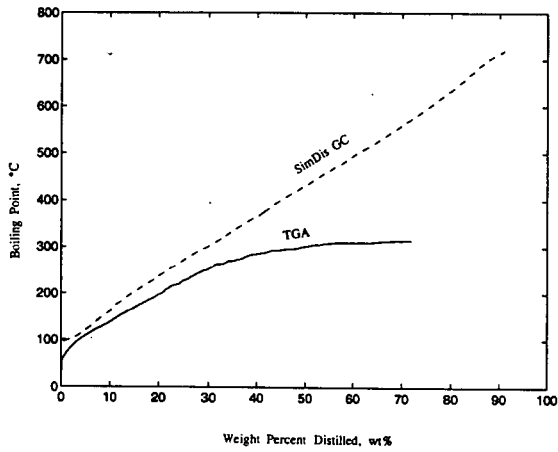


Figure 12 wt% vs T_b of a crude oil determined by TG and SimDis GC

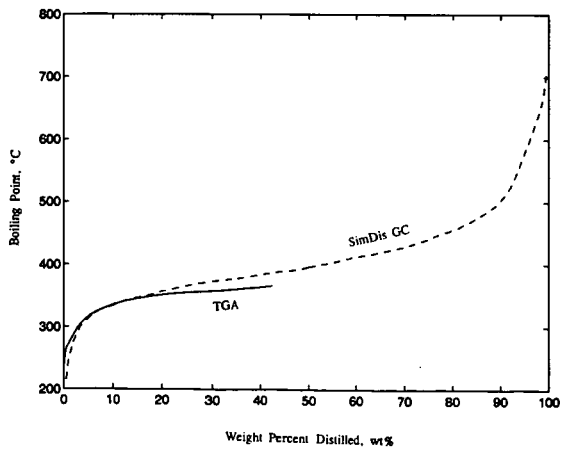


Figure 13 wt% vs T_b of a decanted oil determined by TG and SimDis GC